

Impurity engineering of Czochralski silicon

Xuegong Yu, Jiahe Chen, Xiangyang Ma, Deren Yang *

State Key Laboratory of Silicon Materials and Department of Materials Science and Engineering, Zhejiang University, Hangzhou 310027, People's Republic of China

ARTICLE INFO

Article history:

Available online 20 February 2013

Keywords:

Czochralski silicon
Co-doping technology
Impurity engineering
Defects
Oxygen precipitate
Void

ABSTRACT

Microelectronic devices with high integration level and functional complexity are always requiring larger diameter and more perfect Czochralski (CZ) silicon wafers. Therefore, the defects, playing the key role in the quality control of silicon materials, have to be well controlled during crystal growth and device fabrication. Co-doping nitrogen (N), germanium (Ge) or carbon (C) into CZ silicon to control defect dynamics and to change defect evolution, so-called "impurity engineering", has been developed in recent years, and has been widely applied in the fabrication of higher quality CZ silicon used for microelectronics nowadays. This article is to present an overview of the current status of impurity engineering in CZ silicon, based on the co-doping technologies of N, Ge and C. The fundamental properties of these three co-dopants and their interaction with point defects in CZ silicon are firstly introduced. The bulk of the article is focused on the effects of co-dopants on the formation of oxygen precipitates related to internal gettering (IG) of devices for metal contaminants, and voids associated with the gate oxide integrity (GOI) of devices in CZ silicon. Finally, the improvement of CZ silicon mechanical strength by co-doping technology is described.

© 2013 Elsevier B.V. All rights reserved.

1. Introduction

With the increase of the diameter, defects play a more and more important role in the quality control of Czochralski (CZ) silicon materials and devices. For modern ultra-large scale integrated circuits (ULSI) whose design rule goes towards 32 nm era, the most important work is to control voids and oxygen precipitates which originate from point defects including impurities, since these two defects can both cause the failure of gate oxide integrity (GOI) of metal-oxide-semiconductor (MOS) devices and generate leakage current [1]. Meanwhile, the management of metal contamination is also one of the most important aspects of successful device manufacture. All these circumstances are creating more demand for the control or utilization of the defects in CZ silicon, fitting the request of semiconductor devices with high integration level.

Last 50 years, great efforts have been given to control defects in CZ silicon. The mainstream idea and technology is to manage point defects (self-interstitial and vacancy) and avoid impurities (metal, light elements, etc.). In recent years, a novel technology, in which harmless impurities are co-doped into CZ silicon during crystal growth to improve the quality of silicon materials, so-called "impurity engineering" [2], has been developed, and has been

widely applied in the fabrication of higher quality CZ silicon used for ultra-large scale integrate circuit (ULSI) in the world.

It is well known that ULSI devices need high purity crystal CZ silicon. All of impurities except those for electrical doping should be avoided during the fabrication of silicon wafers. For impurity engineering, nitrogen (N), germanium (Ge) and carbon (C), which are known to be electrically neutral co-dopants in silicon, are doped into CZ silicon to modulate the defect dynamics and change defect evolution for the improvement of the material quality and the device yield. Those impurity atoms prefer to interact with point defects and then form various complexes. This necessarily affects the formation of defects, such as voids, oxidization-induced-stacking faults ring (OSF-ring), thermal donors (TDs) and oxygen (O) precipitates in CZ silicon. Correspondingly, the electrical stability, GOI and internal gettering (IG) of devices can significantly be improved. Apart from these, those co-doped impurity atoms in silicon lattice can interact with dislocations, helpful for the improvement of the wafer strength. The goal of this article is to present an overview of the current status of impurity engineering in CZ silicon, based on the co-doping technologies of N, Ge and C.

The fundamental properties of N, Ge and C in silicon, including segregation, solubility and diffusivity, are firstly described. Among them the diffusion of N is still like a puzzle. These co-dopants can interact with point defects to form different complexes, such as N–O, N–O–V, Ge–V, Ge–V–O and C–O. The formation of co-dopant related complexes plays an essential role in determining the quality of CZ silicon during growth and device processing. For

* Corresponding author.

E-mail address: mseyang@zju.edu.cn (D. Yang).

instance, the N–O complexes with electrical activity act as shallow thermal donors (STDs) in silicon, slightly changing the carrier concentration of silicon crystals.

Oxygen is an unavoidable impurity in CZ silicon crystal, originated from the contamination from silica crucibles. It can form TDs and oxygen precipitates, and induce secondary defects. The generation of TDs will result in the variation of material resistivity. Co-dopants can suppress the formation of TDs in silicon by reducing the rate of generation and the maximum concentration of TDs. The oxygen precipitation is related to the IG ability of silicon wafer which is a stand-by process of metal contamination being rendered harmless in the event of a failure of contamination control. Co-dopants can enhance the growth of oxygen precipitates and related secondary defects acting as IG sites and therefore improve the wafer IG ability. The IG process of co-doped silicon wafer could be accomplished by a single-step annealing. This is significant for the reduction of the thermal budget of IG technology and the simplification of annealing steps for device fabrication. These results will be also overviewed in this paper.

One of the purposes of this paper is to show the influence of co-dopants on the voids in CZ silicon. The voids result from the aggregation of excess vacancies during CZ silicon crystal growth. They are the most important defects in modern microelectronics, reducing the GOI of MOS devices. Since the co-dopants can enhance the formation of grown-in oxygen precipitates at high temperatures, a portion of vacancies will be lost prior to the generation of voids during crystal growth. The surviving vacancies contributing to the formation of voids during subsequent cooling are reduced. It results in the reduction of characteristic formation temperature of voids controlled by super-saturation of vacancies. So, the co-doping can create a larger number of smaller voids with less thermal stability in CZ silicon. The small voids are easily annealed out, which is preferable in microelectronics industry.

The effect of co-dopants on the mechanical strength of CZ silicon will finally be introduced. Co-dopants can improve the mechanical strength of CZ silicon wafers. Due to the locking effect of co-dopants on dislocations, the propagation of dislocations in the co-doped silicon is more difficult. It results from the fact that co-dopants can modulate the lattice stress of silicon crystal and cause larger activation energy for dislocation movement. Also, co-dopants can improve the upper and lower yield points of silicon materials, which is associated with the enhancement of oxygen precipitates by co-dopant or alloy hardening by co-dopants in silicon. The higher mechanical strength of co-doped silicon can reduce the cutting breakage and the wafer warpage, therefore improving the device yield.

2. Co-doping technologies

Nitrogen, germanium and carbon are generally not electrically active in silicon. Their co-doping in CZ silicon has been used to improve the quality of silicon materials in recent years. In this section, the fundamental properties of these co-dopants in silicon have first been introduced, including the solubility, diffusivity, segregation and measurement technique. The nitrogen has a small solubility and segregation coefficient in silicon, so it is hard to obtain the high concentration of nitrogen in silicon crystal. The diffusion of nitrogen in silicon is still like puzzle, even though most researchers believe it is a fast diffuser. Germanium, the same group IV element as silicon, can mix with silicon at any ratio to form GeSi alloy. However, for co-doping in CZ silicon crystal without dislocation generation, the germanium concentration in the crystal should be controlled below $10^{20}/\text{cm}^3$. Since it usually is at the substitutional site in silicon lattice, the diffusion of germanium is

quite slow. Its segregation in silicon is still controversial, and various results have been reported by different groups. Carbon in silicon can exist in various forms. Its solubility at silicon melt point is usually in the order of $10^{17}/\text{cm}^3$. The interstitial carbon is a fast diffuser, which could be electrically active. Afterwards, various co-doping technologies of these species during CZ silicon crystal growth will be elaborated, e.g. gas doping, solid doping. For nitrogen and carbon, the gas doping is more effective than their solid doping, while the solid doping of germanium is more convenient during CZ silicon crystal growth.

2.1. Material physics of co-dopants

2.1.1. Nitrogen

In liquid silicon, the N solubility is about $6 \times 10^{18}/\text{cm}^3$, which can be obtained by quenching experiments [3]. When the N concentration in the silicon melt is above this value, needles of silicon nitride (Si_3N_4) could segregate at the melt surface, resulting in the failure of dislocation-free single crystal CZ silicon growth. The solid solubility of N in silicon at the melting point lies in the range of $4.5\text{--}10 \times 10^{15}$ atoms/ cm^3 , dependent on the practical crystal growth rate. Consequently, the equilibrium segregation coefficient of N between solid and liquid silicon is quite small, which can be determined as 7×10^{-4} [3].

The N or N-related complexes in silicon can be characterized by various techniques, including charged particle activation analysis (CPAA) [4], deep level transient spectroscopy (DLTS) [5], Rutherford backscattering spectrometry (RBS), Auger electron spectroscopy (AES), electron paramagnetic resonance (EPR), luminescence and electrical resistivity [6,7]. They were sufficient for the early N ion-implantation investigations, but most of them could not reach the sensitivities required to measure a low concentration of N in co-doped CZ Si as low as 10^{15} cm^{-3} . Efforts have been concentrated around Fourier transformed infrared (FTIR) absorption and secondary ion mass spectroscopy (SIMS). SIMS can measure the total N concentration, independent of its chemical states, but the detection limit is around $1 \times 10^{14} \text{ cm}^{-3}$ for the specialized instruments, limited by the background N concentration [8]. The N content can be also measured by IR absorption measurements via the presence of N-related vibration modes. The N is known to exhibit an IR absorption peak at 963 cm^{-1} [4], with a calibration coefficient of $1.83 \times 10^{17} \text{ cm}^{-2}$, which has been assigned to the N dimer [9,10]. Another N dimer line is reported at 766 cm^{-1} , with a calibration coefficient of $4.45 \times 10^{17} \text{ cm}^{-2}$ [11]. However, a fraction of N atoms have formed complexes with oxygen impurities in CZ silicon. In that case, FTIR cannot estimate the total N concentration correctly [4]. Recently, various detection limits of N concentration by FTIR method have been reported, i.e., Nakatsu et al. [12] ($9 \times 10^{13} \text{ cm}^{-3}$), Ono and Horikawa [13] ($3 \times 10^{13} \text{ cm}^{-3}$), and Porrini et al. [14] ($5 \times 10^{13} \text{ cm}^{-3}$). However, an accurate method to calibrate the absorption into an absolute concentration is not yet established by now.

The diffusivity of N in silicon is still a puzzle, despite of more than 40 years' investigation. Generally, there exist several N species in CZ silicon crystals, including electrically active N-related complexes, N dimers, and other possible configurations of monomer N [15]. Numerical simulations indicate that the N monomer has a migration activation energy of 0.4 eV [16,17], while the N dimer has a much larger migration activation energy of 2.5 eV [18–20], which is assumed to be practically immobile. The experimental measurements of the N diffusivity in silicon are limited to its relatively low concentration and the detective techniques. The first measurement of N diffusion coefficient attempted by Clark et al. was based on Hall effect [21]. After implanting N^{14+} ions to form an n-type surface layer in the high resistive p-type silicon, the evolution of the p–n junction depth

with the anneal temperature and time reflects the N¹⁴⁺ diffusion behavior. Then, the N diffusion coefficient can be expressed as

$$D = 0.87 \exp\left(-\frac{3.29 \text{ eV}}{kT}\right) (\text{cm}^2/\text{s}) \quad (2-1)$$

where k is the Boltzmann constant and T the absolute temperature. Unfortunately, this equation is not reliable for the substitutional N. Next, Denisova et al. tried to anneal a p-type high resistive silicon sample in the N₂ ambient in the temperature range 700–1200 °C [22]. After irradiating the samples followed by a further 800 °C anneal, an inversion layer associated with the N diffusion layer is formed. By measuring the evolution of p-n junction depth, the diffusivity of N in silicon can be deduced as follows

$$D = 0.03 \exp\left(-\frac{2.63 \text{ eV}}{kT}\right) (\text{cm}^2/\text{s}) \quad (2-2)$$

However, it should be mentioned that the high-temperature anneal above 800 °C usually results in the formation of a SiO₂ or Si₃N₄ film which inhibits the N diffusion, so the equation above has some error at the temperature above 800 °C.

The profiles of out-diffused N in silicon measured by SIMS technique [23], are now widely considered to be the most reliable. Based on the error function simulation, the N diffusivity can be expressed as:

$$D = 2700 \exp\left(-\frac{2.8 \text{ eV}}{kT}\right) (\text{cm}^2/\text{s}) \quad (2-3)$$

Moreover, it was found that the total amount of out-diffused N corresponds with the variation of IR absorption at the N dimer band. This indicates that the N impurities in silicon diffuse as the form of dimers. However, further experiments suggest that the diffusivity of N in silicon is more complicated. Hockett [24] suggested that N dimers may not be the only species responsible for transport, since a small fraction of N diffused rapidly whilst the majority remained immobile. Recently, Mannino et al. found that N diffusion can be enhanced in CZ silicon, due to the existence of oxygen [25]. Voronkov and Falster proposed a dissociative mechanism to explain the N diffusion in silicon [26], in which N transport proceeds via dissociation of the practically immobile dimers into mobile monomers by oxygen catalyzing. The monomer diffusivity obtained by this dissociative model is shown below

$$D = 0.25 \exp\left(-\frac{1.25 \text{ eV}}{kT}\right) (\text{cm}^2/\text{s}). \quad (2-4)$$

2.1.2. Germanium

Ge, as one of the isovalent elements with silicon, usually occupies substitutional sites in the silicon lattice. Due to its larger radius, Ge can cause a volume expansion ($\Delta V/V_{\text{Si}}$) of ~4%. It is completely miscible with silicon to form GeSi alloy with any ratio. The Ge concentration in silicon can be accessible by SIMS, inductively coupled plasma mass spectroscopy (ICP-MS), RBS, energy dispersive X-ray spectrometry (EDX), FTIR and so on. Among them, the ICP-MS is often used, with a typical detect limitation of 10–100 atoms per trillion. Since Ge forms bonds with silicon in the lattice, they can cause an absorption band of 710 cm⁻¹ in the infrared absorption spectrum at room temperature [27]. The Ge concentration in CZ silicon can be calculated by the following formula

$$[\text{Ge}] = k \times 10^{20} \alpha_{\max} W_{1/2} (\text{}/\text{cm}^3) \quad (2-5)$$

where $k = 1.211$ is the conversion factor, α_{\max} the absorption coefficient and $W_{1/2}$ the band width of half maximum (BWHM) [28].

The segregation of Ge in silicon has been investigated for many years, but the results are not consistent because of different

calculating methods. Thurmond firstly reported that the segregation coefficient of Ge is 0.33 [29], obtained from crystal pulling experiments and an analysis of the Ge–Si phase diagram. However, the evaluation of Ge concentration in the silicon melt was difficult in their experiment, which causes a big error in the value of the segregation coefficient. Later on, Rea et al. acquired an effective segregation coefficient of 0.68 by designing an experiment to avoid this error [30]. Zhang et al. further clarified that the effective segregation coefficient of Ge in silicon is 0.69, and the equilibrium segregation coefficient is 0.63 [31]. The Ge equilibrium segregation coefficient has been modified into 0.62 by Niu et al. [32]. Recently the research group from Zhejiang University has grown a series of Ge doped CZ (GCZ) silicon crystals with the Ge concentrations ranging from 10¹⁶ to 10²⁰/cm³. Based on both the experimental results and theoretical calculations, they obtained an effective segregation coefficient of 0.56 for the Ge in silicon, and the equilibrium segregation coefficient should be 0.5 [33]. Nevertheless, even though the accurate segregation coefficient of Ge is still controversial, it is no doubt that this value must be smaller than 1.0. Thus, the Ge concentration increases along the CZ silicon crystal axis from seed-end to tail-end.

The Ge diffusion in silicon was first investigated by radioactive tracer experiments, in which the isotope ⁷¹Ge with a half-life of 11 days was utilized [34]. Petrov et al. [35] acquired the diffusion coefficient of Ge in the temperature range of 1150–1350 °C as follows

$$D = 6.26 \times 10^5 \exp\left(-\frac{5.28 \text{ eV}}{kT}\right) (\text{cm}^2/\text{s}) \quad (2-6)$$

However, McVay and DuCharme [34] reported a different result by the same method as shown below

$$D = 1.54 \times 10^3 \exp\left(-\frac{4.7 \pm 0.2 \text{ eV}}{kT}\right) (\text{cm}^2/\text{s}) \quad (2-7)$$

By combining the SIMS measurements and the fitting of the Ge diffusion profiles with a complementary error function, Ogino et al. obtained the Ge diffusion coefficient as follows [36]

$$D = 7.55 \times 10^3 \exp\left(-\frac{5.08 \text{ eV}}{kT}\right) (\text{cm}^2/\text{s}) \quad (2-8)$$

Later on, Pichler [37] claimed that the Ge diffusion coefficient in silicon should be expressed as

$$D = 1.72 \times 10^3 \exp\left(-\frac{4.830 \text{ eV}}{kT}\right) (\text{cm}^2/\text{s}) \quad (2-9)$$

Hettich et al. have investigated the behaviors of Ge diffusion in an extended temperature range [38]. They reported a non-Arrhenius behavior of Ge diffusivity with a kink at the temperature of 1050 °C. Therefore, the characteristics of Ge diffusion in silicon could be separated into regimes, i.e., a high-temperature regime (1100–1300 °C) with the activation energy of 5.3 eV and a low-temperature regime (850–1000 °C) with the significantly lower activation energy of 4.1 eV. This kink point has also been verified by Dorner et al. [39] and Bouchetout et al. [40]. It is attributed to the evolution in the mechanism of Ge diffusion at different temperature ranges. The impurity diffusion in silicon is generally based on either interstitial or vacancy mechanisms. The temperature dependence of Ge diffusion in silicon is related to a change from an interstitial mechanism at high temperatures to a vacancy mechanism at low temperatures. Fahey et al. [41] investigated the effect of vacancy and interstitial injection on the Ge diffusion in silicon. They estimated that under the 1050 °C equilibrium conditions, 30–40% Ge atoms diffuse by an interstitial-assisted mechanism and the other 60–70% by a vacancy

mechanism if assuming vacancy-interstitial interchange to take place by a kick-out reaction.

2.1.3. Carbon

C is generally incorporated into the silicon melt via CO or CO₂ vapor phase transport. In modern CZ silicon, C is usually in the order of 10¹⁶ cm⁻³, below the detection limit of FTIR measurement. The situation is very different in the case of intentional C co-doping, where the average C concentration could be in the order of 10¹⁷ cm⁻³. The equilibrium solubility of C in liquid silicon is 4 × 10¹⁸ cm⁻³, while that in solid silicon is 3.5 × 10¹⁷ cm⁻³ at the melting point [42,43]. The solid solubility of C in silicon (C_{carbon}) as a function of temperatures can be expressed as [44]

$$C_{\text{carbon}} = 4 \times 10^{24} \exp\left(-\frac{2.4 \text{ eV}}{kT}\right) (\text{cm}^3) \quad (2-10)$$

It has been reported that the existence of oxygen can increase the maximum solubility of C, which can reach to ~10¹⁸ cm⁻³ in an oxygen-rich silicon crystal. The segregation coefficient of C in silicon have clarified to be 0.07 by various experiments [42], which is much smaller than 1.

The C concentration in CZ silicon can be characterized by the FTIR technique. The IR absorption related to the localized vibration mode of isolated C is at 605 cm⁻¹ [45]. It is well explained by models taking into account lattice distortion by the small C atoms. Unfortunately, this 605 cm⁻¹ line is superimposed on the strongly and rapidly varying intrinsic two-phonon absorption bands, limiting the sensitivity of this technique to a low-C concentration. In order to increase the measurement sensitivity, the Si sample is required to have a thickness of larger than 2 mm, with double surfaces being mirror-like polished to reduce the light scattering. The FWHM of the absorption peak should be about 6 cm⁻¹. The intensity of the 605 cm⁻¹ line is proportional to the substitutional C concentration and the conversion equation for the absorption coefficient (α) into the C concentration is shown by [46]

$$C_{\text{carbon}} = 1 \times 10^{17} \alpha (\text{cm}^3) \quad (2-11)$$

Prolonged anneal generally leads to the reduction in the intensity of the 605 cm⁻¹ band, whether at high or low temperatures. The reason is the formation of SiC precipitates at high temperatures, or the formation of C-related complexes with other impurities like oxygen at lower temperatures.

The diffusion coefficient of C (D_c) in CZ silicon is first investigated by Newman and Wakefield [47] based on a radio-tracer technique of ¹⁴C. By diffusing the ¹⁴C source into a CZ silicon sample, the C concentrations in the successive layers after grinding were measured. The diffusion coefficient of C can be obtained by [47]

$$D_c = 1.9 \exp\left(-\frac{3.1 \pm 0.2 \text{ eV}}{kT}\right) (\text{cm}^2/\text{s}) \quad (2-12)$$

Rollert et al. carried out similar experiments and obtained the values of D_c consistent with those reported by Newman et al., as shown by [48]

$$D_c = 0.95 \exp\left(-\frac{3.04 \pm 0.05 \text{ eV}}{kT}\right) (\text{cm}^2/\text{s}) \quad (2-13)$$

Since most of C atoms are at the substitutional sites of silicon lattice, its diffusion rate in silicon can be modified by point defects, such as excess vacancies and self-interstitials [49,50]. If self-interstitials prevail, the enhancement of C diffusivity has been observed by SIMS technique. This enhancement results from the interaction between substitutional C and self-interstitials. Substitutional C atoms can be ejected into the silicon lattice as interstitials when they capture the self-interstitials. However, under the vacancy-rich conditions, the C diffusivity would

become smaller, due to the decrease of self-interstitials. Ladd et al. performed three different kinds of ambient for the experiments of C diffusion in silicon, namely nitrogen, oxygen and POCl₃ ambient [50]. They found the diffusivities of C in oxygen and phosphorus ambient are 3 or 40 times larger than that in N₂. The reason is that the silicon oxide formation in the oxygen and phosphorus ambient is a process of injecting self-interstitials from the surface into the bulk, while the silicon nitride formation in N₂ ambient is a process of injecting vacancies [50]. Different from substitutional C, interstitial C is highly mobile. It is generally located at a split-interstitial where a C and a silicon atom share a lattice site and are aligned along one of the three <0 0 1> directions. If the interstitial C is charged, the electron paramagnetic resonance (EPR) spectra technique can also be used to measure the diffusivity of interstitial C. By combining the IR and EPR measurement, the diffusion coefficient of interstitial C has been obtained as follows [51]

$$D_{ci} = 0.44 \exp\left(-\frac{0.87 \text{ eV}}{kT}\right) (\text{cm}^2/\text{s}) \quad (2-14)$$

The diffusion activation energy of interstitial C in silicon was further modified to be 0.86 eV by Chappell et al. [52].

2.2. Co-doping technology

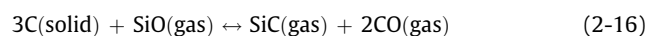
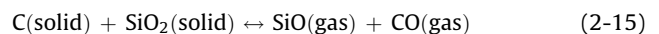
2.2.1. Gas doping

In the history of silicon crystal growth, N₂ gas was once considered to be unsuitable for the protective gas. Kaiser and Thurmond [53] reported that in floating-zone (FZ) silicon crystal growth, N would react with the silicon severely under an atmosphere, which induces the formation of Si₃N₄ precipitates and therefore inhibits the growth of single crystal. Upon lowering the pressure, a glow discharge would happen, induced by the RF field used to heat the silicon, and then the surface of silicon melt is covered with Si₃N₄ needles within a few seconds [53].

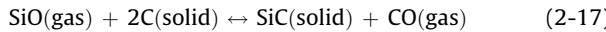
N doping in CZ silicon using gas source was first introduced by Que et al. [54–56]. They used N₂ or N₂/Ar mixture under reduced pressure as the protective gas for crystal growth and successfully obtained N-doped CZ (NCZ) silicon crystals. The protective N₂ atmosphere should have a purity of higher than 99.9995%. To ensure the efficient elimination of SiO above the melt, the N₂ gas flow rate should be controlled at a relatively high speed. With the decrease of N₂ pressure, the chemical reaction of N₂ with the molten silicon becomes weak, and therefore the final N concentration in silicon crystals is controllable. The N concentration in the tail-end of crystals is usually less than 5 × 10¹⁵ atom/cm³. When the N₂ pressure is controlled well, silicon crystal growth could not be disturbed by silicon nitride and a high yield of dislocation-free and swirl-free single crystal is obtained. The N concentration mostly depends upon the pressure and flow rate during melting of polycrystalline charge instead of the pressure during the period of crystal growth. Using N₂ as the protective atmosphere under reduced pressure could be a cost-effective method for NCZ silicon crystal growth.

C doping in silicon can occur from CO absorption by silicon melt during CZ silicon crystal growth. Thermo-chemical reactions that are likely to occur in crystal puller equipments, to produce CO, are understood as follows [57]

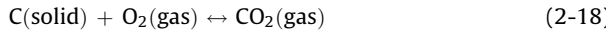
(a) Reactions between silica crucibles and graphite holders:



(b) Reactions between SiO and graphite:



(c) Reactions between graphite and oxygen:



Since the C vapor pressure is extremely low, it is admitted that, once a CO molecule is trapped by the melt, C will stay and become incorporated later on solid silicon according to the freezing segregation law.

It should be noticed that uncontrolled CO generation may give rise to silicon carbide production via the following reaction



Solid silicon carbide particles, if produced by reaction between the silicon melt and the C monoxide over the melt, can be driven by the melt flow towards the freezing interface. Due to the presence of these particles, an interface breakdown usually occurs, followed by the formation of polycrystalline grains. Thus, the formation of silicon carbide must be avoided for the growth of CZ silicon single crystals. Schmid and Khattak [58] have reported that the replacement of graphite retainer with molybdenum, which could eliminate the contact of graphite with the silica crucible, would depress the major source of CO originating and therefore reduce the possibility of the formation of silicon carbide.

For the growth of silicon crystals with high-C concentration, Carle et al. [57] proposed some improvements to pulling processes and equipments, which can also avoid the formation of polycrystalline silicon grains at the melt interface. In their preferred embodiment, where conventional pullers are employed, the seals at the rotating shaft apertures are removed and the oxygen partial pressure is enhanced during a short and controlled time by creating a pressure depression. This depression may be indirectly caused by different Ar flow settings to control oxygen leakage from ambient. As the Ar flow is of prime incidence on oxygen and carbon content in the crystal, high-C content crystals can be produced. Moreover, the desired and reproducible amounts of C in silicon crystals can be obtained through continuously recording the monitoring of CO concentration in the puller atmosphere during crystal pulling.

2.2.2. Solid doping

For solid doping of N into silicon, silicon nitride powders are often used. The most important parameters of the powders may be purity and size. The purity of powders should be better than 1 ppm. The powder size is associated with the time required for its complete dissolution into the molten silicon. If the powder does not completely dissolve, it may result in the generation of dislocations and even grain boundaries in the silicon ingot [59]. The N-containing powder may be added to the crucible prior to any heating of the polycrystalline silicon material or added during the melting of the poly-silicon nuggets. The silicon nitride can also be coated on the inner walls of crucibles. During the melting process, the coated silicon nitride can gradually dissolve into the silicon melt and this dissolution even continues during the whole pulling process. This makes it difficult to derive how much silicon nitride has entered into the melt and consequently the resultant N concentration in silicon. So, this technique is usually combined with empirical experience.

Since the dopants such as III/V Group elements, including boron, phosphorus, antimony and arsenic, should be added into the melt in order to achieve the p/n conduction type of silicon. These dopants can be introduced through currently known methods. Here especially mentioned is boron-doped p-type silicon. A boron

nitride (BN) powder can be used for not only the N source but also the III Group dopant source. But, as the amount of boron and N equals each other in stoichiometric ratio, this method is only applicable for lightly boron-doped silicon. In addition, BN is even more refractory than silicon nitride at the melt point of silicon so that the powder size should be further reduced to guarantee the complete dissolution of BN in the melt silicon, and meanwhile the duration time of the melting process should be prolonged.

The doping of Ge in silicon is based on the addition of either high purity Ge raw material or the high purity SiGe alloy. Unlike the solid source for C and N doping, high purity Ge-containing dopants are very easy to fabricate, and they are not required to have uniform and small size. Ge-containing solid source cannot be powder-like because Ge or SiGe alloy is very easily oxidized. According to the Si–Ge binary phase diagram, Ge has unlimited solubility in silicon melt and a melting point lower than Si. In this sense, if high purity Ge is applied as the doping source, it will completely melt when silicon raw materials are all solid, and after the complete transformation from solid silicon to molten Si, Ge can completely dissolve in silicon solvent, where there will be few small un-molten Ge particles that may cause imperfection of silicon lattices. As for SiGe, the melting mechanism is the same as for pure Ge so that it should play the same role in the crystal growth process of Ge particle-doped CZ (GCZ) silicon.

The solid C doping source is safer, more convenient and economical than the gaseous source C monoxide. The criteria for selecting the appropriate C dopant are two factors, i.e., purity and facility of dissolving in silicon melt. The typical C dopant can be high purity C or silicon carbide and the form of the solid source can be various. Most common is in the form of powder. Like silicon nitride, silicon carbide has a melting point higher than 1700 °C and C is more difficult to melt below 3000 °C and also it can hardly become alloy with silicon in the silicon melt. These properties make C or silicon carbide very slowly dissolve in the silicon melt. In the case that the C or silicon carbide powder is unable to dissolve, there is a large quantity of small C or silicon carbide particles in the melt. The consequence will be so terrible that dislocations and grain boundaries can stem from the sites where the small particles stay, the same as that occurs for the silicon nitride particle case. The other approach is the employment of stick-like C source, which is dependent on the erosion of C or silicon carbide stick by the revolutionary melt flux. This method comprises soaking a C-containing stick of a predetermined shape with silicon melt to elute C in the surface layer part of sticks, whereby C is doped so that the C concentration in the melt becomes the target value. By using this method, the eluted amount of C from the C-containing stick into the melt can be precisely controlled and good reproducibility can be guaranteed.

3. Complexes of co-dopants with point defects

Nitrogen, germanium and carbon usually can interact with point defects in silicon, and then influence the formation of defects. Firstly, all these co-dopants can interact with the oxygen impurity to form oxygen-related complex. The nitrogen–oxygen complexes are electrically active, which act as the shallow thermal donors in silicon. They will change the carrier concentration in silicon, e.g. compensating the hole concentration in p-type silicon, and increasing the electron concentration in n-type silicon. A number of experiments have clarified that nitrogen–oxygen, carbon–oxygen and germanium–oxygen complexes can become the nuclei of oxygen precipitates at low temperature. In addition, these co-dopants can also interact with vacancy to form vacancy-related complexes. This will change the concentration of free vacancies and therefore tailor the formation of vacancy-related defects. Furthermore, these vacancy-related complexes can also further

interact with oxygen and then become the nuclei of oxygen precipitates in silicon at high temperature. This section will be focused on the formation process, mechanism and fundamental properties of these complexes in silicon crystal.

3.1. N-related complexes

N plays an important role in modifying the properties of CZ silicon crystals. Silicon wafers with larger diameter for microelectronic application and wafers with thinner thickness for photovoltaic application benefit from the strength hardening due to N doping, originated from the dislocation locking effect [60]. N also enhances oxygen precipitation by interacting with oxygen atoms [9], and reduces vacancy and interstitial related defects such as voids and A-swirl [61,62], respectively. All these behaviors relate to the fact that N in silicon inclines to interact with intrinsic point defects such as vacancies and silicon self-interstitials, modifying the early stage of point defect clustering dynamics, and interact with light impurities. Nitrogen in silicon prevails in the form of N–N pair, forming a four-member ring with the adjacent silicon. Furthermore, N–O complexes form unavoidably in CZ silicon. On one hand, a family of electrically active NO_x ($x = 1, 2, 3, \dots$) defects as the shallow thermal donors (STDs) exist. On the other hand, $\text{N}_2\text{O}_x\text{V}_y$ ($x = 1, 2; y = 1, 2$) defects build up as the derivative of N–N by the agglomeration of interstitial oxygen and vacancies. These complexes are believed to strongly control the formation of oxygen precipitates and voids in NCZ silicon.

Several STDs induced by NO_x complexes were firstly reported by Suezawa et al. [63,64]. A typical FTIR spectrum of STDs is shown in Fig. 1 [65]. Three series of bands of the $1s-2p_0$, $1s-2p_{\pm}$, $1s-3p_{\pm}$ transition can be detected in the range of $190-270 \text{ cm}^{-1}$. In each bands, eight different species were recognized, generally labeled as $\text{N}-\text{O}-x$ ($x = 1, 2, 3, \dots$) in Table 1. Among them, the species from $\text{N}-\text{O}-1$ to $\text{N}-\text{O}-6$ were assigned by Suezawa et al. [64] and the other two ($\text{N}-\text{O}-6'$ and $\text{N}-\text{O}-8$) were found by Wagner et al. [66]. Several ionization energies of the STDs have been estimated, as shown in Table 2 [65]. There are good agreements between the observed transition energies and the results of the effective mass approximation calculated for the STD states in silicon.

The absorption coefficients of all four transitions ($\text{N}-\text{O}-1$, $\text{N}-\text{O}-2$, $\text{N}-\text{O}-3$, $\text{N}-\text{O}-5$) exhibit an increase with the N content, which can be described by square root dependence [67,68]. According to the mass-action law for the reaction $n\text{N} + m\text{O} \rightarrow \text{N}_n\text{O}_m$, it leads to the

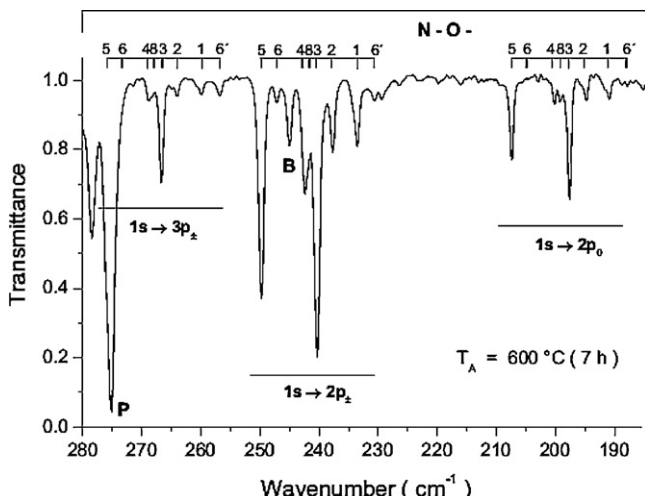


Fig. 1. FTIR spectrum of STD defects [65], in which three series of bands of the $1s-2p_0$, $1s-2p_{\pm}$, $1s-3p_{\pm}$ transition can be seen in the range of $190-270 \text{ cm}^{-1}$ related to N–O related shallow donors.

Table 1

The peak positions of STD transition measured at 8 K [66].

STD species	$1s-2p_0 (\text{cm}^{-1})$	$1s-2p_{\pm} (\text{cm}^{-1})$	$1s-3p_{\pm} (\text{cm}^{-1})$
N-O-1	190.8	233.8	260.1
N-O-2	194.9	237.8	264.2
N-O-3	197.7	240.4	266.8
N-O-4	200.2	242.5	269.0
N-O-5	207.4	249.8	276.4
N-O-6	204.4	247.0	274.2
N-O-6'	187.9	230.6	256.9
N-O-8	199.1	241.5	268.2

Table 2

Ionization energies of the shallow donors [66].

Donor	Ionization energy (meV)
Groups I, II and III	
1	35.38
2	35.90
3	36.21
4	36.45
5	37.38

integrated absorption values equal to $[N]^n[O_i]^m$. The N predominantly exists in the N_2 form, and the concentrations of interstitial N atoms [N_i] can be expressed as $[\text{N}_i] \approx (\rho N/2)^{1/2} \exp(-E/2kT)$, where ρ is the lattice site density. Note that the square root dependence is obtained in the expression. This coincidence shows that the STDs should involve only one N atom. The oxygen concentration dependence of the STDs had been investigated by Wagner et al. [66,69]. The chemical compositions of the electrically active N–O complexes in silicon were determined in a specially doped ingot with variable oxygen concentrations and a fixed N concentration by FTIR technique. The result shows that the $\text{N}-\text{O}-5$, with its absorption at 249.8 cm^{-1} in $1s \rightarrow 2p_{\pm}$ transition, has a linear dependency, proving $\text{N}-\text{O}-5$ to be NO ($m = 1$). The other two species of $\text{N}-\text{O}-4$ (242.5 cm^{-1}) and $\text{N}-\text{O}-6'$ (256.9 cm^{-1}) also show the linearity between $[\text{NO}_m]$ and $[\text{O}_i]$, therefore they have the same NO stoichiometry. $\text{N}-\text{O}-3$ with its transitions $1s \rightarrow 2p_{\pm}$ at 240.4 cm^{-1} has a square dependence on $[\text{O}_i]$, indicating that it has a NO_2 composition. The power dependency $m = 3$ of the complexes $\text{N}-\text{O}-1$ (233.8 cm^{-1}), $\text{N}-\text{O}-2$ (237.8 cm^{-1}), and $\text{N}-\text{O}-8$ (241.5 cm^{-1}) identify these STDs as the NO_3 defects. However, the composition of $\text{N}-\text{O}-6$ still remains unknown.

Qi et al. studied the local vibration models (LVMs) of NO_x complexes in the middle range IR (MIR) spectra [70]. Strong absorption bands occur at 963 and 766 cm^{-1} , which have been assigned to N_2 pairs. Three additional bands at 1026 , 996 , and 801 cm^{-1} were exclusively observed in CZ silicon, related to NO_x complexes. Jones et al. studied the isotopic effects on these LVMs in CZ silicon [71]. All the modes shift with ^{15}N , showing N atoms to be involved in the complex. These absorption bands were also observed by Wagner et al. [11]. Especially the absorption intensity of 801 cm^{-1} has a linear dependence on the product of $[\text{N}][\text{O}_i]$, indicating that these bands arise from the NO complex. Fujita et al. calculated the atomic structures, binding energies and LVMs of the NO and NO_2 complexes [72]. They predicted three LVMs at 1001 , 801 , and 722 cm^{-1} related to NO complexes. The LVMs including different isotope substitutions of N and O are presented in Table 3.

Table 3

Local vibrational modes of the N–Oxygen (NO) defects in silicon [73].

$^{14}\text{N}^{16}\text{O}$	$^{15}\text{N}^{16}\text{O}$	$^{14}\text{N}^{18}\text{O}$
1001	974	999
801	783	800
722	721	690

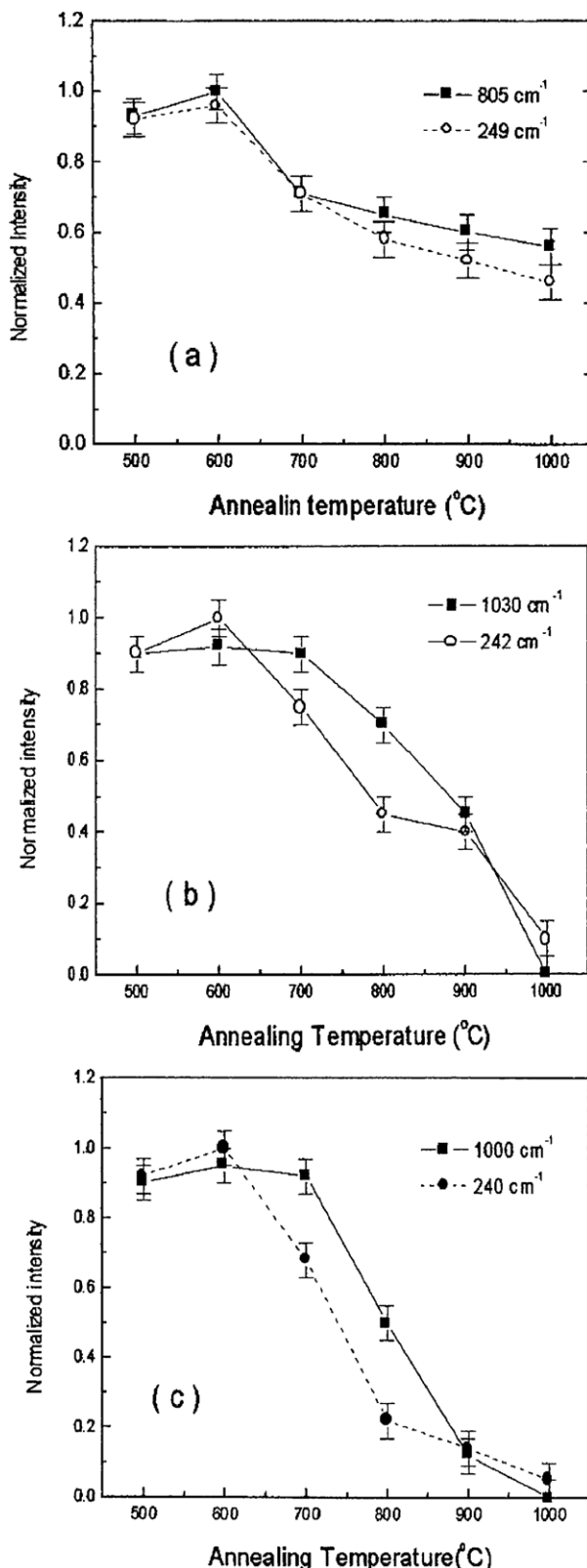


Fig. 2. The intensity of the optical absorption lines at different wavenumbers in the NCZ silicon annealed for 10 min [73]. (a) The normalized intensity of the line at 805 cm^{-1} and at 249 cm^{-1} at different temperatures; (b) the normalized intensity of the line at 1030 cm^{-1} and 242 cm^{-1} at different temperatures; (c) the normalized intensity of the line at 1000 cm^{-1} and 240 cm^{-1} at different temperatures.

Table 4

Local vibrational modes of the two lowest energy configurations of the N-oxygen-pair (NO_2) defect, including isotope substitutions of the involved defect atoms [66].

N-O-O	$^{14}\text{N}^{16}\text{O}^{16}\text{O}$	$^{14}\text{N}^{16}\text{O}^{18}\text{O}$	$^{14}\text{N}^{18}\text{O}^{16}\text{O}$	$^{14}\text{N}^{18}\text{O}^{18}\text{O}$	$^{15}\text{N}^{16}\text{O}^{16}\text{O}$
1022 (N)	1022 (N)	1018 (N)	1018 (N)	996 (N)	
977 (O2)	934 (O2)	976 (O2)	933 (O2)	976 (O2)	
812 (N,O1)	812 (N,O1)	805 (N)	805 (N)	805 (O1,N)	
794 (N,O1)	793 (O1,N)	766 (O1)	765 (O1)	781 (N)	
670 (O2)	661 (O2)	667 (O2)	657 (O2)	670 (O2)	
O-N-O	$^{16}\text{N}^{14}\text{O}^{16}\text{O}$	$^{16}\text{N}^{14}\text{O}^{18}\text{O}$	$^{18}\text{N}^{14}\text{O}^{16}\text{O}$	$^{18}\text{N}^{14}\text{O}^{18}\text{O}$	$^{16}\text{N}^{15}\text{O}^{16}\text{O}$
1084 (N)	1083 (N)	1082 (N)	1081 (N)	1054 (N)	
970 (O2)	929 (O2)	970 (O2)	928 (O2)	969 (O2)	
856 (N)	855 (N)	856 (N)	855 (N)	836 (N)	
751 (O1)	751 (O1)	716 (O1)	716 (O1)	750 (O1)	
658 (O2)	649 (O2)	658 (O2)	649 (O2)	658 (O2)	

Yang et al. studied the LVMs at 1030 , 1000 and 805 cm^{-1} after annealing in the temperature range of 450 – $1150\text{ }^\circ\text{C}$ [73]. Fig. 2(a) shows the normalized intensity of the lines at 805 cm^{-1} and at 249 cm^{-1} during different temperature annealing. The intensity variation of the 805 cm^{-1} line was the same as that of 249 cm^{-1} line, which is the transition absorption peak of N-O-5 having the N-O ring structure. Fig. 2(b) shows the normalized intensity of the 1030 cm^{-1} line following the decrease of transition absorption peak of N-O-4 at 242 cm^{-1} , which also corresponds to the N-O ring structure. So, the peaks at 805 and 1030 cm^{-1} are both attributed to the LVMs of N-O complex. The theoretical calculation has revealed the LVMs of both the NO_2 structures (O-N-O and N-O-O), as shown in Table 4 [66]. Two LVMs at 1070 and 860 cm^{-1} close to the calculated frequencies of 1084 and 856 cm^{-1} shown in Table 4 were found in the experiment. It suggests that the LVMs at 1070 and 860 cm^{-1} may arise from the NO_2 complex with O-N-O configuration. Experiments show that the 860 cm^{-1} line has a similar behavior to the 240 cm^{-1} , which is the $1s \rightarrow 2p_{\pm}$ transition of N-O-3. Also, the LVMs at 1070 and 1000 cm^{-1} have a correlation with 240 cm^{-1} , suggesting that the absorption bands at 1070 and 1000 cm^{-1} , together with the band at 860 cm^{-1} must be attributed to the LVMs of NO_2 complexes.

Jones et al. firstly proposed a planar O-N-O structure with a C_{2v} symmetry for NO_m complexes, in which a pair of over-coordinated O atoms binds with a substitutional N core atom [74]. Later on, Ewels et al. claimed that the substitutional N replacing by an interstitial N core atom in NO_2 is the most stable center [68]. The idea of a four-member N-O ring, which is very similar to the N_2 pair structure, replacing a N atom by one oxygen atom, as the core structure of a N-O complex came from Gali et al. [75], see the N-O ring in Fig. 3 [67]. Meanwhile, they suggested that the interstitial oxygen atoms can further be attracted to N-O cores to create the N-O shallow donor family [67]. It is easy to realize that the N-O complex with a four-member ring structure is a single donor. The trivalent oxygen can accommodate three electrons in bonds and

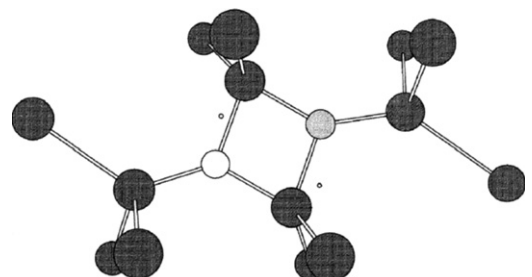


Fig. 3. The structure of NO complex with four-member ring. (Dark shaded circles: Si, light shaded circle: N, empty circle: O, the small circles represent the original lattice positions) [67].

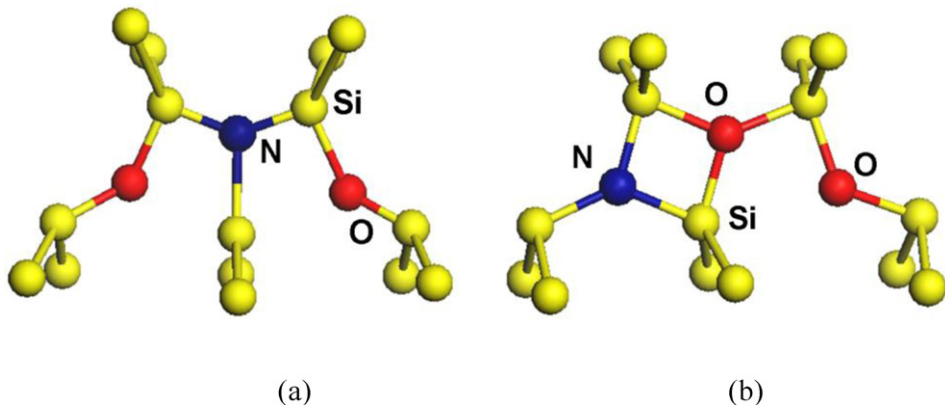


Fig. 4. Two possible structures for the NO_2 complex [69]. (a) C_{2v} symmetries; (b) C_{1h} symmetries.

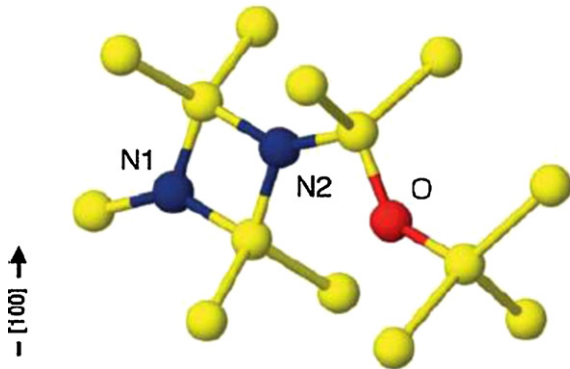


Fig. 5. The structure of N-pair-oxygen (N_2O) defect in silicon. The blue (dark grey) atoms correspond to N, whereas the red (grey) atom refers to oxygen [78].(For interpretation of the references to color in this figure legend, the reader is referred to the web version of the article.)

two more in a lone pair orbital perpendicular to those bonds. The sixth valence electron of oxygen will be excited to conduction band, acting as a donor species. However, the electron spin resonance (ESR) results [76] show that the STDs have a C_{2v} symmetry, which is in conflict with monoclinic N–O ring. There are two likely structures for the NO_2 defect which have C_{2v} and C_{1h} symmetries, respectively, depending on whether the second oxygen abuts N or the first O atom, shown in Fig. 4. Hara et al. suggested the O–N–O structure illustrated in Fig. 4(a), has C_{2v} symmetries [69]. On the contrary, the N–O–O was later found to be the minimum energy structure of the NO_2 complex, with a binding energy of 1.1–1.4 eV [77].

Fig. 5 shows the structure of a N_2O complex, in which the oxygen atoms are bound to the N_2 pair. The trapping of oxygen

atoms can be attributed to the strain field surrounding the N_2 pair. According to the calculated frequencies based on the structure of (NN)–O, the modes at 1016, 992, 870 and 749 cm^{-1} were found, seeming closed to the experimental modes at 1026, 996, and 801 cm^{-1} [78]. Also, the binding energy of 1.0–1.2 eV was obtained for the N_2O complexes by theoretical calculation, which was in agreement with the experimental value of 1 eV [60,79]. Another N–O configuration in CZ silicon is the N_2O_2 complex formed by a N_2O complex continuing to trap an interstitial oxygen atom. The infrared absorption bands at 1018 and 810 cm^{-1} were regarded as the LVMS of N_2O_2 complexes [80]. The N_2O_2 complex has two likely structures. Fig. 6 shows the NNOO structure with the second oxygen situated next to the first oxygen atom, and the ONNO structure with the second oxygen situated at a bond center site next to the N_2 pair. It was found that the ONNO structure is more stable, and the binding energy is 0.9 eV, which is a little larger than that of the NNOO structure [80].

Apart from the interaction between N and oxygen mentioned above, the coupling of N with the intrinsic point defects especially vacancies is also important. The existence of N-vacancy complexes was confirmed through positron annihilation spectroscopy by Adam et al. [81]. A deep level transient spectroscopy (DLTS) signal of $E_c - 0.42$ eV defect found in the NCZ silicon was also attributed to the formation of N-vacancy complexes [82]. So far, the vibration properties, the atomic structure and the formation energy of these N–V–O complexes in silicon have been intensively studied [83–88]. The local vibration modes at 551 and 653 cm^{-1} lines found in N-implanted FZ silicon were recently regarded as the vibration of VN_2 and V_2N_2 complexes [89]. Meanwhile, a 739 cm^{-1} line might be assigned to the $\text{V}_2\text{N}_2\text{O}$ or $\text{V}_2\text{N}_2\text{O}_2$ vibrations [85]. Fig. 7(a–c) shows the atomic structure of VN_2 , VN_2O and VN_2O_2 complexes, respectively, and (d–f) corresponds to the structure of V_2N_2 , $\text{V}_2\text{N}_2\text{O}$ and $\text{V}_2\text{N}_2\text{O}_2$ complexes, respectively [85]. As shown in Fig. 7(a), the

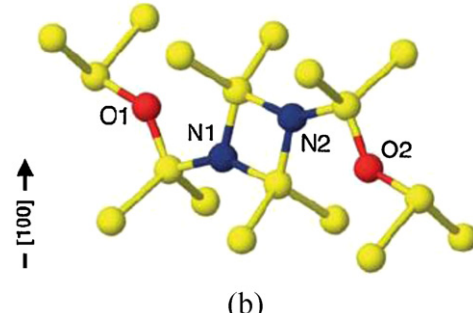


Fig. 6. The structure of N-pair-oxygen-pair (N_2O_2) defect in silicon. The blue (dark grey) atoms correspond to N, whereas the red (grey) atoms refer to oxygen. (a) The NNOO configuration. (b) The ONNO configuration [80].(For interpretation of the references to color in this figure legend, the reader is referred to the web version of the article.)

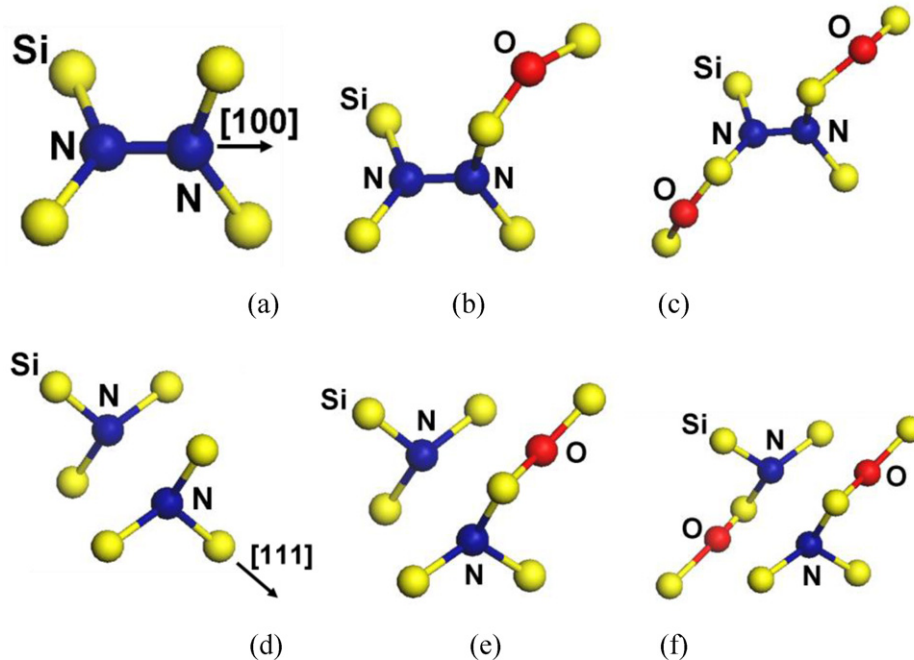


Fig. 7. The atomic structure of (a) VN_2 , (b) VN_2O , (c) VN_2O_2 , (d) V_2N_2 , (e) $\text{V}_2\text{N}_2\text{O}$ and (f) $\text{V}_2\text{N}_2\text{O}_2$ complexes [85].

neutral VN₂ complex is formed by inserting a N–N pair at a vacancy site in the center of a tetrahedron. The central bond of the N–N pair is aligned along <1 0 0> whereas the four N–Si bonds point to the summits of the tetrahedron, and lie in two perpendicular {1 1 0} planes which makes the symmetry group of VN₂ of D_{2d} type. The V₂N₂ complex is created by inserting two N atoms in the vacancy sites of a relaxed vacancy dimer, see Fig. 7(d). The V₂N₂ has a D_{3d} symmetry. The VN₂ and V₂N₂ could react with an interstitial oxygen atom to form a stable complex at high temperatures. There are various sites of the oxygen atom around the V₂N₂, shown in Fig. 8. The calculation result shows oxygen at B3 site has the lowest formation energy, followed by the B5 site and then B2 site [84,90]. The oxygen sites with the minimum energy around the VN₂ complexes also have similar results. The reason is that the VN₂, and V₂N₂ complexes exert a tensile strain on the surrounding lattice, expanding the first neighboring Si–Si bonds, especially the B3 bonds. And the oxygen atom at B3 site will move towards the empty space of N₂V₂, further reducing the energy. There are several equivalent sites to B3 and it could capture second oxygen atoms to form the V₂N₂O₂ complex, shown in Fig. 7(f), and capture more oxygen atoms to forming V₂N₂O_n complexes and act as the nuclei of oxygen precipitates.

Table 5 lists the formation energies of these $V_mN_2O_n$ complexes [90]. The formation energy for N_2 is about 3.95 eV at the ground state, showing that N_2 is a very stable complex. The formation energy of VN_2 complexes is about 0.21 eV when formed from N_i and N_s and is about 1.8 eV thus more stable, when formed from the coupling of N_2 with a silicon vacancy. Nevertheless, the small energy gain suggests that the VN_2 would easily be dissociated at a

Fig. 8. Considered sites of an O atom coupling to the N₂–V₂ complex. B1 is the bond center of the N–Si bond. B2, B3, B4, and B5 are the bond centers of the Si–Si bonds. I1 and I2 are the interstitial sites. Except for I1, the sites have several equivalent sites, but for simplicity they are not shown. The B3 site has 12 equivalent sites and some of them are indicated by B3' [84,90].

relatively high temperature. It will turn back to N_2 via reaction $VN_2 + I \rightarrow N_2$. Though, the VN_2 is a metastable complex, it is an active complex during crystal growth as it contributes to the formation of very stable V_2N_2 complexes. Seen from the table, the V_2N_2 complex reveals its high stability due to the large energy gain.

Likewise, the energy gain is about 0.70 and 0.95 eV for the V_2N_2O and $V_2N_2O_2$ complexes, respectively. In contrary, the quasi-chemical reaction forming the VN_2O complex is slightly exothermic with the formation energy of -0.15 eV, and when capturing an oxygen dimer, the formation energy becomes positive 0.51 eV. This indicates that the formation of VN_2O_2 complexes is unstable.

3.2. Ge-related complexes

Ge doping in CZ silicon can suppress the formation of TDs [91,92], improve the hardness against electron radiation [93], restrain the dislocation movement [94], suppress crystal originated particles (COPs) and enhance the oxygen precipitates for internal gettering [95]. These properties of GCZ silicon are strongly associated with the interaction of Ge with point defects. In the late 1980's, radiation-induced defects in GCZ silicon have been widely studied and it is found that Ge atoms tend to interact with vacancies to form Ge-V centers [96]. The Ge-V pair in CZ silicon has been studied by electron paramagnetic resonance (EPR) [97], IR [93] and deep level transient spectroscopy (DLTS) [98] techniques. The EPR measurements show the spectrum of a vacancy in GCZ silicon is roughly similar to that of an isolated vacancy (V) except in the hyperfine structure with several satellites [97]. Vacancies are trapped next to substitutional Ge. By selective illumination, charge states can be generated [97]. The electronic structure of GeV^+ and GeV^- were found to be slightly perturbed from that for V^+ and V^- in silicon crystal [97], and their distortions and level positions appear very similar to those for the isolated vacancy [98].

The binding energy of Ge-V is about ~ 0.27 eV [99]. The equilibrium concentration of vacancies in GCZ silicon with irradiation is significantly higher than that in the conventional CZ silicon [100]. The vacancies can be released from Ge atoms in the irradiated silicon by annealing [93,98,100]. Watkins [101] reported that the consequent release of vacancies could be observed as a growth in the $12\text{ }\mu\text{m}$ band when the vacancies in turn were trapped by oxygen atoms to form O-V (A-centers). Brelot and Charlemagne also studied the stability of Ge-V in n-type silicon containing 3×10^{20} Ge atoms/ cm^3 by IR technique [93]. There was no $12\text{ }\mu\text{m}$ absorption line related to V-O after a 90 K electron irradiation. The A-centers appear only after annealing between 200 and 280 K . This means that the Ge acts as an efficient trap for vacancies at low temperatures, and the trapped vacancies can be released from the Ge-V centers by thermal activation in the range of 200 – 280 K . The electrical levels of Ge-V pairs in GCZ silicon have not been directly measured. The dangling bond reconstructions reveal an only slightly perturbed vacancy, and its general behavior versus electrical properties such as Fermi level, optical excitation, appears identical to that of the isolated vacancy [102]. The DLTS results of the n-type Ge-Si alloy after electron radiation [98] show that the energy level of Ge-V complexes is about $E_c - 0.29$ eV, with a capture cross-section of $5 \times 10^{-16}\text{ cm}^2$ for electrons.

Chroneos et al. [99] found that the total energy of the configurations for the multi-vacancies involved GCZ silicon super-cells would follow the bond-length-related rules by first-principles simulation. Vacancies tend to bind with Ge atoms and relax the local lattice deformation stresses in silicon. Therefore, it seems that Ge atoms in CZ silicon crystals act as nuclei sites for Ge-V pairs [99]. In this way, it is therefore proposed that the vacancy could transfer to the surroundings of the generated Ge-V pairs with a probable routing of $\text{Ge} \rightarrow \text{GeV} \rightarrow \text{GeV}_2 \rightarrow \text{GeV}_3 \rightarrow \text{GeV}_m$ ($m = 4, 5, 6, \dots$) transformation. Using the law of mass action, the relative concentrations of defect clusters can be expressed as follows [99]

$$\frac{[\text{Ge}_m\text{V}_n]}{[\text{Ge}]^m[\text{V}]^n} = \exp\left(\frac{-E_b}{k_B T}\right) \quad (3-1)$$

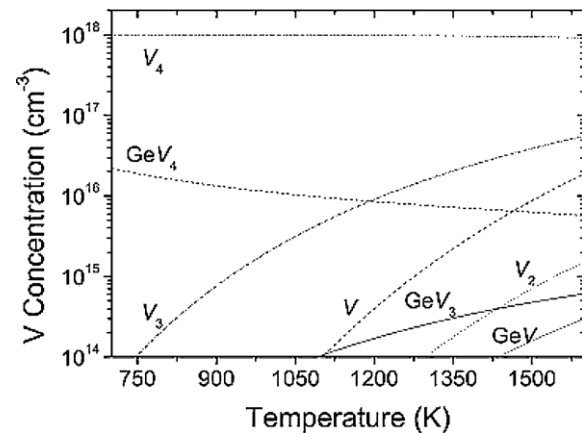


Fig. 9. The temperature dependence of the concentration of V_n clusters in comparison to the concentration of GeV_n clusters for a Ge concentration of 10^{19} cm^{-3} , an initial V super-saturation of 10^{18} cm^{-3} [99].

where E_b is the binding energy of the clusters, $[\text{Ge}_m\text{V}_n]$ the concentration of a Ge_mV_n cluster, $[\text{Ge}]$ the concentration of unbound Ge atoms, $[\text{V}]$ the concentration of unbound V, k_B Boltzmann's constant, and T the temperature. Fig. 9 shows the variation of the concentration of GeV_n clusters and V_n clusters with the temperature. $[\text{GeV}_n]$ is lower than $[\text{V}_n]$ at the whole temperature range. The binding energies of GeV_n clusters are higher than that of V_n clusters by a value of 0.35 eV. It indicates that Ge cannot act as a site to trap a significant proportion of vacancies.

Interstitial oxygen atoms can also be captured by Ge atoms to form stable Ge-O complexes, but the oxygen atom should be located at the third-nearest-neighbor site to the Ge atom [103,104]. The interstitial oxygen occupies the bridging positions between two silicon atoms forming the Si_2O molecule, which causes IR absorption bands at $30, 1100$ and 1200 cm^{-1} , and which benefit different LVMs of Si_2O quasi-molecule [105]. In heavily doped GCZ silicon, the oscillator strength of the 1200 cm^{-1} band absorption and the peak separations between the 1100 cm^{-1} band absorptions were largely reduced, which are attributed to the perturbation of Si-O-Si centers by the nearby Ge atoms [106]. Furthermore, three additional low-frequency IR absorption lines located at $1130, 1127$ and 1184 cm^{-1} was detected in GCZ silicon with a Ge concentration of $2 \times 10^{20}\text{ cm}^{-3}$ [107]. The shifted positions of other bands are ascribed to the weakened harmonic coupling between the rotational and asymmetric vibration modes of the Si-O-Si molecule [106]. For higher values of the Ge content, a broad, low-frequency band was found [108], attributed to the vibrations of the Si_2O units with several nearest-neighbor lattice sites occupied by Ge atoms. The observed absorption bands can be described as the vibration of interstitial oxygen disturbed by Ge atoms located in the nearest 2nd, 3rd and 4th coordination spheres relative to an oxygen atom [109], see Fig. 10.

Theoretical calculations also demonstrate the stability and the configurations of different possible Ge-O complexes in CZ silicon [103]. The oxygen atom is preferable to stay away from the Ge atom and most likely to form Si_2O molecules. However, these molecules may have Ge atoms in their neighborhood [110]. This is supported by the much lower formation enthalpy (-910.7 kJ/mol) of SiO_2 (α -quartz), than that (-580.0 kJ/mol) of GeO_2 (rutile) [111]. But, it is possible to form Si-O-Ge molecules [110]. Note that the effect of the Ge atoms on the geometry and vibration properties of the Si_2O molecules is not significant.

In order to relieve the lattice stress, Ge atoms incline to react with vacancies and interstitial oxygen to form related complexes [105]. VO defects containing a core Ge atom (one of the neighbors or next neighbors of the vacancy) are referred as GeVO complexes

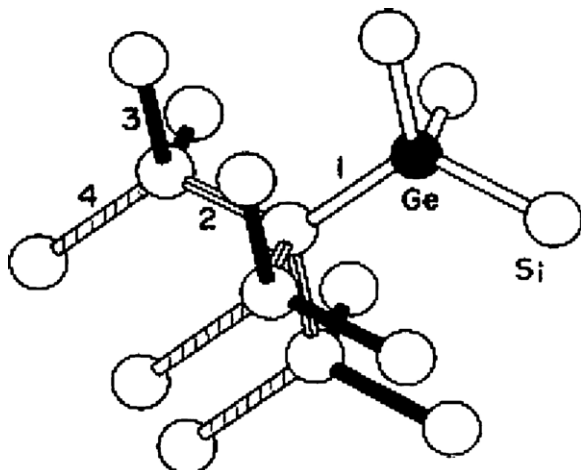


Fig. 10. Part of the silicon crystal lattice around the substitutional Ge atom, showing the first-, second-, third- and fourth-neighbor bonds to the Ge atom [109].

[113]. The following equation illustrates the formation of GeVO by the VO defect diffusing toward Ge [105,111].



The structure of VO in the $\text{Si}_{1-x}\text{Ge}_x$ crystals has been studied by DLTS and ab initio modeling. Fig. 11 shows the considered structures of the GeVO complex. The formation energy of GeVO at sites of b , a' and b' are 0.07, 0.19 and 0.09 eV, respectively, by ab initio modeling [111]. The binding energy of the deeper GeVO complex is found to be about 0.18 eV from the DLTS studies. From the FTIR measurements it is known that the 839.2 cm^{-1} band grows at the expense of the 834.6 cm^{-1} band, both of them lying above the main band of VO at 830 cm^{-1} [111]. Therefore, the 839.2 cm^{-1} band to $\text{VO}-\text{Ge}_{a'}$, and the 834.6 cm^{-1} band are assigned to $\text{VO}-\text{Ge}_b$ and/or $\text{VO}-\text{Ge}_b'$ defect forms. This assignment is also supported by the relative defect stability and respective electric levels. Most of stable GeVO complexes produce an acceptor state very close to that of VO, but $\text{VO}-\text{Ge}_{a'}$ has a deeper level, i.e., 20 meV deeper than VO (2/0). The acceptor state of GeVO is more localized than that of VO. Markevich et al. found from the DLTS studies at least three configurations of VO centers with distinct levels and the energy level shifted upward from the level of the dominant configuration in as-irradiated GCZ Si material. On isochronal annealing in the temperature range of 200–300 °C, the dominant VO defect transforms into another one whose level is about 25 meV deeper [111].

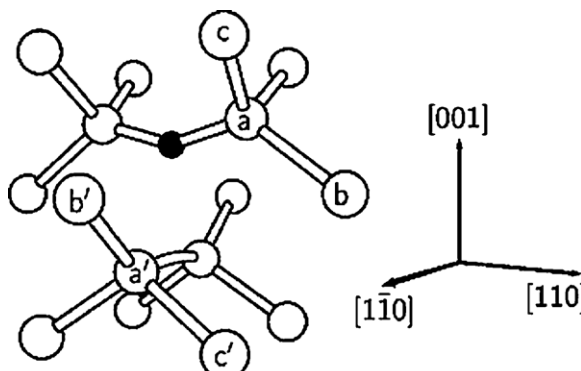


Fig. 11. The VO-Ge complexes considered here result from substituting 1st- or 2nd-neighboring silicon atoms by Ge. These structures are labeled with letters from a to c and $a'-c'$ [111].

Ge atoms in silicon can effectively compete with oxygen in trapping vacancies [103] and therefore a gradual increase in the concentration of VO defect is observed versus Ge content [112,113]. Taking into account a noticeable fraction of oxygen atoms with nearby Ge atoms in CZ silicon [114]. It is believed that such defects may be more effective traps for vacancies than isolated oxygen atoms due to a larger cross-section for vacancy capture [104,115]. After vacancy capture by Ge, the electronic properties and thermal stability of GeVO are expected to differ from those of the A-centers, and their annealing via vacancy dissociation gives rise to A-center formation [115]. During crystal growth, the concentration of free vacancies is higher prior to void formation, so the GeVO complexes are usually formed. These GeVO complexes can become the nuclei of oxygen precipitates by further trapping more oxygen atoms and then enhance oxygen precipitation at high temperatures.

3.3. Carbon-related complexes

Carbon can also interact with oxygen atoms, vacancies and self-interstitials, resulting in the formation of various complexes. It is known that the substitutional carbon (C_s) is an effective trap for self-interstitials. Therefore, the self-interstitial pushes out a carbon atom from a substitutional site and generates a highly mobile interstitial carbon in silicon. However, the interstitial carbon is mobile at room temperature, and then a series of reactions are triggered by them. One of them is the formation of the C_iO_i complexes, which was known as C3 centers [116]. If extra self-interstitials are available, the C_iO_i complex itself can become a trap for self-interstitials and lead to the formation of $Si_iC_iO_i$ (C4 center) [117]. The C_iO_i complex has been investigated by means of many methods in recent years, including EPR, DLTS, photoluminescence (PL) and FTIR. The C_iO_i complex, identified by EPR spectrum labeled as Si-G12 with spin $S = 1/2$ and C_{1h} symmetry, was first reported in 1964. A donor level at $E_v + 0.38 \text{ eV}$ observed by DLTS in C-rich CZ silicon has been assigned to C_iO_i complex [118], and the 790 meV C-line in PL spectrum is also ascribed to this defect [119,120]. The low-temperature FTIR measurement shows that the absorption bands at $1116.3, 865.9, 742.8, 588, 549.9, 529 \text{ cm}^{-1}$ are related to the C_iO_i pair [121,122]. In fact, Davies et al. [123] examined the relationship between the C3 center and 790 meV spectra on the same samples, and found that the absorption in the C3 and 790 meV lines are proportional to each other for a large variety of electron irradiation dose, annealing conditions and C concentrations.

The stable structure of C_iO_i is a ring in the $\{0\bar{1}1\}$ plane shown by Backlund and Estreicher [124], with three O-Si bonds at 1.8, 1.8, and 1.9 Å and three C-Si bonds at 1.8, 1.8 and 1.7 Å, respectively. Furthermore, they also calculated the binding energies relative to the dissociated defects in the 0 and + charge states, $C_i^0 + O_i^0 \rightarrow C_iO_i^0 + 1.64 \text{ eV}$ and $C_i^+ + O_i^0 \rightarrow C_iO_i^+ + 1.72 \text{ eV}$, which is in agreement with other authors' results. The C4 defect has a donor level at $E_v + 0.11 \text{ eV}$ and a rather shallow acceptor level at $E_c - 0.09 \text{ eV}$. Besides, the $Si_iC_iO_i$ complex has the -1, 0 and +1 three charge states. It should be mentioned that, except the C_iO_i and $Si_iC_iO_i$ complexes, the C-O defects also include other complexes, such as C_iO_i-H and C_nO_m .

Infrared absorption spectra of the C_iO_i complex have been intensively analyzed and a number of bands have been reported. As mentioned above, six vibration modes for C_iO_i defects are known at $1115, 865, 742, 586, 550$ and 528 cm^{-1} , related to ^{16}O , ^{12}C and ^{28}Si . Whether these bands undergo a shift when isotope substitution occur, such as ^{18}O replaces ^{16}O or ^{12}C changes for ^{13}C , is an interesting topic. The calculated and observed infrared absorption bands of C_iO_i for different C and oxygen isotopes summarized by Backlund and Estreicher are shown in Table 6 [124]. The C_iO_i pair is

Table 6Frequencies (in cm^{-1}) of local modes of $\text{C}_i\text{-O}_i$ [124].

$^{12}\text{C}^{16}\text{O}^{28}\text{Si}$	$^{12}\text{C}^{18}\text{O}^{28}\text{Si}$	$^{13}\text{C}^{16}\text{O}^{28}\text{Si}$	$^{14}\text{C}^{16}\text{O}^{28}\text{Si}$	$^{12}\text{C}^{16}\text{O}^{30}\text{Si}$
1141	1140	1101	1067	1136
925	925	898	874	917
625	624	624	624	604
604	598	604	604	589
565	562	564	564	550
559	558	558	558	541

stable up to 600 K during the annealing process [125]. Ge doping can affect the binding energy of the silicon interstitial clusters and then the reaction $\text{C}_s + \text{I} \rightarrow \text{C}_i$ and $\text{C}_i + \text{O}_i \rightarrow \text{C}_i\text{O}_i$ can start at lower temperatures. The annealing out of C_iO_i (862 cm^{-1}) defects is accompanied by the emergence of a weak band at 1048 cm^{-1} in IR absorption spectra. The band at 1048 cm^{-1} is assigned to C_sO_{2i} defects generated by the reaction $\text{C}_i\text{O}_i + \text{VO} \rightarrow \text{C}_s\text{O}_{2i}$ [126].

Two IR absorption bands of the C4 center ($\text{Si}_i\text{C}_i\text{O}_i$) are located at 940 and 1024 cm^{-1} [121]. Murin et al. [121] performed isochronal annealing on the irradiated n-type silicon wafers in 25°C step for 30 min in the temperature range of 75 – 325°C . It is found that the 940 and 1024 cm^{-1} bands are transformed into three new bands at 724 (O-related), 952 and 973 cm^{-1} (both C-related) in the temperature range of 150 – 200°C . These lines disappear at about 300 – 325°C and new bands at 969 cm^{-1} (O-related) and at 951 and 977 cm^{-1} (C-related) emerge.

The $\text{C}_i\text{-C}_s$ complexes [119] can be formed as follows



This process is quite similar to the formation of C_iO_i complexes. There is a competitive relationship between C_s and O_i on the trapping of the C_i atoms to form the complexes. The ratio of the capture radius of C_s and O_i is determined to be ~ 3 [127]. Hence, in crystalline silicon, if $[\text{O}_i] \gg [\text{C}_s]$, most of the interstitial carbon atoms are trapped by O_i . With the increase of $[\text{C}_s]$, more C_i atoms are trapped by C_s , instead of O_i atoms. At that time, the $\text{C}_i\text{-C}_s$ complex is the dominant defect in CZ silicon. The formation of $\text{C}_i\text{-C}_s$ complexes in crystalline silicon can give rise to the optical absorption and luminescence [128], so it can be characterized by PL and IR techniques [129,130]. Furthermore, there are also some other important ways for the characterization of this defect center, such as EPR [131,132], photoconductivity [133], DLTS and optically detect magnetic resonance [116,134].

The $\text{C}_i\text{-C}_s$ complex has been demonstrated as a metastable structure, i.e., this kind of defect can be stable up to $\sim 250^\circ\text{C}$ [143], and will dissociate into C_i and C_s with the increase of temperatures. Wong and Streetman [136] pointed out that the concentration of $\text{C}_i\text{-C}_s$ decreases exponentially with the annealing time as follows

$$n = n_0 \exp\left(-\frac{t}{\tau}\right) \quad (3-4)$$

with the decay time τ obeying

$$\tau = \tau_0 \exp\left(\frac{E}{kT}\right) \quad (3-5)$$

$\tau_0 = 8 \times 10^{-11} \text{ s}$, $E = 1340 \text{ meV}$. The $\text{C}_i\text{-C}_s$ complex can combine with interstitial silicon atoms and form another kind of complex as below [145]



Davies and Newman [135] claimed that in irradiated silicon samples, the annealing property of the $\text{C}_i\text{-C}_s$ complex is dependent on the radiation dose. Its thermal annealing decay process also obeys a single exponential relationship, but has a different value of activation energy ($E = 1700 \pm 50 \text{ meV}$) and pre-exponential factor

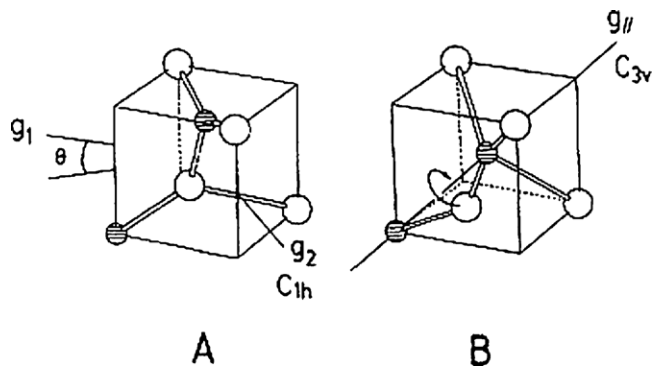


Fig. 12. Modes for the two configuration of the $\text{C}_i\text{-C}_s$ complex [116]. The A form is related to the LVM bands at $594.6, 596.9, 722.4, 872.6$ and 953 cm^{-1} while the B form is related to the LVM bands at $540.4, 543.3, 579.8, 640.6, 730.4$ and 842.4 cm^{-1} .

($\tau_0 = (4 \pm 3) \times 10^{-14} \text{ s}$). At a larger dose, there will be more interstitial silicon atoms in the material. A huge number of interstitial silicon atoms will induce a fast dissociation process of the $\text{C}_i\text{-C}_s$ complex [146].

The $\text{C}_i\text{-C}_s$ complex usually has two configurations [116], namely A form and B form, see Fig. 12. Through the detection of infrared spectroscopy, it is found that five LVM bands at $594.6, 596.9, 722.4, 872.6$ and 953 cm^{-1} are related to the A form and six LVM bands at $540.4, 543.3, 579.8, 640.6, 730.4$ and 842.4 cm^{-1} are related to the B form [137]. The characterization of the defects by EPR and DLTS [116] revealed that the A form belongs to the point group of the C_{1h} , and represents the global minimum in energy for the singly positive charge state (A^+) or singly negative one (A^-). The atomic model [116] of this kind of configuration is constructed as a $\langle 1\ 0\ 0 \rangle$ -oriented Si-C split-interstitial adjacent to a second substitutional carbon atom. The B configuration is favor to be in the neutral charge state and also belongs to the C_{1h} point group [135]. Its atomic structure [116] is believed to be of two equivalent substitutional carbon atoms at neighboring lattice sites with an interstitial silicon atom located between them. Further studies deduced that A configuration has a donor ($0/+$) and an acceptor energy level ($-/-0$) in the band gap at $E_v + 90 \text{ meV}$ and $E_c - 170 \text{ meV}$ [20] respectively. Besides, these two configurations of the $\text{C}_i\text{-C}_s$ complex can convert into each other [116] with the aid of external energy supply.

4. Co-dopants and oxygen-related defects

The oxygen impurities in silicon originate from the contamination from the crucible. During the thermal processing of IC fabrication the supersaturated interstitial oxygen atoms can aggregate into some small cluster or precipitates. It is well known that the thermal donors (TDs) are naturally the small oxygen cluster, which can change the resistivity of crystal. Oxygen precipitates can act as the gettering sites for unavoidable harmful metal contaminants during the IC fabrication, which are very important for the increase of manufacturing yield of IC fabrication. However, excessive oxygen precipitation (OP) accompanied with punch-out dislocations results in a decrease in the mechanical strength of CZ silicon. Therefore, well-controlled OP in CZ silicon is of significance for improving performance and yield of ICs. Nowadays, the thermal processing temperatures of IC fabrication have been substantially decreased. Under the circumstance, in order not to generate oxygen precipitates in the device active region, the initial oxygen concentration in silicon wafers is demanded to be lowered. Thus, how to suppress the TDs and enhance OP in CZ silicon is an issue of significance. Co-doping of electrically inactive impurities such as nitrogen, germanium and

carbon into CZ silicon has been proved to be a viable pathway to deal with these oxygen-related defects.

4.1. Thermal donors

Oxygen-related TDs are electrically active microdefects in CZ silicon. They are generally generated by heat treatments in the temperature range of 350–500 °C, with the energy levels close to the conduction band edge [138,139]. Up to now, 16 individual neutral TD species with different ionization energies ranging from 49.9 to 69.2 meV and nine single-charged TD species with ionization energies ranging from 156.3 to 116.0 meV have been observed in IR spectra [140]. Since the TDs affect the electrical properties of CZ silicon, they are undesirable for commercial CZ silicon wafers, which can be eliminated by the heat treatments at temperatures above 500 °C for a period of time.

Although the exact structures of oxygen-related TDs are not essentially known, the kinetics of TD formation has been clarified [141]. Overall, the interstitial oxygen concentration ($[O_i]$) is the most important factor to influence the formation of TDs [142]. It is well recognized that the generation rate and the maximum concentration of TDs are proportional to the fourth and third powers of $[O_i]$, respectively [141,143]. Rationally, the entities which can interact with oxygen atoms will affect the formation of TDs. As a matter of fact, secondary impurities such as N, Ge and C exhibit suppression effects on TDs [144–148]. Note that, in the case of N co-doping, another STDs are generated due to the formation of N-O complexes [148]. In the following, the effects of co-doping of N, Ge and C into CZ silicon on the oxygen-related TDs are elucidated in detail.

The N has two-fold effects on the generation of donors in CZ silicon. On one hand, N affects on the formation of TDs associated only with oxygen impurity [144]; on the other hand, a family of STDs related to both N and oxygen impurities forms at temperatures around 650 °C [11,63,149], as mentioned above. Using photothermal ionization spectroscopy, Griffin [149] found that while N doping suppressed the formation of TDs, it enhanced the formation of certain STDs. However, they did not identify such STDs as the N-O complexes but suggested a catalytic role of N in the formation of STDs. By electrical and infrared absorption measurements, it was suggested that the behavior of STDs resembles that of the TDs in CZ silicon crystals, but they are monovalent donors with the same levels as those of neutral TDs [150]. By means of low-temperature far-infrared spectroscopy, as shown in Fig. 13, Yang et al. [144] found that N suppresses the formation of TDs in CZ silicon annealed at 450 °C, while N interacts with oxygen atoms to form N-O complexes which are related to the STDs. The interaction of N and oxygen atoms is supposed to reduce the TDs. Moreover, they found that the resistivity of NCZ silicon annealed at temperatures ranging from 650 to 1000 °C changes with the annealing time and temperatures, which is due to the formation and elimination of the N-O complex related STDs. In this way, STDs can be essentially annihilated by the annealing at 900 °C and above, during which the N-O complexes attract more oxygen atoms to form larger electrically inactive clusters [77].

The effect of C on the formation of TDs in CZ silicon has been intensively investigated to reach a consensus that C exerts an inhibition effect. Taking a typical result for example, Lindström and Hallberg [151] proved that the retarded TD formation occurred in CZ silicon containing C with a concentration of $6 \times 10^{16} \text{ cm}^{-3}$, while the TDs hardly generated as the C concentration reached to $5 \times 10^{17} \text{ cm}^{-3}$ even after 180 h anneal at 450 °C. The mechanism for such a suppressing effect can be interpreted in terms of the interactions between C atoms and silicon self-interstitials or interstitial oxygen atoms based on different TD_{N-O} models.

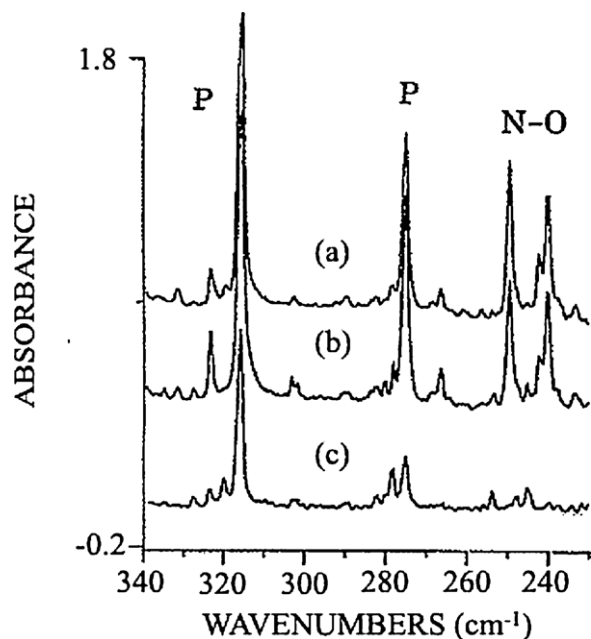


Fig. 13. Spectra of FTIR related to thermal donors and shallow thermal donors in CZ silicon measured at low temperature. (a) High [N], (b) low [N], (c) N undoped [144].

According to the 'self-interstitial model' for TDs, a Si–O–Si–O chain is supposed to be the fundamental configuration of TDs [143,152]. During the formation of the above-mentioned chains, the chains may collapse at some points due to the stress, resulting in punched-out interstitial silicon atoms. Such release of silicon self-interstitials during 450 °C annealing was once experimentally observed. Furthermore, the core of the TDs was proposed to be a divalent silicon interstitial combined with a pair of adjacent interstitial oxygen atoms [152]. The formation of this core forces two electrons into a lone pair p-like orbital on the divalent silicon atom, thus accounting for the double donor character of TDs [143]. As sufficient C atoms are present, the mobile silicon self-interstitials will be trapped by the substitutional C atoms through the $C_s + Si_i \rightarrow C_i + Si_s$ reaction. Therefore, fewer silicon self-interstitials are available for the formation of TDs.

Another widely accepted model of TDs is the ' O_2 model' [153]. In this model, the TDs are believed to be the oxygen clusters formed through the aggregation of fast-diffusing molecular-like di-oxygen atoms: $O_2 + O_2 \rightarrow O_4$ (TD). The inhibition effect of C on the TD formation may be related to the formation of C–O complexes [154]. It has been suggested that two possibilities may be envisaged with the O_2 model. One is the trapping of interstitial oxygen atoms by C atoms, leading to C_i-O_i complexes, which are found to form in C-doped CZ silicon, exhibiting infrared (IR) absorption lines at 738 cm^{-1} [166]. Theoretical calculations also confirm the existence of the C_i-O_i complexes [68,155]. The formation of such C_i-O_i complexes reduces the O_i concentration and, furthermore, decreases the formation rate and the maximum concentration of TDs. Moreover, certain clusters of C and oxygen as revealed by the IR bands around 1012 and 1026 cm^{-1} were found to form during 450 °C annealing [151]. As a result, the formation of TDs was suppressed. Another possibility in the framework of the ' O_2 model' is the frequent occurrence of trapping/detrapping of O_2 molecules at C atoms [153]. This case lowers the effective diffusivity of O_2 molecules rather than the interstitial oxygen concentration. The trapping of O_2 molecules by C was proved by the observation of $C-O_2$ complexes [156]. Although the C

suppression of TDs can be understood from different standpoints, it is still an open question due to the exact configuration of TDs not being essentially disclosed. Fortunately, from the engineering point of view, TDs can be effectively killed and the C suppressing effect on TDs is worthy to be utilized.

It has been reported that the TD formation is retarded in oxygen-rich SiGe alloy with more than 1% Ge content [145]. In GCZ silicon, the Ge concentration is usually below 10^{20} cm^{-3} , much lower than that in the SiGe alloy. In this case, however, the Ge doping still suppresses the formation of TDs in CZ silicon. Li et al. [146] found that the generation rate of TDs in the CZ silicon co-doped with 10^{18} cm^{-3} Ge atoms was much smaller than that in the conventional CZ silicon during the annealing at 450°C . Low-temperature far- and medium-IR spectra as shown in Fig. 14 indicate that although the Ge doping suppresses the formation of TDs, it does not change the wavenumbers of the TD-related absorption bands. This result implies that the Ge doping does not affect the configuration of TDs [157]. The retardation effect of Ge on TDs has been tentatively explained in terms of interactions between Ge atoms with vacancies and oxygen atoms [158]. The Ge doping introduces compressive stress into silicon matrix, which can be relieved by attraction of vacancies. The consequent Ge–V complexes can further combine with oxygen atoms during the TD formation annealing. Therefore, the number of oxygen atoms available for TDs is decreased, thus leading to the retarded TD formation.

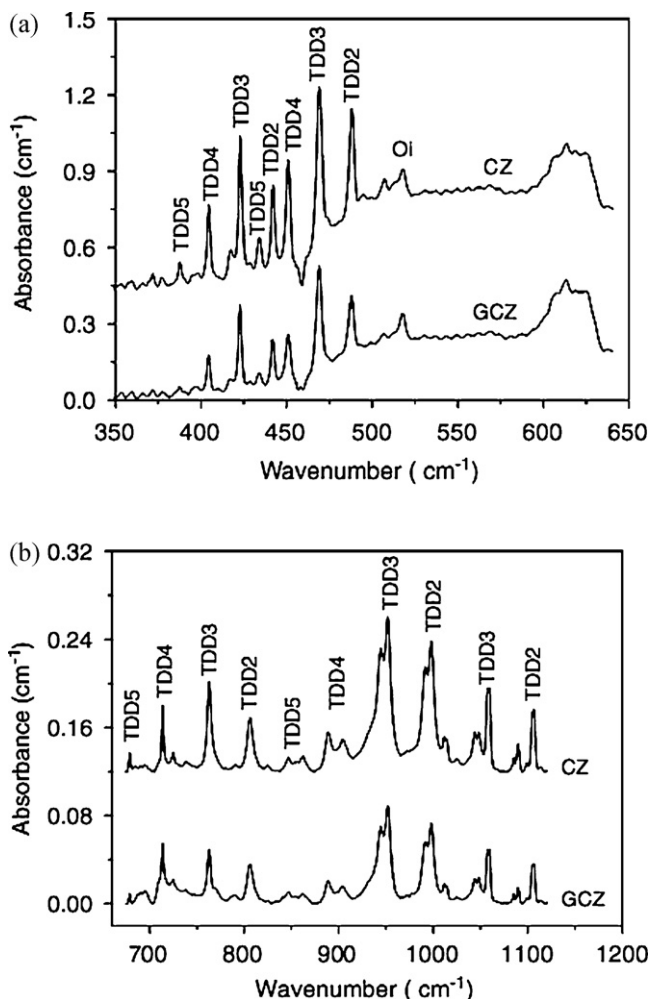


Fig. 14. Low-temperature far-IR spectra (a) and mid-IR spectra (b) of the silicon with and without Ge doping. Samples subjected to 650°C , 30 min + 450°C , 4 h annealing [157].

4.2. Oxygen precipitates

During thermal processing in IC fabrication, the supersaturated interstitial oxygen atoms in CZ silicon can aggregate into oxygen precipitates and further induce secondary lattice defects. Such precipitates and defects act as gettering sites for unavoidable harmful metal contaminants during the IC fabrication [159]. This property of CZ silicon is very important for the increase of manufacturing yield of IC fabrication. However, excessive oxygen precipitation (OP) accompanied by punch-out dislocations results in a decrease in the mechanical strength of CZ silicon [160]. Therefore, well-controlled OP in CZ silicon is of significance for improving performance and yield of ICs.

The ever-smaller feature size of ICs puts much more stringent requirements on the control of metal contamination and defects in CZ silicon wafers. In terms of oxygen-related issues, CZ silicon wafers are required to possess stronger IG capability and, moreover, the device active areas that are generally located at near-surface region of silicon wafers should be essentially free of OP. Nowadays, thermal processing temperatures of IC fabrication have been substantially decreased. Under these circumstances, the initial oxygen concentration in silicon wafers is demanded to be lowered in order not to generate oxygen precipitates in the device active region. The reduction of initial oxygen concentrations in CZ silicon and the decrease of IC processing temperatures, as mentioned above, are not beneficial for OP and therefore the IG capability of CZ silicon. How to enhance OP in CZ silicon is an issue of significance. Co-doping of electrically inactive impurities such as N, Ge and C into CZ silicon has been proved to be a viable pathway to introduce heterogeneous nuclei and thus enhancing OP. In the following, the effects of co-doping N, Ge and C into CZ silicon on OP are reviewed.

4.2.1. Effects of N on OP

During CZ silicon growth, the degree of super-saturation of interstitial oxygen becomes progressively larger along with the cooling process. Thus, grown-in oxygen precipitates form via heterogeneous nucleation mechanism in a certain temperature range. The formation of grown-in oxygen precipitates depends on versatile factors such as initial oxygen concentrations, characteristic parameter of V/G for CZ silicon growth, cooling rate and the secondary impurities (e.g. N and C) [161]. To date, the exact mechanism for the formation of grown-in oxygen precipitates has not been clarified. The grown-in oxygen precipitates significantly affect the performance of CZ silicon in the following regards: (1) a part of grown-in oxygen precipitates can grow up during the device fabrication to become gettering sites for harmful metal impurities [62]; (2) certain grown-in oxygen precipitates may act as the nuclei for oxidation-induced-stacking faults which are detrimental to device yield [162]; (3) appropriately sized grown-in oxygen precipitates exert strengthening effect on silicon [163]. Consequently, well control of grown-in oxygen precipitates is an important technological concern in CZ silicon growth. It has been proved that the co-doping of N significantly affect the formation of grown-in oxygen precipitates.

Yu et al. [62] investigated the variations of $[O_i]$ due to dissolution of grown-in oxygen precipitates at 1270°C in NCZ and conventional CZ silicon wafers which were produced under nearly the same conditions. The increased $[O_i]$ in NCZ silicon was essentially higher, indicating that N co-doping enhanced the formation of grown-in oxygen precipitates. Karoui et al. [164] found that the pre-annealing at 1250°C hardly affects the density of oxygen precipitates formed in NCZ silicon by the low–high two-step annealing. This result showed that the N co-doping facilitated the formation of grown-in oxygen precipitates which could be stable at temperatures above 1250°C . Aihara et al. [165] pointed

out that N doping enhanced the formation of grown-in oxygen precipitates stable over 800 °C. Nakai et al. [166] reported that the density of grown-in oxygen precipitates increases with N concentration but hardly relies on the initial $[O_i]$ in NCZ silicon. Their work further indicated that the size of grown-in oxygen precipitates was larger than critical radius r_c at 1100 °C, with a nearly uniform size distribution rather than a Boltzmann distribution which generally occurs for the grown-in oxygen precipitates in conventional CZ silicon. Such results as mentioned above are manifested as Fig. 15. Yu et al. [62] also obtained the

similar results as mentioned above. Regarding the nucleation temperature of grown-in oxygen precipitates in NCZ silicon, Nakai et al. [166] estimated that it was in the range of 1000–1040 °C dependent on the N concentration. However, Yu et al. [62,167] believed that the large sized grown-in oxygen precipitates formed prior to the formation of voids (around 1100 °C). Although the consensus has not been reached for the effect of N doping on the onset of grown-in oxygen precipitates, it is definite that the N doping facilitates the formation of grown-in oxygen precipitates at higher temperatures in comparison with the case of conventional CZ silicon.

Yu et al. [62] once investigated oxygen precipitation in the mixed-type NCZ silicon containing a “P-band”, which gives rise to a well known narrow ring of OSFs in oxidized wafers. They found that oxygen precipitation within the “P-band” was weaker than that within the void region when subjected to one-step high-temperature annealing. However, the scenario resulted from the low-high two-step annealing was quite the contrary. Such oxygen precipitation behavior in the mixed-type NCZ silicon was in sharp contrast to that in the mixed-type CZ silicon. Based on the experimental facts, it was derived that the formation of large sized grown-in oxygen precipitates was enhanced by $N_2-V_2-O_x$ complexes in the void region, while the small sized grown-in oxygen precipitates formed more significantly in the “P-band” via the N_mO_n complexes as the heterogeneous nucleation centers.

N is believed to be involved in the formation of grown-in oxygen precipitates in NCZ silicon. This is, however, a phenomenological derivation to large extent. Direct evidences for the existence of N in the grown-in oxygen precipitates can be given by TEM characterization. Aihara et al. [165] observed grown-in oxygen precipitates with a size of ~50 nm in the NCZ silicon with a N concentration of $3 \times 10^{15} \text{ cm}^{-3}$. As shown in Fig. 16, the precipitates have a shape elongated in a $\langle 1\ 1\ 0 \rangle$ direction and accompanied by a strain field. Moreover, substantial N content is detected in the oxygen precipitates by EDX. Fujimori et al. [168] found that the grown-in oxygen precipitates in the NCZ silicon with a N concentration of $6.2 \times 10^{14} \text{ cm}^{-3}$ were in the form of 14-sided polyhedron bounded by eight $\{1\ 1\ 1\}$ and six $\{1\ 0\ 0\}$ faces, with a size range of 20–30 nm and accompanying the small whisker-like defects. Similarly, they also detected the N content in such the polyhedral precipitates by EDAX. Interestingly, Fujimori et al. claimed that nitride precipitates in the form of 32-sided polyhedron bounded by eight $\{1\ 1\ 1\}$ and 24 $\{3\ 1\ 1\}$ faces were found in their as-grown NCZ silicon [168].

It can be concluded that N is an enabler for grown-in oxygen precipitates in CZ silicon. The size, density and morphology of the grown-in oxygen precipitates depend strongly on N and oxygen concentrations as well as thermal history of NCZ silicon. The interaction among N, oxygen and point defects (i.e. vacancy and interstitial) dictates the early stage of grown-in oxygen precipitate formation. This point will be further elucidated in the following. The enhanced formation of the grown-in oxygen precipitates has two-fold effects on the IG of NCZ silicon. The advantageous effect is that based on the grown-in oxygen precipitates sufficient bulk microdefects (BMDs) acting as IG sites can be formed with a low thermal budget process (e.g. just single-step high-temperature annealing). However, the adverse effect may be manifested as the occurrence of near-surface defects originated from the grown-in oxygen precipitates [9,164,169]. Therefore, in order to exert the positive effect of the N enhanced formation of grown-in oxygen precipitates, N doping and the thermal history of CZ silicon growth should be elaborately engineered in each specific case.

In terms of oxygen precipitation, N doping exhibits the effects not only on the size and density, but also on the morphology of oxygen precipitates. For the conventional CZ silicon, the morphologies of oxygen precipitates can exhibit as sphere, polyhedron,

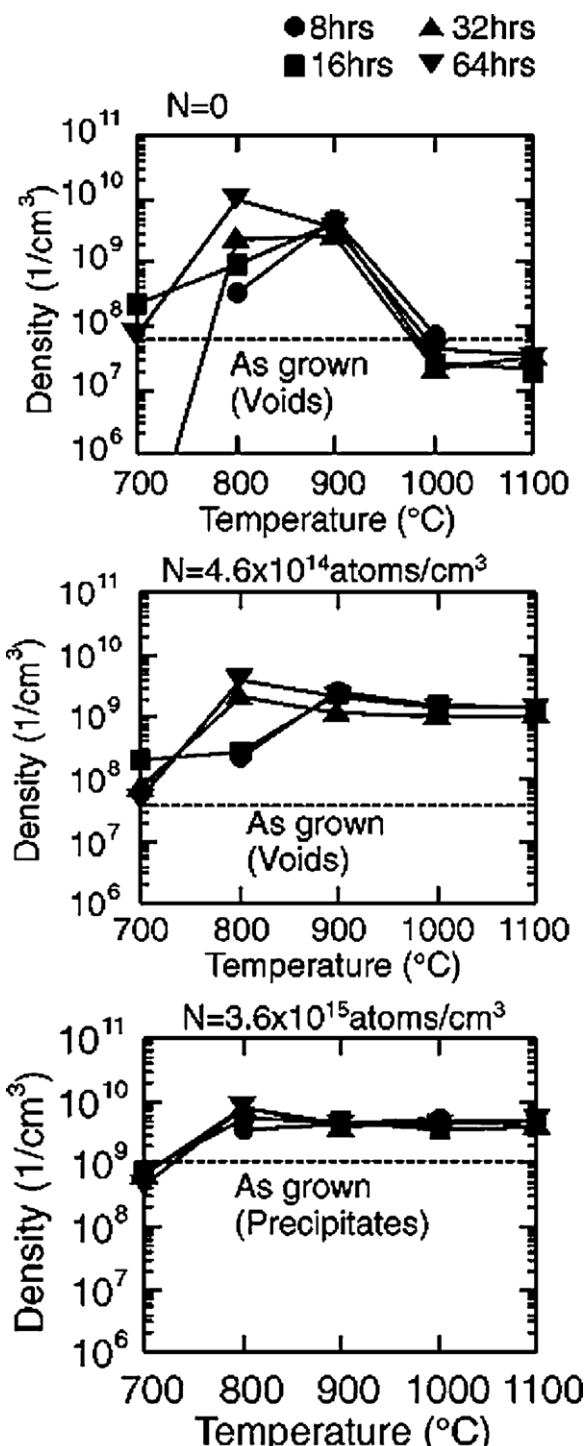


Fig. 15. Oxygen precipitate density after a single-step heat treatment at 700 °C together with the grown-in defect density [166].

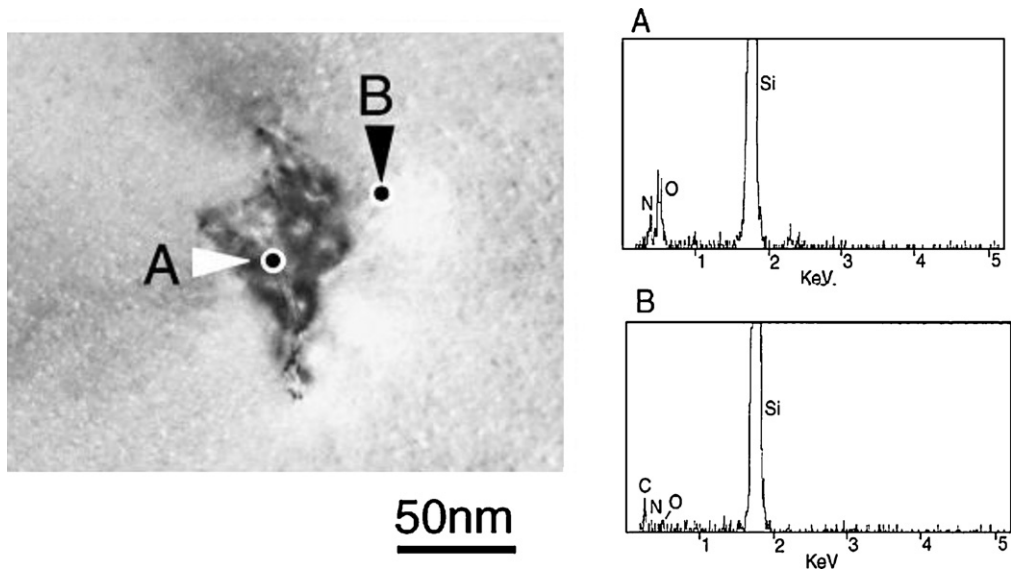


Fig. 16. TEM image and EDAX analysis results of grown-in defects in the crystal with the N concentration of 3×10^{15} atoms/cm³ [165].

octahedron, platelet and ribbon, determined primarily by annealing temperatures [44,164,170,171]. Such the morphologies of oxygen precipitates have also been observed in NCZ silicon. However, with the same annealing scheme, the morphologies of oxygen precipitates in NCZ silicon could be quite different from those in the conventional CZ silicon. Yang et al. [172,173] found that oxygen precipitates in NCZ silicon subjected to single-step high-temperature annealing or low-high two-step annealing could be of cubic shape with the edge length of about 400 Å, paralleling to the <1 1 0> or <1 1 1> orientation, as shown in Fig. 17(a). Those in the conventional CZ silicon subjected to the same annealing are generally with the morphology of octahedron or polyhedron. Rozgonyi et al. [174] performed nanoscale analysis of oxygen precipitates in NCZ silicon after low-high annealing. They found that the microstructures of defects existing in the near-surface and bulk regions are different. Concretely speaking, strain-free octahedral precipitates connected with a series of stacking faults were found in the near-surface region. An umbrella-like defect configuration comprising a platelet precipitate and a condensate of self-interstitials was found in the bulk, as shown by Fig. 17(b). The oxygen precipitation behavior was believed to be related to the coupling of vacancies and N atoms, which in turn affected the interstitial condensation.

Shimura and Hockett [169] believed that the substitutional N atoms plays an important role in the heterogeneous nucleation of oxygen precipitates. The atomic radius of N (0.70 Å) is much smaller than that of silicon (1.17 Å). Substitutional N atoms, like substitutional C atoms, introduce a lattice contraction, thus leading to enhanced oxygen precipitation. Abe et al. [175] suggested that N–O complexes can act as heterogeneous nucleation centers for oxygen precipitation. In any case, the interaction among N, point defects and oxygen has been considered to be crucial for the early stage of oxygen precipitation. First-principles calculations by Kageshima et al. [83,176,177] revealed that the most stable N₂V₂ complexes, substantially formed after point defect generation during crystal growth, can exist at the temperature of void aggregation. Positron annihilation spectroscopy has proved that N–V complexes indeed form in N-doped silicon [81]. Based on density functional theory and semi-empirical Hartree–Fock calculations, Karoui et al. [9,164,178] pointed out that the N₂V₂ complexes have strong capability for attracting oxygen atoms, thus forming a grown-in oxygen precipitate nucleus of roughly 2 nm in diameter. Thus, Yu et al. [62,179,180] phenomenologically suggested that at high temperatures prior to void aggregation the N₂V₂ complexes bind oxygen to form N₂V₂O_x ($x > 1$) complexes which facilitate the formation of large grown-in oxygen

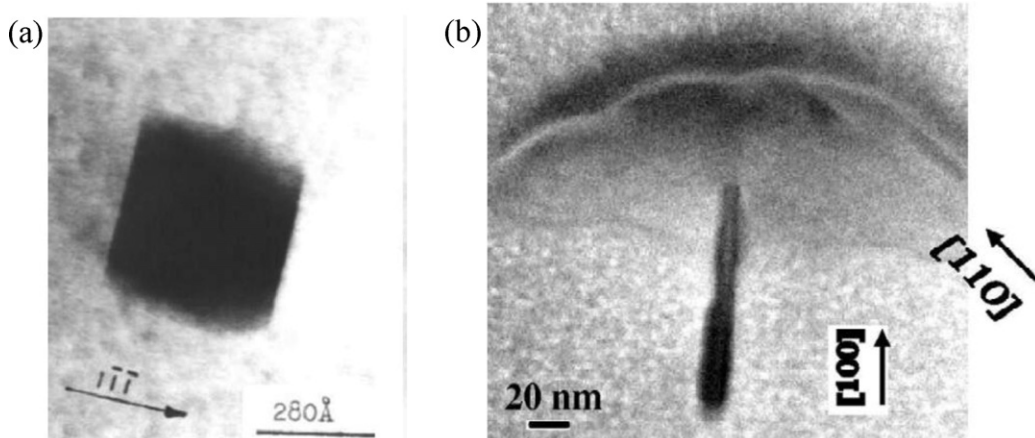


Fig. 17. OP in Lo-Hi heat-treated NCZ silicon: (a) oxygen precipitate of cubic morphology and (b) umbrella-like defect configuration comprising a platelet precipitate and a condensate of self-interstitials [172,174].

precipitates; moreover, in the low-temperature range of 750–450 °C the N₂ pairs can directly bind oxygen to form N_mO_n ($m, n > 1$) complexes, which act as the heterogeneous nuclei for small grown-in oxygen precipitates. von Ammon et al. [61] proposed that in NCZ silicon the high oxygen content favors the formation of NO complexes rather than N₂V ones at high temperatures, while, the N₂V complexes could form at low temperatures. Moreover, they believed that the N enhanced oxygen precipitation is not only attributed to a higher free vacancy concentration but also to the effective removal of silicon interstitials by the N₂V complexes. A recent density functional theory study accomplished by Karoui [88] and showed that the N₂O_n and N₂V₂O_n ($n = 1, 2$) complexes formed from N₂ and N₂V₂ species are the most stable N–O complexes, which can act as nucleation centers for oxygen precipitates. They believe that the increase in the number of nucleation sites due to N–V–O coupling explains the high density of stable grown-in oxygen precipitates and the delay in the void formation in NCZ silicon.

4.2.2. Effect of Ge on OP

Ge doping can enhance the formation of grown-in oxygen precipitates [158,181]. By high-temperature annealing, e.g. 1270 °C, to dissolve the grown-in oxygen precipitates, the increased oxygen concentration in GCZ silicon is higher than that in the control CZ silicon. Meanwhile, the prolonged isothermal annealing at 800 and 1000 °C significantly can lead to more oxygen precipitation in GCZ silicon. If the conventional and GCZ silicon wafers are both subjected to the ramping anneal from various low temperatures to a high temperature, followed by an isothermal anneal, it is found that Ge doping facilitates the formation of grown-in oxygen precipitates in large size. Thus, it is believed that Ge doping can improve heterogeneous nuclei for oxygen precipitation during CZ silicon growth.

Ge doping also enhances the nucleation of oxygen precipitates in CZ silicon during the post annealing [182–185]. It has been revealed that Ge doping can enhance the nucleation of oxygen precipitates in a wide temperature range from 650 to 1150 °C. However, the enhancement of Ge doping on oxygen precipitates is more pronounced at the temperatures above 850 °C, compared with that at a lower temperature. Generally, it is known that the super-saturation of O_i is too small to enable homogeneous nucleation of oxygen precipitates in CZ silicon during the high-temperature annealing, e.g. 1000 °C or above. But, the oxygen precipitates formed by isothermal annealing at high temperatures are smaller and denser in GCZ silicon than those in CZ silicon. This is ascribed to an increase in the density of heterogeneous nuclei, due to the formation of Ge-related complexes and the reduction of the critical size for oxygen precipitates by Ge doping.

It is well accepted that rapid thermal processing (RTP) at high temperatures enhances oxygen precipitation in CZ silicon subjected to the subsequent thermal treatments. The vacancies introduced by high-temperature RTP usually combine with oxygen to form VO₂ complexes at certain temperatures below a critical point, which act as the heterogeneous nuclei of oxygen precipitates [161,186,187]. In the case of GCZ silicon, the interaction between oxygen and vacancy is influenced and therefore oxygen precipitation will be modified, due to Ge doping. Wu et al. [188] have reported that the nucleation of oxygen precipitates can be greatly enhanced in the temperatures range from 650 to 1050 °C after the 1260 °C RTP pre-treatment, as shown by Fig. 18. At the relatively lower temperatures, i.e., 650–750 °C, most of the vacancies form the VO₂ complexes with oxygen, which dominate the nucleation of oxygen precipitates [186]. The interaction of Ge atoms with vacancies is negligible. However, the Ge atoms will directly combine with the supersaturated oxygen atoms to form Ge–O complexes, which can enhance heterogeneous nuclei of oxygen

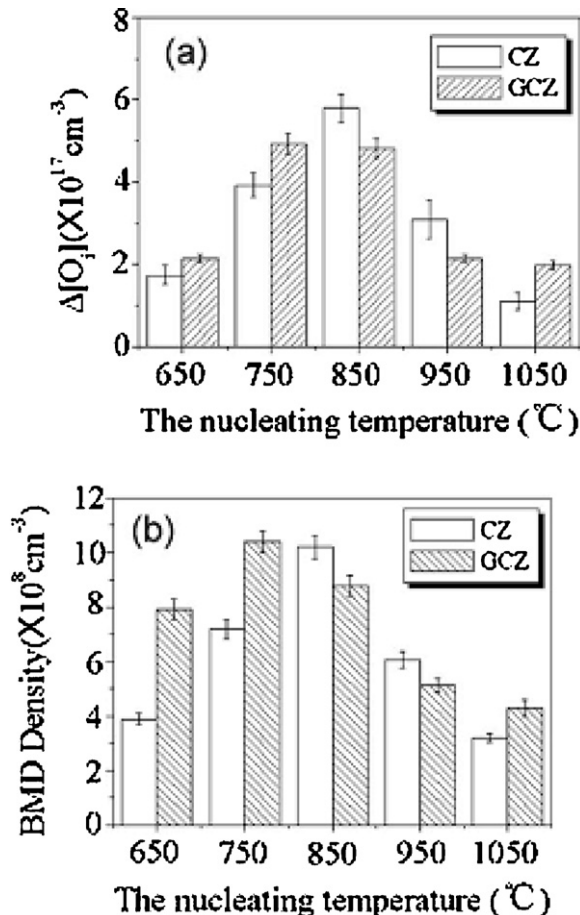


Fig. 18. (a) $\Delta[O_i]$ and (b) BMDs density of the CZ and GCZ silicon annealed at x ($x = 650, 750, 850, 950$, and 1050) °C/4 h + 1050 °C/16 h with the RTA pre-treatment at 1260 °C for 60 s [188].

precipitates during the following annealing below 650 °C [103]. At medium temperatures, i.e., 850–950 °C, a portion of vacancies combines with the Ge atoms to form remarkable Ge–V complexes [91,98]. This interaction could also lead to the dissociation of VO₂ complexes, which in turn improves the interaction between the Ge atoms and vacancies. Although the Ge–V complexes can further trap oxygen atoms and act as the nuclei of oxygen precipitates, they are less favorable energetically than VO₂ complexes in the nucleation. At high temperatures, i.e., 1050 °C or above, more free vacancies are available and therefore a large number of Ge–V or Ge–V–O complexes generate. These complexes are dominant in the heterogeneous nucleation of oxygen precipitates in GCZ silicon [189].

Ge doping also affects the morphology of oxygen precipitates in CZ silicon [183,190]. Generally speaking, platelet precipitates are inclined to form at intermediate temperatures (750–950 °C), while polyhedron precipitates at higher temperatures [191,192]. Fig. 19 compares the morphologies of oxygen precipitates in GCZ silicon with those in conventional CZ silicon [183]. It can be seen that after prolonged annealing at 800 °C, platelet precipitates dominate in conventional CZ silicon, while both particle-like precipitates and platelet ones in GCZ silicon with a concentration of 10^{18} cm^{-3} . After the annealing at 1000 °C or above, polyhedral oxygen precipitates appear in conventional CZ silicon, but both platelet and polyhedral oxygen precipitates are entangled in GCZ silicon. The particle-like and platelet oxygen precipitates formed in GCZ silicon can be easily dissolved by high-temperature annealing. It should be mentioned that when the Ge doping level is in the order of 10^{16} cm^{-3} or below,

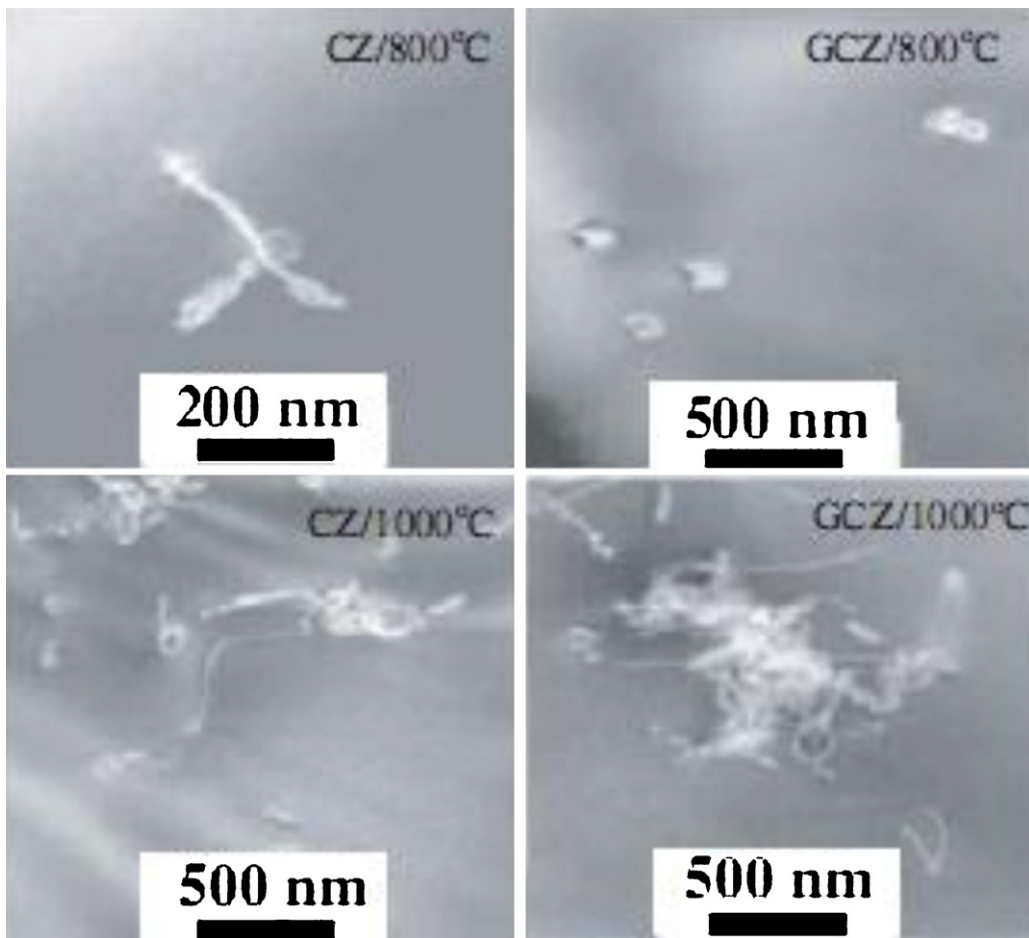


Fig. 19. TEM micrographs of the precipitates observed in the samples subjected to the 225 h annealing at 800 and 1000 °C. (a) CZ, 800 °C, (b) Ge doped CZ, 800 °C, (c) CZ, 1000 °C, (d) Ge doped CZ, 1000 °C [183].

the oxygen precipitate morphologies in GCZ silicon exhibit no substantial difference from those in conventional CZ silicon.

Since the covalent radius of Ge atom is larger than that of silicon atom, lattice strain must arise from the incorporation of substitutional Ge atoms in silicon lattice. The strain can be reduced by the generation of vacancies, which has been experimentally verified by Vanhellemont et al. [100]. Moreover, it is revealed that the formation energy of vacancies in GCZ silicon is much smaller than that in CZ silicon [100]. First-principles calculations show that the vacancies tend to accumulate around Ge atoms, and therefore suppress the formation of vacancy clusters to some extent [91]. Low-temperature FTIR characterization of neutron-irradiated GCZ silicon revealed that the formation of VO complexes is retarded, and meanwhile, the Ge-V-O complexes are numerously generated [193,194]. Yang et al. [189] proposed that various Ge-related complexes can act as heterogeneous nuclei of oxygen precipitates in CZ silicon at different temperatures. At high temperatures prior to the void formation, the vacancies tend to combine with Ge atoms and form Ge-V complexes. These complexes further capture oxygen atoms to transform into stable Ge-V-O complexes, which act as the heterogeneous nucleation sites for the formation of grown-in oxygen precipitates at high temperatures during the crystal cooling. In the late stage, the amount of residual free vacancies is limited, but the super-saturation of interstitial oxygen becomes larger. In this case, the Ge atoms could directly combine with oxygen atoms to form Ge-O complexes, which act as the heterogeneous nuclei for oxygen precipitation at the low

temperatures (<900 °C) during crystal growth. Theoretical calculations based on density functional theory also demonstrate that Ge-O complex is energetically stable when the captured oxygen atom is located at the third-nearest-neighbor site to the Ge atom [103].

4.2.3. Effect of C on OP

There is a wealth of experimental evidence that C enhances oxygen precipitation, exhibiting an increase of precipitate density and a simultaneously decreased C concentration in the silicon matrix [191,195,196]. Tan et al. [197,198] pointed out that the enhancement of oxygen precipitation is due to a direct role of C in nucleation through influencing nuclei interfacial energy and an indirect role via its influence on relieving the strain around oxygen precipitates. C-O complexes were proposed to be the heterogeneous nuclei of oxygen precipitates. Furthermore, Shimura et al. [199–201] confirmed that C directly provides heterogeneous nuclei, so-called “C3 centers”, for oxygen precipitation at temperatures lower than a critical value (T_c) in the range of 800–850 °C. However, C only plays a catalytic role at temperatures higher than T_c . Sun et al. [202] reported that substitutional C has an insignificant effect on heterogeneous nucleation, but it can interact with silicon interstitials. Such Cs-Si_i interaction reduces the supersaturation of silicon interstitials, which releases the strains around the oxygen precipitates and therefore enhances oxygen precipitation. According to the correlation of oxygen with carbon during oxygen precipitation, Liu et al. [203] believed that there is a critical

precipitate size which distinguishes the C behavior in oxygen precipitation. They actively participate in oxygen precipitates smaller than the critical size, but are less involved in oxygen precipitates larger than the critical size.

For oxygen precipitation in CZ silicon subjected to Lo-Hi two-step annealing, the interstitial oxygen content in CZ silicon could exhibit an initial decrease with the extension of low-temperature annealing time, followed by an increase and a final decrease. Herein, the ‘abnormal’ increase of oxygen content refers to retardation effect. Although C doping is not essential in retardation effect, high-content C enhances the retardation effect of oxygen precipitation. Ogino [196] found that oxygen precipitation in CZ silicon with a high concentration of C was suppressed during the Lo-Hi two-step annealing with respect to that in conventional CZ silicon. It is believed that C enhances nucleation of oxygen precipitates significantly during low-temperature annealing and therefore the growth of small oxygen precipitates is retarded during the following high-temperature annealing.

It has been revealed that C doping exhibits remarkable effects on the oxygen precipitate morphology and the formation of secondary defects associated with oxygen precipitation. The oxygen precipitates formed by low-temperature anneal in high-C CZ silicon usually take an octahedral shape, rather than the platelet one which generally occurs in low-C CZ silicon [204,205]. Such morphology change in high-C silicon is possibly related to the effects of C or/and point defects on strain energies, formed at the very early stage of oxygen precipitation. In the case of high-temperature annealing, the colony of small loops are the primary secondary defects in high-C CZ silicon, induced by square {1 0 0} platelet precipitates. It is quite different from the situation in low-C CZ silicon, which features punched-out dislocation loops and precipitate-dislocation complexes. It is supposed that at high temperatures substitutional C atoms might act as the sites for point defect clusters near large precipitates. Moreover, high-content C in CZ silicon suppresses the formation of rod-like defects, but enhances the formation of small amorphous precipitates during prolonged annealing at 650 °C. Londos et al. [206] found that high-content C facilitates the formation of spherical oxygen precipitates and simultaneous dissolution of the disc-like precipitates at high temperatures, based on the measurement of infrared spectroscopy. Such oxygen precipitation behavior is due to the C catalytic role, which minimizes the interfacial energy between precipitates and substrate.

5. Influence of co-dopants on voids

As one of the main grown-in microdefects in modern large diameter CZ silicon, voids located at the near-surface of wafers, degrade the GOI of MOS devices and therefore reduce the yield of ULSI [207,208]. Besides, the GOI yield in every CZ silicon wafer was in proportion to the density of void defects [209]. Void defects have been referred to by various names based on the method of their detection, such as the crystal originated particles (COPs) emerging at the wafer surface after SC-1 cleaning [210], flow pattern defects (FPDs) revealed by Secco solution etching without agitation [211] and light scattering tomography defects (LSTDs) detected by IR-light scattering [189,212]. Ueki et al. [213] have clarified that the void defects formed during CZ silicon crystal growth are related to the agglomeration of vacancies. The defects are believed to be of octahedral structures surrounded by several {1 1 1} crystal planes with a nanometer-thick oxide layer [214].

It has been established that grown-in microdefects in CZ silicon were controlled by the ratio of the growth rate (V) and the axial temperature gradient (G) [186]. An accepted theory is based on the recombination of vacancies and self-interstitials in the near-interface silicon crystal area. At a low V/G value, the recombination

loss of point defects is partly compensated by the diffusion, so the survived point defects are self-interstitials which have a higher diffusivity and the interstitial-type microdefects were formed; while the V/G exceeds a critical value, the contribution of diffusion is extremely small, so the survived defects are vacancies which are of higher initial concentration and the microdefects were found to be vacancy-type, such as voids [186,215]. Furthermore, the cooling rate of a crystal near 1100 °C after crystallization is known to determine the density void defects [216]. If a crystal is fast cooled through the clustering temperature range, the fine COPs are formed in high density. In a slow cooled crystal, however, larger COPs can grow and the density of the fine COPs is somewhat reduced because the nucleation of vacancy clusters is suppressed. It is worth pointing out that the density of void defects is proportional to the cooling rate to the power of 1.5 and inversely proportional to the square root of vacancy concentration at the defect formation temperature [186]. Note that the driving force of the void formation is the gain in the volume free energy related to the vacancy super-saturation.

The presence of void defects exhibits deleterious effect on devices performance such as enhanced leakage current. It is therefore very important to control void defects in the process of silicon crystal growth. The techniques to control void defects have been developed over the years, and three different ways have been widely accepted: thermally controlled CZ silicon crystal ingot growth [217], high-temperature annealing [218] and high-cost epitaxial wafers. As an economic alternative, intentional impurity doping in CZ silicon during crystal growth has been also suggested recently, including N doping, Ge doping and C doping [219–221].

5.1. Grown-in voids

5.1.1. Nitrogen doping

Two opposite viewpoints of the effect of N doping on grown-in voids in CZ silicon have been proposed. One is that N doping increases the density of grown-in voids but decreases their sizes [219], and the other considers that the N doping decreases the density of grown-in voids [61]. Voronkov and Falster [222] assume that voids are formed by vacancy aggregation and the N impurity is an efficient trap for vacancies. In float-zone (FZ) silicon crystals with a small amount of N concentration (10^{14} cm^{-3}), the formation of voids is sufficiently suppressed. On the contrary, N doping results in a strongly increased void density in CZ silicon crystals. For conventional CZ silicon, voids are produced typically at about 1100 °C, while in N-doped CZ silicon the vacancy trapping by N at this temperature is strong. The major fraction of vacancies exists as trapped VN complexes and only a minor fraction as free vacancies V, so the void nucleation rate becomes negligible at 1100 °C. In addition, in NCZ silicon the oxygen content favors the formation of NO complexes at high temperatures, implying that no N–N pair is available to react with vacancies, and defect suppression effect is reduced.

Park et al. [219] have investigated the effect of N doping in a fast-pulled CZ silicon crystal on vacancy-related defects. It is well known that the pulling rate of CZ silicon crystal seriously affects the vacancy concentration and the defect density in the process of crystal growth. For a low-cost silicon substrate, a high pulling rate should be required. However, this causes the increase of vacancy-related defects. The FPD density for conventional and N-doped samples in the fast-pulled CZ silicon crystal was measured. It was found that the FPD was formed on the whole wafer in very high density of about 800 cm^{-2} in conventional silicon, the density of FPDs in NCZ silicon were reduced remarkably and its effect seems to depend on the doping concentration. They considered the N plays a role to disturb the growth of vacancy clusters by reducing the vacancy-rich region and the vacancy concentration. In

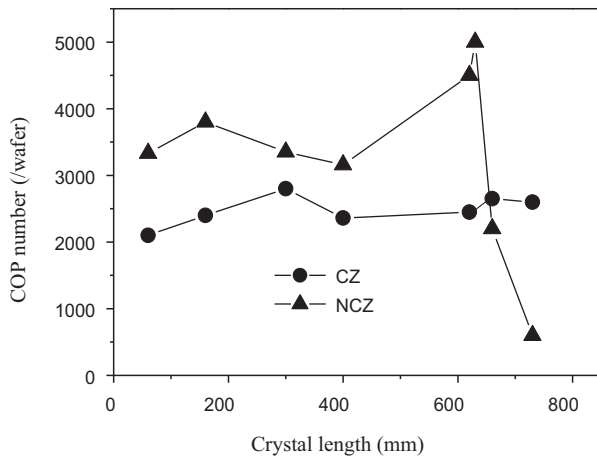


Fig. 20. Number distribution of grown-in COPs along the axial direction of the CZ and NCZ silicon crystals after being cleaned in SC-1 solution for 1 h [220].

addition, Voronkov and Falster also suggested that the void growth is diffusion-limited, just like in conventional silicon crystals, but the free vacancy concentration is remarkably reduced because of vacancy trapping by N [222].

Yu et al. [220] have studied the effect of N doping on grown-in COPs during crystal growth. The axial profile of grown-in COPs along the crystal axis direction of CZ and NCZ silicon were shown in Fig. 20. In general, the number of COPs in conventional CZ silicon is much lower than that in NCZ silicon, indicating that N doping significantly increases the density of COPs under the same crystal growth conditions. Besides, it was also observed that the number of grown-in COPs in the CZ silicon remains constant along the crystal axis direction, while in the NCZ silicon, the number of COPs of the tail part is much higher than those of the seed-head and middle parts of the crystal. More interestingly, the number of COPs reduces dramatically at the tail portion of the crystal. Comparing the size profiles of grown-in COPs in the CZ and NCZ wafers sampled from the tail portion of crystals, there was significant difference: the percentage of the small COPs with the size of 0.11–0.12 μm increases and that of COPs larger than 0.12 μm decreases remarkably in the NCZ Si samples within the detection limit of the particle counters than undoped CZ ones. However, the total number of the COPs on the NCZ wafers is much larger than that on the CZ wafer. N doping facilitates the formation of denser grown-in COPs with smaller sizes, so it is considered that N doping reduces the super-saturation of vacancies prior to the formation of voids and then decreases the onset temperature of void formation.

von Ammon et al. [61] found that the increase of N doping concentration can increase the defect-free zones in FZ grown silicon crystal until the nitrogen content extends over the entire crystal volume. The inner COP region shrinks until it disappears in the center of the crystal at $0.8 \times 10^{14} \text{ cm}^{-3}$, while the inner boundary of the outer A-swirl region is shifted towards the crystal rim, until the A-swirl vanishes at $1.35 \times 10^{14} \text{ cm}^{-3}$, as shown in Fig. 21. They proposed that the dominant reaction paths for the suppression of vacancy and Si interstitial aggregation in silicon proceed via $\text{N}_2 + \text{V} \rightarrow \text{N}_2\text{V}$ and $\text{N}_2\text{V} + \text{I} \rightarrow \text{N}_2$, respectively. Moreover, they suggested that the shift of the boundaries of the COP- and the A-swirl region as a function of the nitrogen concentration can be used to directly measure the radial variation of vacancy and silicon interstitial concentrations, respectively, just after V-I recombination is completed. Measured values are in excellent agreement with the theoretical calculations, if the incorporation of substitutional and single interstitial nitrogen at the growth interface is assumed with a ratio of around 1:7.

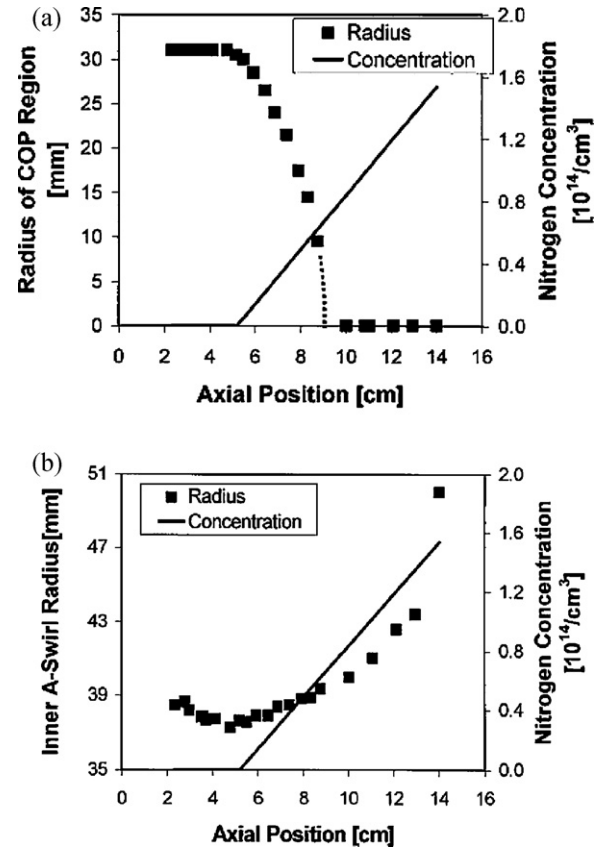


Fig. 21. Radial shift of the boundary of the COP region (a) and the inner boundary of the A-swirl region, (b) as a function of the nitrogen concentrations [61].

Nakai et al. [223] investigated the crystal defects in epitaxial layers on NCZ silicon substrates. It was found that there are two types of crystal defects generated in the epitaxial layer: stacking faults induced by a nitrogen-doped substrate (N-SF) and elliptical pits (E-pits). From the investigation of the dependence of N-SF and E-pit formation on the quality of nitrogen-doped substrates, it was revealed that the control of both nitrogen concentration and crystal growth parameter of the CZ-Si ingots is effective for suppressing N-SF and E-pit formation. Interestingly, they also reported that carbon co-doping in addition to nitrogen doping can suppresses N-SF and E-pit generation and clarify that the epitaxial layer grown on a nitrogen and carbon co-doped substrate is one of the candidates for realizing epitaxial wafers having high internal gettering ability.

5.1.2. Germanium doping

To investigate the effect of Ge on FPDs, three GCZ silicon crystals with different Ge concentrations and one conventional CZ silicon crystal without Ge doping were pulled under almost the same growth conditions [189]. According to the doping weight-in quantity of Ge, the Ge concentration in the respective head samples of the GCZ1, GCZ2 and GCZ3 silicon was estimated to be about $\sim 10^{15}$, 10^{16} and 10^{17} cm^{-3} , and the Ge concentration in the tail sample of each GCZ silicon crystal was approximately one order of magnitude higher than that in the head samples.

The FPD densities in the as-grown CZ and GCZ silicon samples with different Ge concentrations are shown in Fig. 22. It can be seen that the FPD densities in the head samples of the CZ, GCZ1 and GCZ2 silicon crystals were about $4.5 \times 10^5 \text{ cm}^{-3}$, while that of the head sample of the GCZ3 with a relatively higher Ge concentration of about 10^{17} cm^{-3} was only about $9 \times 10^4 \text{ cm}^{-3}$. For the CZ silicon

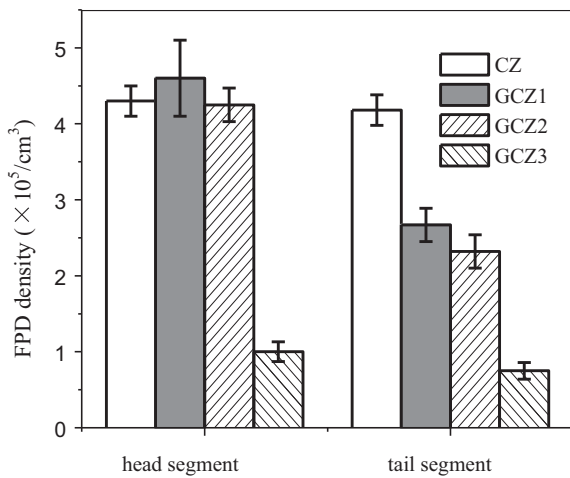


Fig. 22. FPD densities in the as-grown CZ and GCZ Si samples with the different Ge concentrations [189].

crystal, the FPD density of the tail sample was almost the same as that of the head sample. However, for the GCZ1, GCZ2 and GCZ3 Si crystals, the FPD densities of the tail samples were less than those of the head samples. Furthermore, the FPD densities of the tail samples of the GCZ Si decreased with the increase of Ge concentration. Accordingly, it can be concluded that Ge doping can significantly suppress voids in GCZ Si crystals.

Fig. 23 shows the size profiles of grown-in COPs in both the CZ and GCZ silicon wafers [221]. As can be seen, an increase in the percentage of COPs which are smaller ($0.11\text{--}0.12 \mu\text{m}$), and a

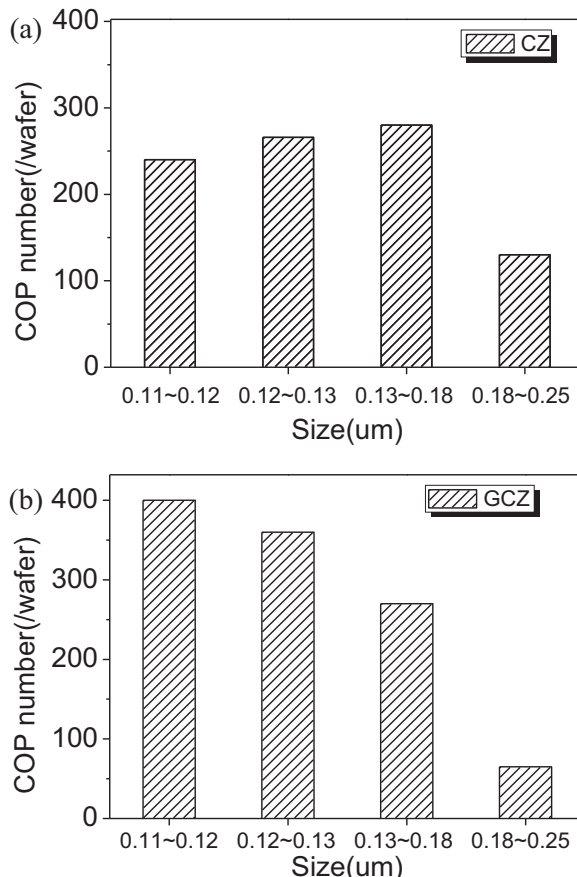


Fig. 23. Density and size profiles of the COPs on (a) CZ, and (b) GCZ silicon wafers [221].

decrease in the percentage of COPs which are larger (over $0.12 \mu\text{m}$) in the GCZ silicon wafers compared to those in the CZ silicon wafers has been suggested. The total amount of grown-in COPs on the GCZ silicon wafers was actually more than that on the CZ wafers, meaning Ge doping could induce a higher density of COPs generated with smaller sizes. As noted, the evolution of COPs in as-grown GCZ silicon seems not to coincide with the result given by FPDs detection. It is worthwhile to point out that the FPDs are believed to be deduced by larger voids, i.e., only those whose radius is larger than the critical radius r_c can bring enough hydrogen bubbles to etch wafer surface and leave flow patterns. Suggested by the results of COPs detection, the quantity of larger voids in GCZ silicon crystals is less than that in CZ silicon. Therefore, it is reasonable to conclude that the fewer FPDs in the GCZ silicon samples are associated with the lack of larger voids while the higher density COPs on the GCZ silicon wafers is mainly contributed by smaller size voids.

Yu et al. [226] have investigated the FPDs distribution in GCZ silicon wafer with light and heavy dopants either boron (B) or phosphorus (P). It was also found that the FPD densities in the lightly doped (both B and P) GCZ silicon decrease with the increase of Ge concentrations; in the heavily B-doped GCZ silicon, the FPDs are denser compared with the heavily B-doped CZ silicon, whereas the reverse case in the heavily P-doped GCZ and CZ silicon were observed.

5.1.3. Carbon doping

No electrical activities would have been brought to silicon wafers by C doping because C mainly exists on substitutional sites. C is known to modify the properties of grown-in microdefects in silicon crystal at relatively low concentrations as reported by Porrini [224]. It was found that C increases the value of the ratio V/G thus expanding the interstitial region of a crystal and the microdefects density is remarkably changed by C doping. The COPs could be impeded by C doping in CZ silicon. It was reported by Takahashi et al. [225] that C induces a significant reduction in the size of voids observed by TEM. This effect indicates a strong vacancy trapping by C and with reduced size and slightly reduced void density, the amount of vacancies contained in the voids is strongly diminished.

5.2. Annealing behavior

5.2.1. Nitrogen doping

The annealing behavior of voids in NCZ silicon have been investigated in pure hydrogen atmosphere by Yu et al. [220], and they also discussed the dissolution of the voids in NCZ silicon in detail. It was found that the radical size profile of grown-in COPs of NCZ silicon wafers cut from the tail portion of the crystal was the same as that of CZ wafers, that is to say, the density of COPs in smaller size along the radial direction increased, while that in larger size decreased. The COP mappings of the CZ and NCZ tail wafers experienced annealing in hydrogen in the temperature range of $1150\text{--}1200^\circ\text{C}$ for 1–2 h was shown in Fig. 24. It was obvious that there was a high density of COPs both in CZ and NCZ as-grown silicon. When subjected to annealing at 1150°C for 2 h, the COPs could be largely removed on NCZ wafers, while those on the CZ wafers were hardly removed. After 1200°C annealing for 1 h, since the COPs on both the silicon wafers were basically eliminated, however, it should be mentioned that, the number of COPs in the CZ wafers still remained to some extent. This shows that the thermal stability of COPs on the NCZ wafers is poorer than that on the CZ wafers. Besides, it was also found that the COPs in the outer part of the wafers were dissolved more easily than those in the inner.

As mentioned above, N doping in CZ silicon has been considered to decrease the concentration of vacancies, which impeded the

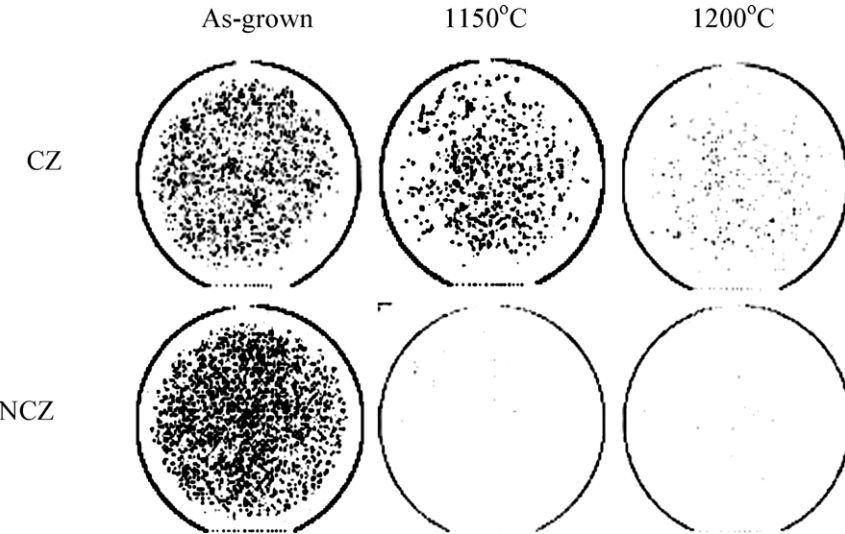


Fig. 24. COP maps of the CZ and NCZ wafers cut from the tail portions of the crystals before and after annealing in hydrogen at different temperatures [220].

formation of voids. It is also concluded by Voronkov and Falster [222] that the N doping is in favor of generating denser voids with smaller size due to the reduction in C_0 . Moreover, they considered that the dissolution process of voids consists of two steps. At first, the oxide films on the inner wall of voids are dissolved. Because of the out-diffusion of oxygen during annealing in hydrogen, the oxygen concentration in the sub-surface of CZ silicon wafers is lower than the solid solubility, so the oxide films are dissolved by the catalysis of hydrogen which results in the collapse of voids. Then surface silicon atoms on the inner wall of voids are mobile to reconstruct and vacancies diffuse out of the surface. Above all, the voids in the NCZ silicon can be more easily dissolved than those in the conventional CZ silicon.

5.2.2. Germanium doping

Experiments have clarified that the thermal stability of FPDs in GCZ silicon is much poorer than that in CZ silicon. The FPD densities in both the CZ and GCZ silicon samples before and after different annealing are shown in Fig. 25 [189]. It was evident that, after the 1050 °C/2 h annealing, the FPD density in the GCZ silicon is significantly reduced, while that in the CZ silicon crystals remains almost constant. Although the FPD density in the CZ silicon wafer decreased to a considerable extent after 1150 °C annealing for 2 h, it was still much higher than that in the GCZ

wafer. However, after 1200 °C/2 h annealing, the FPD densities in both the CZ and GCZ silicon wafers decreased to nearly the same level. The prolonged annealing at high temperatures has no notable effect on the annihilation of FPDs. That is, the FPDs in the GCZ silicon crystals can be annihilated at lower temperatures than those in the CZ crystal, implying the thermal stability of voids in the GCZ silicon crystals is much poorer, i.e., the voids in the GCZ silicon crystals can be eliminated by high-temperature anneals with a low-cost heat budget.

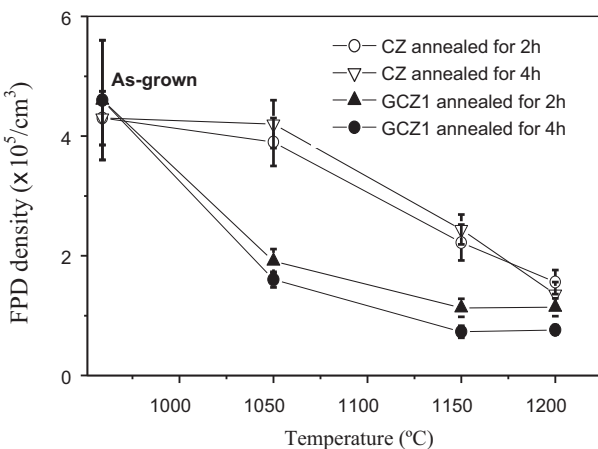
Similar with FPDs, poorer thermal stability of COPs could be also detected in GCZ silicon compared to CZ silicon. After annealing in hydrogen at 1200 °C, COP density on the GCZ silicon was much lower than that on the CZ silicon, indicating that the COPs on the CZ silicon wafer can be annihilated more easily by Ge doping [221]. Actually, at the sub-surface (such as at the depth of 30 μm) in the annealed wafers, it was also found that more grown-in COPs were annihilated on the GCZ silicon wafers than on the CZ ones. Ge doping could reduce the thermal stability of grown-in COPs not only on the surface but also in the bulk of the GCZ silicon wafers. Consequently, it is suggested that Ge doping could effectively deteriorate the thermal stability of grown-in COPs on wafers.

It is interesting to propose the mechanism of Ge impacting void defects by forming Ge-related complexes. Ge atoms can react with the intrinsic point defects in CZ silicon crystals, so that the formation of vacancy-based microdefects, such as P-band and voids, will be influenced by Ge doping. Meanwhile, the Ge atoms located on substitutional sites of the silicon cause lattice distortion and hence mechanical stress. To relieve the stress, Ge tends to react with vacancy and/or oxygen to form $\text{Ge}-\text{V}_m$ or $\text{Ge}-\text{V}_n-\text{O}_m$ ($m, n \geq 1$) complexes when GCZ wafers are annealed at high temperatures, and that the complexes would survive at low temperatures and become the nuclei of oxygen precipitates. Thus, prior to the nucleation of voids, the nuclei of oxygen precipitates can grow by rapid diffusion of oxygen and absorption of a considerable number of vacancies at high temperatures. Accordingly, the number of surviving vacancies contributing to the formation of voids during subsequent cooling is reduced.

The driving force for void formation, f , is the gain in volume free energy per vacancy associated with vacancy super-saturation, which can be expressed as

$$f = k_B T \log \left(\frac{C_0}{C_e} \right) \quad (5-1)$$

Fig. 25. FPD densities in both the CZ and GCZ silicon samples before and after different high-temperature annealing [189].



where k_B is Boltzman's constant, T the void nucleation temperature, C_e the equilibrium vacancy concentration, and C_0 the initial vacancy concentration (the actual vacancy concentration in as-grown silicon). From equation (5-1) and bearing in mind that C_g strongly decreases with decreasing temperature, it can be found that the void nucleation temperature T will be lower when the initial vacancy concentration C_0 is reduced by Ge doping in CZ silicon crystal. Therefore, voids are suppressed in as-grown GCZ silicon crystal, especially for those with large volume voids which are believed to be the origin of FPDs. This can also explain the fact that the FPD density decreases with the increase of Ge concentration. Additionally, the voids could be formed during lower temperature annealing because of the pronounced vacancy consumption caused by the formation of the Ge-related complexes. In fact, when binding temperature of Ge and vacancies T_b is higher than the nucleation temperature of voids T_n , void formation will be strongly or completely suppressed, due to the lack of free vacancies [215]. Because T_b is probably higher than T_n , the void formation will be suppressed due to the decrease in free vacancies which results in the decrease of C_0 . According to Voronkov's results, the density N and size R (assuming spherical voids in silicon lattice and the radius R standing for their size) of voids in CZ silicon crystals accord with the relational expression as follows:

$$N = \left(\frac{1.72}{4\pi m^*} \right) \left(\frac{qE^*}{Dk_B T^2} \right)^{3/2} \left(\frac{2C_0}{\rho} \right)^{-1/2} \quad (5-2)$$

$$R = 1.35(m^*)^{1/3} \left(\frac{C_0 D k_B T^2}{q E^*} \right)^{1/2} \quad (5-3)$$

From the equations above, one could conclude that the N and R of voids are directly proportional to the initial vacancy concentration C_0 . Therefore, the formation of lower density FPDs and denser COPs with smaller sizes were believed to be enhanced in GCZ silicon crystals, due to the decrease of the initial vacancy concentration C_0 , as well as the decrease of the formation temperature T of voids. Furthermore, higher Ge concentration in CZ silicon benefits the higher COP density, thus the COP density in the tail portion is higher than that of the head and middle portion of the GCZ silicon crystals.

Moreover, voids in CZ silicon usually form in a narrow temperature range about 300 °C below 1100 °C during crystal growth. They could be annihilated especially in hydrogen gas during elevated temperature annealing due to dissolving the inner oxide films surrounding voids. The removal of the oxide films on the inner walls of grown-in void defects is believed to be the first step in the reduction process, which is an oxygen diffusion-limited process. Then the second step is the shrinkage of voids through the diffusion of vacancies, which is a diffusion-limited process [227]. For GCZ silicon crystal, due to the decrease of void formation temperature T and the increase of void density N , the thickness of inner oxide film of voids in GCZ silicon crystals might be thinner than that in CZ silicon; additionally, the volume of voids in GCZ silicon crystals is considered to be smaller than that in CZ silicon. Therefore, the voids in GCZ silicon could be dissolved by thermal cycle more easily, compared to those in CZ silicon.

5.3. IG technology of co-doped CZ silicon

The IG is a stand-by process to remove the detrimental effect of surface metal contaminants. It requires both a thin defect-free denuded zone (DZ) close to the wafer surfaces and high density of IG sites in the bulk. The gettering sites are induced by oxygen precipitates and their extended defects during heat treatments [30]. The commonly used IG thermal cycle is the high-low-high (Hi-Lo-Hi) sequence, known as Hi-Lo-Hi three-step annealing,

which in principle consists of the following three steps: (1) oxygen out-diffusion heat treatment at a high temperature (>1100 °C) for DZ formation, (2) oxygen precipitate nucleation anneal at a temperature as low as 600–750 °C, and (3) introduction of gettering sites related to oxygen precipitates growth during high-temperature treatment, usually at 1000–1100 °C. In common sense, the width of DZ is decisively affected by oxygen out-diffusion during the first step, while the BMD density and size by the following two. Generally, it takes a long period of furnace operation for such an IG thermal cycle in addition to the time for device fabrication processes. What's more, the effectiveness of Hi-Lo-Hi IG thermal cycles is largely dependent on the initial interstitial oxygen concentration [O_i] and thermal history that the silicon wafer has undergone [228]. It is worthwhile to introduce a rather common technology named as Magic DZ process invented by MEMC [229]. The MDZ process is in principle composed of a RTP at a very high temperature (e.g., 1250 °C) and a L-H thermal cycle typically as 800 °C/4 h + 1000 °C/16 h. In the RTP step, a vacancy concentration profile increasing from the surface to the bulk is installed. The installed vacancy profile therefore controls the precipitate distribution of the wafer after the subsequent L-H process. Meanwhile, due to fast out-diffusion of vacancies near the surface crossing the critical depth, the formation of oxygen precipitates is suppressed where the DZ is located. In other words, the IG structure is controlled by the vacancy rather than the oxygen concentration profile. The reported advantages of RTP are independence on initial oxygen concentrations and thermal history of silicon wafers, reproduction of vacancy profile and easy handling. Nowadays, conventional IG process is confronting challenges from ever-decreasing feature sizes of integrated circuits and diminishing initial oxygen concentration with application of magnetic-field CZ-grown method. In this context, application of IG technology was intensely studied. Up to now, a desirable IG effect, that is a high density of BMDs in the bulk and a suitably wide DZ, has been reported in CZ silicon wafers co-doped with intended impurities.

5.4. Three-step annealing process

5.4.1. Nitrogen doping

It was assumed that absolutely clean DZ could hardly come into formation for NCZ silicon (NCZ) via general heat treatments, in which there should exist plenty of tiny oxygen precipitates [230]. However, recent research demonstrates opposite results. Clear and stable DZ appears in NCZ silicon after conventional three-step annealing. Moreover, IG process based on RTP is also workable on NCZ silicon.

Results from Ref. [231–233] show that there existed a slightly smaller-width DZ in NCZ silicon than in CZ silicon after typical H-L-H three-step annealing. However, denser BMDs appeared in the bulk of NCZ silicon wafers.

To inspect the quality of DZ, prolonged heat treatments were applied on CZ and NCZ silicon wafers after IG treatments. Rigorous Low-High two-step annealing was employed to complete nucleation of oxygen precipitates and further growth. It is illustrated by Fig. 26 that the DZs in the NCZ silicon still remained larger than 10 μm in width, although they shrunk more compared to CZ silicon. It can be concluded that even though N in CZ silicon can enhance oxygen precipitation and thus cause DZ shrinking, it has no significant effect on the DZ's stability during subsequent heat treatments.

The effect of N doping on the density of oxygen precipitates at the cross-section of NCZ silicon was investigated [233]. It was found that much denser BMDs were present in M-like shape in NCZ silicon wafer, while BMDs at relatively low density were uniformly distributed in CZ silicon wafer. Such difference in shape is ascribed

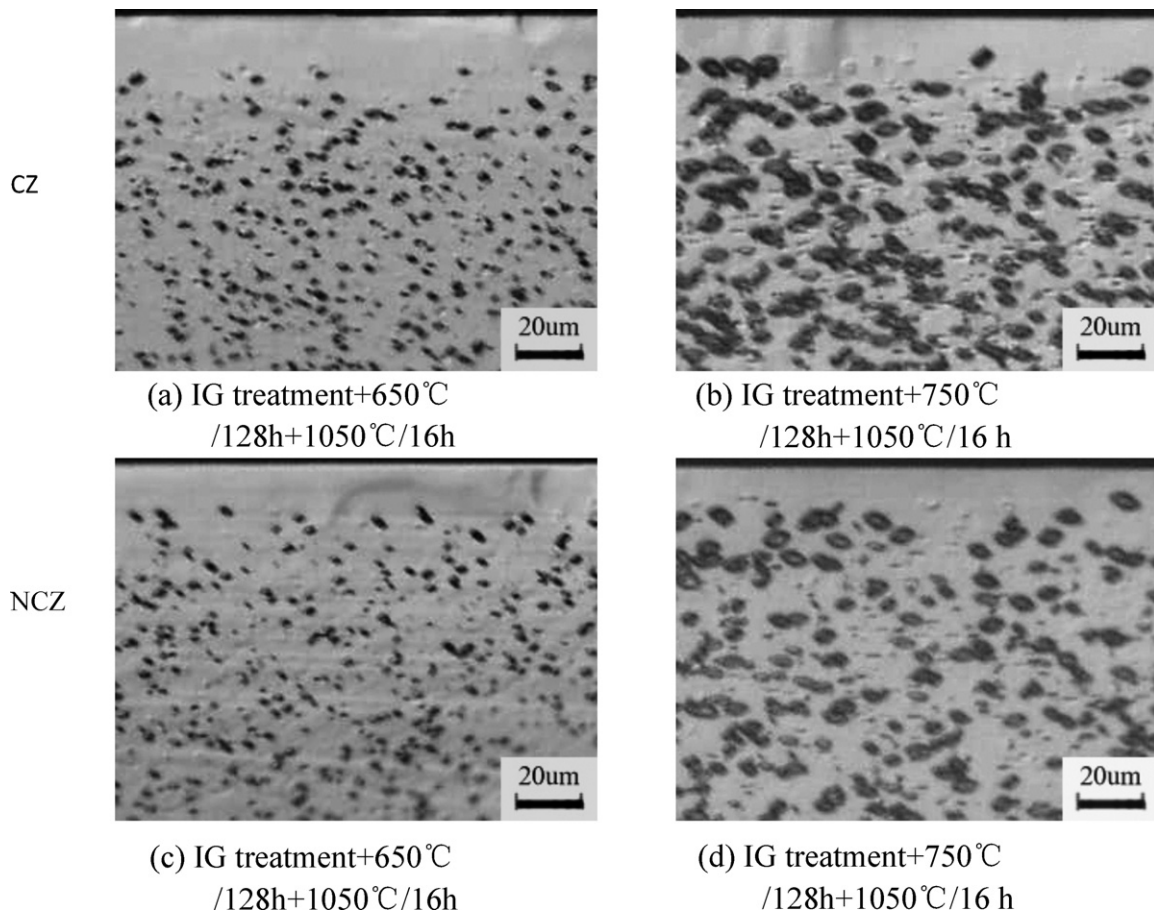


Fig. 26. Optical micrographs of the DZs and BMDs in the cross-section of the CZ silicon and NCZ silicon wafers subjected to low–high two-step in Ar ambient after the IG heat treatment [232].

to different nucleation mechanisms. In CZ silicon wafers, a homogeneous nucleation process dominates, which results in a uniform distribution of oxygen precipitates throughout the cross-section. While in NCZ silicon wafer, N was incorporated into heterogeneous nucleation process during three steps. In conclusion, there is considerable evidence that N co-doped silicon is a kind of promising material employed in fabrication of ULSI devices, because of its favorable DZ in near-surface region and high density BMDs in the bulk.

A slightly narrow but stable DZ was also generated in N-doped silicon wafers after DZ annealing with RTP pre-annealing, compared with conventional CZ silicon [36]. However, the density of oxygen precipitates characterized by BMDs is the same in both kinds of the silicon wafers subjected to 1280 °C/60 s pre-annealing. In the other words, the enhancement effect on oxygen precipitation from N doping is suppressed. N–N pairs introduced during crystal growth probably break up at high temperatures into N_i and N_s. This therefore fails to enhance oxygen precipitation. As a result, the supersaturated vacancies kept from identical rapid thermal process dominate the precipitation, which contribute to the almost same BMD density in both the CZ and NCZ silicon wafers.

For further study, both the CZ and NCZ silicon samples that had formed a DZ were subjected to rigorous oxygen precipitation annealing [234]. It was found that though notable shrinking of DZs happened within both kinds of samples, sufficiently wide DZ remained. On the ground of experimental facts, definite conclusion can be drawn as N does not affect the formation of defect-free DZ in the RTP-based IG process [234]. The [O_i] depth profile in DZ was qualitatively described for deep understanding of IG structure formed by RTP-based IG process. Following prolonged annealing at

450 °C for 100 h, spreading resistance profile (SRP) was employed to characterize the depth distribution of carrier concentration, whose amount was reported proportional to the cube of [O_i] [234]. Within the DZ region, there is a region containing more oxygen than the bulk and outer region where new oxygen precipitates occur during prolonged annealing [235]. However there still exists a DZ wide enough to satisfy requirement of contemporary microelectronic application.

5.4.2. Germanium doping

What has been reported more than once is that the desirable IG structure could be generated in Ge doped silicon wafers with conventional H–L–H three-step annealing [236]. Though the width of DZs gets a little smaller than that in CZ silicon wafers, however, the BMDs present in GCZ silicon are noticeably denser, indicating stronger gettering ability [236]. Work about the effect of germanium doping on oxygen out-diffusion was done in Ref. [237]. The conclusion is drawn that oxygen out-diffusion in silicon could be enhanced by Ge doping in the temperature range between 1050 and 1200 °C. Data from both SRP technique (Fig. 27) and SIMS measurements (Fig. 28) are conformable and verify the above conclusion. The enhancement mechanism is explained as follows: it has been well established that the diffusion of interstitial oxygen atoms in silicon occurs by atomic jumps from a bond-centered site to one of the six equivalent adjacent sites. For Ge doped silicon, the energy barrier height reduces around the substitutional site of Ge atoms, resulting from the introduction of compressive stress by larger atomic radius. As a consequence, a fast “diffusion channel” for interstitial oxygen atoms is generated.

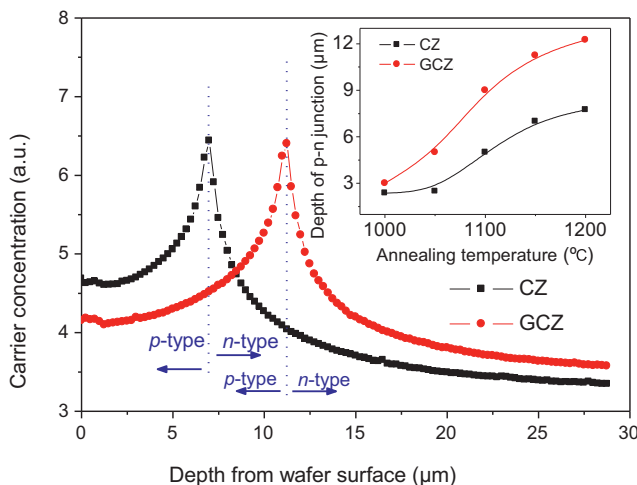


Fig. 27. The carrier concentration profiles of the CZ and the GCZ samples after the two-step thermal treatment 2 h at 1200 $^{\circ}\text{C}$ followed by 100 h at 450 $^{\circ}\text{C}$. The inset shows the correlation of the p-n junction depth versus the annealing temperatures [237].

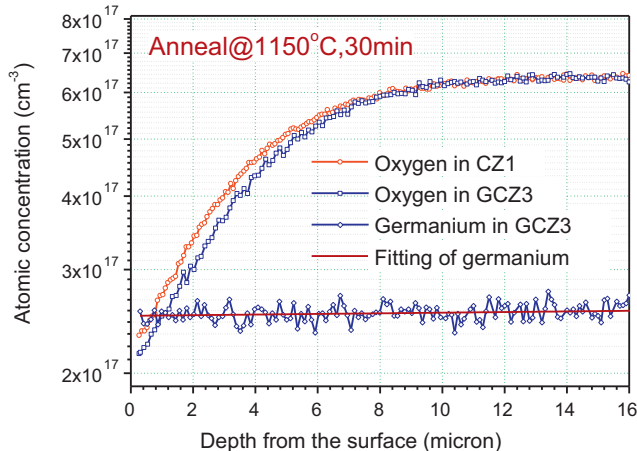


Fig. 28. SIMS profile for both the oxygen and Ge concentrations in the CZ and GCZ samples that were subjected to a 0.5 h anneal performed at 1150 $^{\circ}\text{C}$. The Ge profile was fitted using an exponential decay method [237].

An interesting phenomenon is the smaller width of DZ as obtained in GCZ silicon subjected to H-L-H three-step annealing in spite of promoted oxygen out-diffusion by germanium doping. On the basis of data supporting Ge enhancement on oxygen precipitation, it is reasonably suggested [236] that during the second low-temperature step, Ge can effectively enhance oxygen precipitate nucleation in the near-surface of GCZ silicon, even though the $[O_i]$ is lower than the solubility limit, which results in the DZ shrinkage of GCZ silicon. In addition, applications of IG process based on RTP in GCZ silicon wafers have been investigated. By analyzing the experimental data, a reasonable suggestion was put that the DZ with good quality in near-surface region and higher density of BMD in the bulk could both be formed in GCZ silicon wafers, meaning its latent utility value in IG process of ULSI fabrication [238]. A process simulation of dynamic random access memory (DRAM) fabrication involved with RTP was applied on GCZ silicon wafers. DZ at good quality is present though slightly narrower in width, which can still meet the needs of ULSI devices. Moreover, higher oxygen precipitate density was generated [239].

Afterwards, subsequent anneals were designed to check the existence of tiny oxygen precipitates in DZs, see Fig. 29 [240]. It is worthwhile to figure out that the ADD1 anneal referred in Ref.

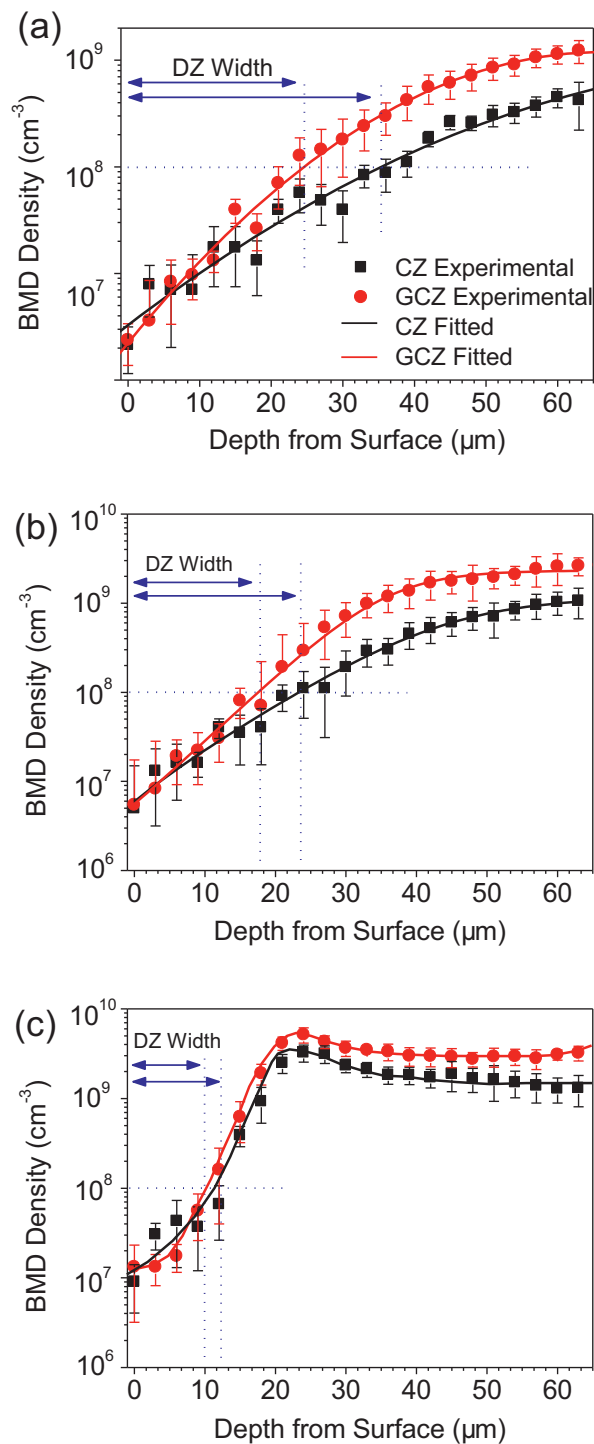


Fig. 29. BMD density profiles in sub-surface for both the conventional and GCZ silicon wafers suffered to (a) the DRAM simulating thermal treatments and the following additional treatments: (b) ADD1 and (c) ADD2 treatments [240].

[215] is aimed to coarsen the tiny oxygen precipitates within DZs by small-rate ramping (1000 $^{\circ}\text{C}/16$ h, ramping up from 800 $^{\circ}\text{C}$ with a rate of 1 $^{\circ}\text{C}/\text{min}$), whereas the ADD2 anneal aims to precipitate the oxygen interstitials within DZs by prolonging nucleation duration (650 $^{\circ}\text{C}/100$ h + 1000 $^{\circ}\text{C}/16$ h). Shrinkage of DZs happened in both kinds of silicon wafers, but the width was sufficient to satisfy the requirement of device fabrication. Namely, the thermal stability of IG structure for Ge doped CZ silicon wafer is as good as for the conventional one. With regard to gettering

capability, GCZ silicon wafers perform better than CZ silicon, ascribe to enhancement of oxygen precipitates in the bulk [241].

Two main impacts of Ge doping on CZ silicon wafers are presented during the denuded zone processing. One is the enhancement of oxygen precipitate nucleation, and the other is the enhancement of oxygen out-diffusion. It is reasonable to accept that these two influences are in competition relationship during the furnace anneals. However, oxygen diffusion strongly depends on the anneal temperature. Generally speaking, it could be speculated that the former effect dominates in most of the thermal period, so that the DZs of smaller width and BMDs at higher density are presented in three-step IG annealing.

5.4.3. Carbon doping

The effect of high-C concentration ($H[C]$, no less than $1 \times 10^{16} \text{ cm}^{-3}$) on the IG structure formed by conventional high-low-high three-step annealing was firstly studied by Chen et al. [241]. The obvious DZs and high density of BMDs were generated in the $H[C]$ CZ silicon. Though the width of DZ in $H[C]$ CZ silicon was a slightly smaller than that in conventional CZ silicon, it is sufficient for device fabrication. Furthermore, a little of denser BMDs were generated in the $H[C]$ CZ silicon implying more impurity gettering sites. Further heat treatments designed to check the existence of tiny precipitates in the DZs were employed. From the photographs in Fig. 30 [241], one can easily find that, a DZ with a width more than $10 \mu\text{m}$ survived after rigorous precipitation treatments. It is suggested that, after the first high-temperature step, out-diffusion of O_i and C_s takes place.

Recently, the carbon co-doping together with N doping was reported to be attractive to suppress the crystal defect generation for epitaxial layers, like OSFs and E-Pits [242]. OSFs and E-pits are normally formed by the agglomeration of self-interstitials around oxygen precipitates in CZ silicon. While for N and C co-doped silicon wafers, Nakai et al. found that the OSF defects can be suppressed by increasing the C co-doping content to NCZ silicon. And they proposed that the strain around the OSF centers decreases by carbon by relaxing strain around oxygen precipitates, and the OSF centers in nitrogen and carbon co-doped substrates cannot gather self-interstitials around it. Therefore, OSFs appear

after two-step oxidation, because the low-temperature heat-treatment results in the increased strain around the OSF centers during its growth, but with smaller densities. Moreover, it is also suggested that carbon has no influence on nitrogen effect for suppressing vacancy agglomeration or for forming grown-in oxygen precipitates, however, carbon might change the morphology of small rod-like voids, perhaps the rod shape becomes round [240].

5.5. One-step annealing technology

5.5.1. Nitrogen doping

Great effort has been made on reducing the thermal budget and simplification of processes for IG technology. Traditionally, it is hard for oxygen to precipitate through one-step annealing. However, as for co-doped CZ silicon emphasized here, favorable IG structures can be generated.

Recent work demonstrates that N doping of silicon wafers can get good quality DZ via one-step annealing, which is difficult for CZ silicon [243]. As shown in Fig. 31, notably denser BMDs appeared in the NCZ silicon compared with the CZ silicon after annealing at the temperature of 1150°C for 4 h. Moreover, it is noted that a clear DZ did appear in the NCZ silicon. That means a great simplification of IG process from conventional H-L-H temperature three-step annealing to the only one-step high-temperature annealing. A further test aiming to check the existence of DZs in the NCZ silicon treated with one-step annealing at high temperature was also carried out [243]. The p-type CZ silicon and NCZ silicon wafers were subjected to $450^\circ\text{C}/80\text{ h}$ annealing, after a one-step IG treatment. During annealing of $450^\circ\text{C}/80\text{ h}$ TDs are substantially produced, compensating p-type carriers and conducting type being reversed. SPR measurements were employed to obtain the TD concentration depth profile whose maximum value was proportional to cubic power of $[O_i]$, thus obtain the depth distribution of $[O_i]$, as shown in Fig. 32. From the CZ silicon a p-n junction was received, indicating that merely out-diffusion of oxygen atoms took place during annealing at 1150°C . However, a p-n-p junction was obtained for NCZ silicon, which also confirms the existence of DZ.

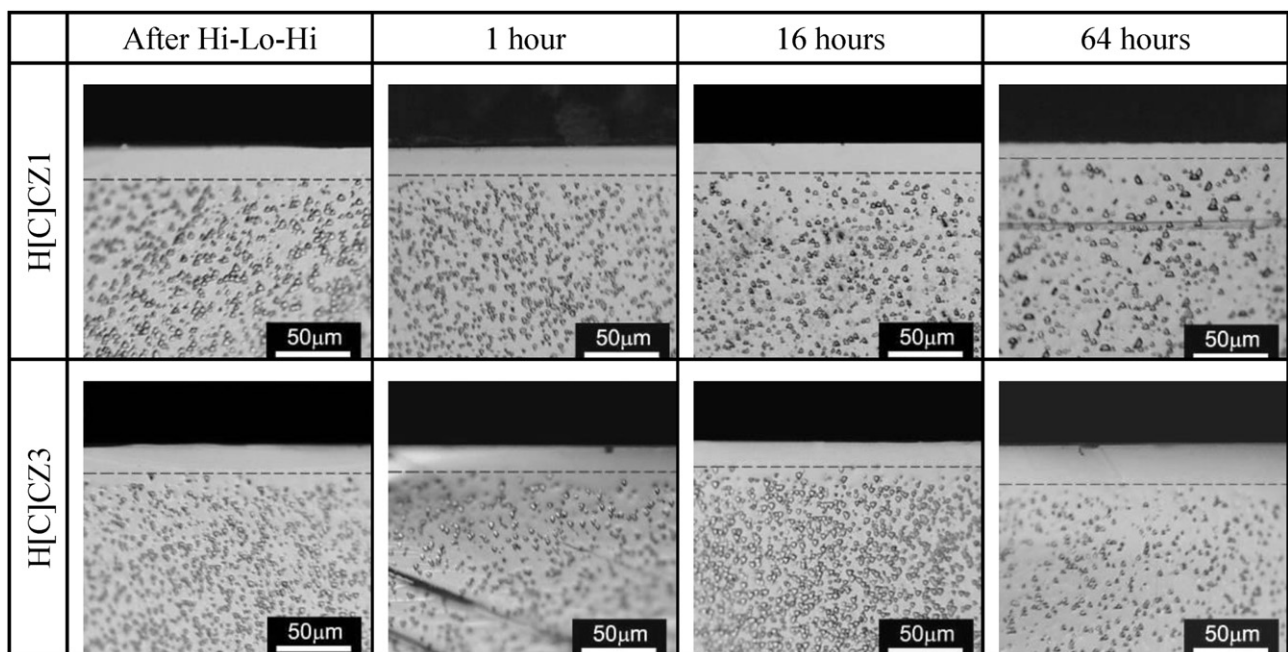


Fig. 30. Cross-sectional optical microphotographs for the L[C] and H[C] CZ silicon wafers after the Hi-Lo-Hi annealing and subjected to the rigorous ramping process following the isothermal annealing at 1050°C for 1, 16 and 64 h, respectively. The dashed lines on them were drawn to show the DZ width for clarity [241].

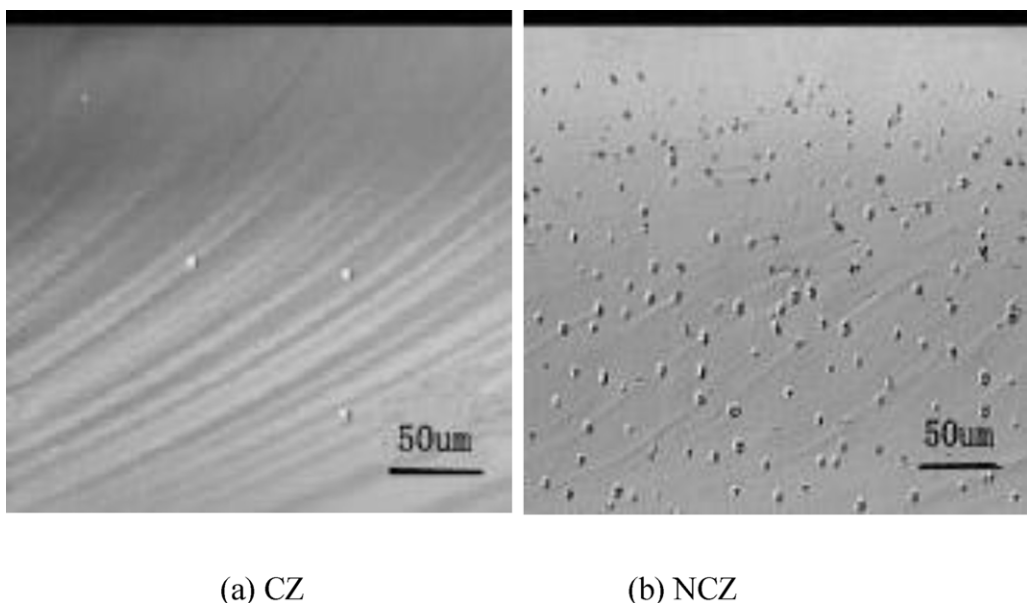


Fig. 31. Optical micrographs of the cross-sections of the CZ silicon and NCZ silicon wafers after annealing at 1150 °C for 4 h [243].

The effect of RTP related process on one-step annealing for the DZ in NCZ was also studied [168]. Without RTP pre-annealing, substantial oxygen precipitates are generated in NCZ silicon in contrast to CZ silicon in which scarcely any ones exist in the bulk, consistent to the previous results. It is supposed that N-N pairs

formed in as-grown NCZ silicon can bind vacancy and oxygen to form the $N_2-V_2-O_x$ ($x > 1$) complexes by the following reaction: $N_2 + 2V + xO \rightarrow N_2-V_2-O_x$. The $N_2-V_2-O_x$ ($x > 1$) complexes thereafter run as heterogeneous nuclei, attracting interstitial oxygen atoms aggregating even though oxygen super-saturation is very low at 1150 °C. Additionally, when the NCZ silicon wafers are subjected to RTP pre-annealing followed by one-step annealing at high temperatures, high density of BMDs is present, much more than those in the CZ silicon with RTP pre-annealing and in the NCZ silicon without RTP pre-annealing. Such effect contributes to recombination of the broken N-N bonds at temperatures (e.g., 1150 °C) lower than the RTP processing temperature. Subsequently, $N_2-V_2-O_x$ complexes are generated by the above reaction.

The other way to greatly simplify the IG process and cut down the thermal budget is ramping anneal which was also intensively studied [244]. What has been proved is that ramping anneal from low to high temperatures at a rate smaller than 3 °C/min causes grown-in oxygen precipitates whose sizes are above r_c to grow up [245]. In brief, a ramping process takes full advantage of grown-in oxygen precipitates, those stayed in the bulk are remained as nuclei and promote precipitation, those located in near-surface region subsequently dissolves when ramping to a high temperature. The IG structure thus forms. It was found that wider DZ and denser BMDs were obtained while ramping from a lower temperature suitable for nucleation, or to a higher temperature suitable for dissolution of oxygen precipitates and for simultaneous out-diffusion of oxygen atoms. Oxygen precipitation in NCZ silicon can occur under the condition of ramping from lower temperatures compared to CZ silicon, which is favored in microelectronics manufacturing.

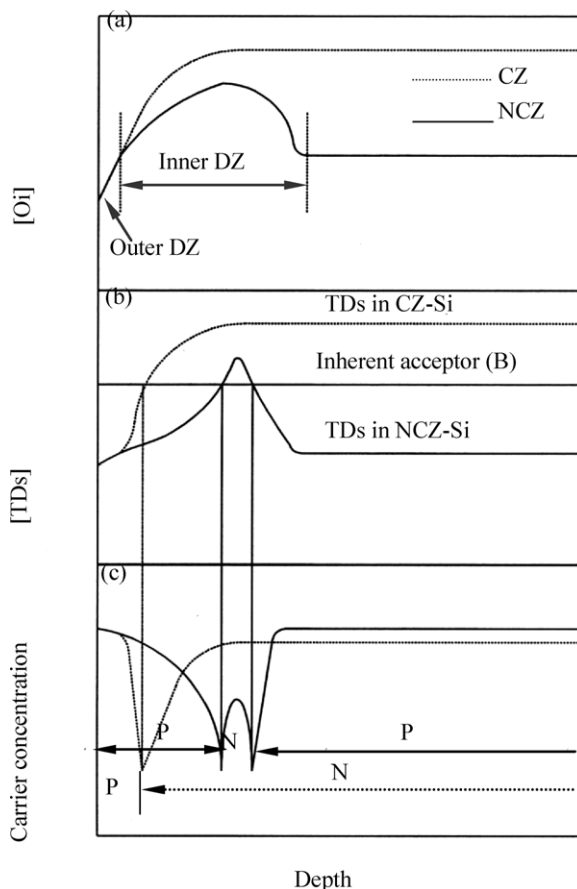


Fig. 32. Schematic diagram for the conceptual model to elucidate the formation of the p-n junction in p-type CZ silicon wafer and the pnp structure in p-type NCZ silicon wafer, subjected to high-temperature ~1150 °C annealing and successive prolonged 450 °C annealing [243].

5.5.2. Germanium doping

Studies on one-step IG annealing for GCZ silicon wafers showed that the desirable IG structure can be also obtained, implying promising application of GCZ silicon to future IC industry. Dense oxygen precipitates were found in GCZ silicon wafers treated with one-step annealing at temperatures as high as 1050 °C. In contrast, DZ was hardly to be found in CZ silicon wafer with same thermal treatments [236]. It is a desirable phenomenon that denuding annealing process can be largely simplified to one-step in CZ silicon wafers with Ge doping.

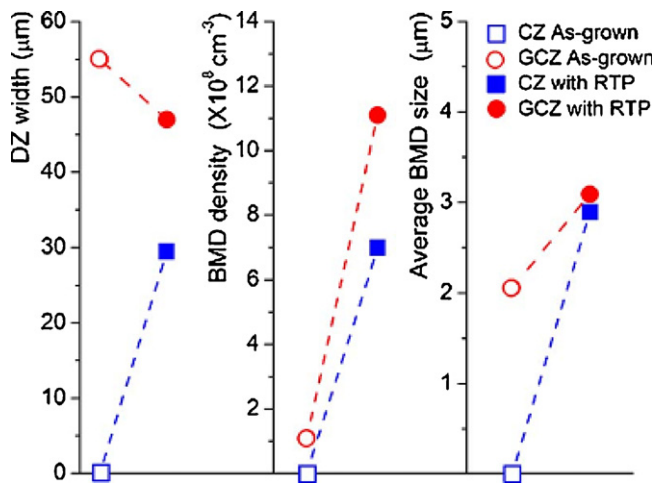


Fig. 33. DZ widths, BMD densities, and their average sizes in both the CZ and GCZ silicon wafers annealed at 1050 °C for 16 h with or without RTA pre-annealing which was performed at 1260 °C for 60 s [237].

Furthermore, denuded zone formation using one-step annealing with RTP pre-annealing also works on GCZ silicon wafers [237,238]. Denser oxygen precipitates were observed in the GCZ silicon wafers after a RTP 1260 °C/60 s followed by conventional 1050 °C/16 h annealing, see Fig. 33. Meanwhile, it is interesting to find that the DZ widths in the GCZ silicon wafers were larger than that in the CZ silicon wafers. The interpretation has been proposed: on one hand, Ge-related complexes trap vacancies at ease for the purpose of releasing lattice stress, leading to more vacancies surviving from the RTP pre-annealing, leading to an enhanced oxygen precipitation due to vacancies generated; on the other hand, the oxygen out-diffusion is promoted in the temperature range of 1050–1200 °C therefore the oxygen concentration in the sub-surface region is too low to generate the obvious oxygen precipitates. The above two effects are the relation of mutual competition and temperature dependent: the promotion of oxygen out-diffusion is quite weak at low temperatures, and therefore the promotion on the enhancement on the out-diffusion of oxygen interstitials instead of the nucleation process of oxygen precipitation dominates the behaviors of Ge atoms in the GCZ silicon during annealing at the temperature of 1050 °C during RTP processing. The DZ width in the GCZ silicon wafers was therefore larger than that of the CZ ones in such case.

6. Influence of co-dopants on wafer mechanical strength

The mechanical properties of CZ silicon wafers are crucial for ensuring manufacturing yield of ICs. Silicon is a brittle material at room temperature, thus being susceptible to breakage or fracture during device manufacturing due to either localized stress at sharp contacts during handling, chemical-mechanical polishing, back-face grinding and dicing, or global stress during robot handling, down force during chemical mechanical polishing, etc. [246,247]. Silicon turns into a ductile material when annealed at temperatures beyond the brittle-ductile transition (BDT) point [248,249]. In this case, the mechanical properties of silicon are dictated by dislocation generation and motion. The stress in the silicon wafer generated at high temperatures may result in warpage which is detrimental for alignment in the lithography process [250], and even worse, may lead to slip lines which are the disastrous killer of device manufacturing yield. In a word, the mechanical properties of silicon at room and elevated temperatures are of great importance for crystal cutting and device manufacturing. For CZ silicon, the primary impurity of oxygen exerts significant effects on

the mechanical properties. Moreover, it has been verified that co-dopants such as N, Ge and C also affect the mechanical properties of CZ silicon in different manners.

6.1. Fracture strength

The effect of N doping on Young's modulus and hardness of silicon has been studied by nano-indentation. N doping with a concentration of $2 \times 10^{15} \text{ cm}^{-3}$ can significantly increase the Young's modulus (from 104 to 182 GPa) and hardness (from 6.49 to 8.11 GPa) of float-zone (FZ) silicon. However, the related mechanism of such the strengthening effect remains unclear [251].

Vedde et al. investigated the room temperature fracture strength of N-doped silicon wafers with a specially designed double ring bending setup. It was shown that FZ silicon wafers with the low concentration N ($< 2 \times 10^{14} \text{ cm}^{-3}$) and oxygen ($3-4 \times 10^{15} \text{ cm}^{-3}$) exhibited a significantly higher fracture strength than conventional CZ ($[O_i]: 7.2-8.6 \times 10^{17} \text{ cm}^{-3}$) or FZ ($[O_i]: 4-15 \times 10^{15} \text{ cm}^{-3}$) silicon wafers, whereas FZ silicon wafers with the high concentration N ($1.7-3.6 \times 10^{15} \text{ cm}^{-3}$) but without oxygen did not possess the improved fracture strength [252]. Besides, for CZ silicon, N doping can improve fracture strength for both grinded and polished wafers [253]. This implies that the improvement in the fracture strength of silicon by N doping relies on the presence of oxygen. High density grown-in oxygen precipitates and N-O complexes are suggested to be responsible for the increase of fracture strength for NCZ silicon [253,254].

Ge doping can improve the fracture strength of the annealed CZ silicon wafers, which is attributed to the formation of high density and small oxygen precipitates [255]. The Ge doping at $\sim 10^{19} \text{ cm}^{-3}$ increases the fracture strength of multicrystalline silicon as well [256]. The mechanical behavior of Ge doped silicon has also been investigated by nano-indentation [257]. As shown in the load-displacement (P-h) curves in Fig. 34, the GCZ silicon with a Ge

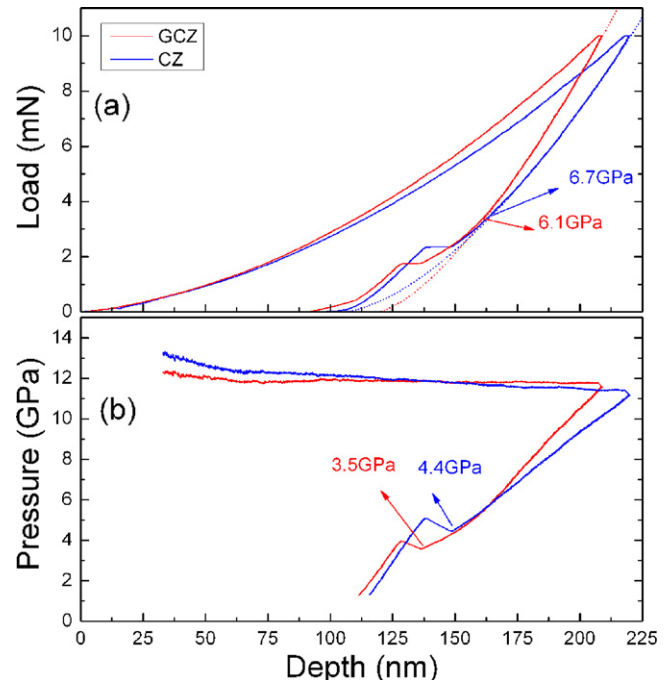


Fig. 34. Nano-indentation tests of the CZ silicon and GCZ silicon specimens. (a) Load-displacement (P-h) curves of the CZ silicon (blue solid line) and GCZ silicon (red dashed line) specimens, with a maximum load of 10 mN and constant loading/unloading rate of 0.05 mN/s. The dotted lines represent the power-law fitting of initial unloading P-h curves. (b) Corresponding average contact pressure versus depth curves of Fig. 34(a) [257]. (For interpretation of the references to color in this figure legend, the reader is referred to the web version of the article.)

concentration of $8 \times 10^{19} \text{ cm}^{-3}$ shows a stiffer mechanical behavior under contact loading with sharper slopes for both loading and unloading segments, smaller maximum indentation depth and smaller residual indentation depth. It is derived from nano-indentation experiments that GCZ silicon has higher Young's modulus and hardness of than ordinary CZ silicon. The improvement in the elastic module of GCZ silicon is supposed to be caused by the promotion effect of Ge doping on metallic phase transformation (Si-I–Si-II phase) during the indentation, which has been confirmed by micro-Raman spectroscopy measurements [255].

C doping has been suggested to increase the micro-hardness of CZ silicon [258]. This may be related to the existence of strong C–Si bonds in C-doped silicon. The influence of C doping on fracture strength of silicon is still not clear. C doping increases the yield strength of silicon crystals when the crystals are initially dislocated and contain oxygen impurity with the concentration higher than about $5 \times 10^{17} \text{ cm}^{-3}$ [259].

6.2. Plastic deformation

It is well known that the interstitial oxygen can suppress slip and warpage of CZ silicon wafers [260,261]. Likewise, the interstitial N has the similar effects. Interestingly, a minor concentration of N ($<3 \times 10^{15} \text{ cm}^{-3}$) is found to be very effective in reducing slips in low-oxygen content silicon wafers [11]. N doping with a concentration of $3.6 \times 10^{15} \text{ cm}^{-3}$ can reduce wafer warpage of CZ silicon wafers during annealing [262]. Moreover, the dislocation glide around an indentation on CZ silicon at high temperatures is found to be significantly suppressed by N doping [260,261].

In CZ silicon with different N concentrations, an increase in the N concentration leads to enhanced upper and lower yield points, as shown in Fig. 35 [263]. N can also increase the upper yield stress of FZ silicon [264]. This implies that N doping can increase the

tolerable processing temperatures at which the plastic deformation of silicon wafers under load can be avoided.

The locking of dislocations by N can be directly evidenced by the increased unlocking stress, which refers to the critical stress for dislocation movement. It is proved that the FZ silicon with higher N concentrations has larger unlocking stresses, implying the increase of N concentration results in a stronger locking effect [266]. The interaction energy between N and dislocations has also been studied by measuring the unlocking stress as a function of temperatures [267]. The experimentally estimated energy for dislocation escaping from the locking of N atom is 4.1 eV, slightly higher than that of 3.6 eV between dislocations and oxygen [249]. This interaction energy cannot be understood in terms of the model in which the dislocations interact with individual impurity atoms. Consequently, it is proposed that impurity atoms segregate at dislocations and pipe diffuse along the dislocation line, forming complexes or clusters which immobile dislocations strongly [267]. Molecular dynamics (MD) modeling suggests that the binding energy of N with edge dislocation ($1.66 \text{ eV}/\text{\AA}$) is slightly lower than that of oxygen ($1.8 \text{ eV}/\text{\AA}$) [265]. In brief, both the experimental and theoretical results agree that N has a strong dislocation locking ability which is comparable with that of oxygen.

High concentration Ge doping can also suppress dislocation generation in silicon. Generally, a so-called Dash necking process is necessary in CZ silicon crystal growth in order to grow a dislocation-free silicon ingot. However, using an appropriately Ge doped silicon seed, dislocation-free GCZ silicon can be grown successfully without the Dash necking process [94]. The generation of dislocations due to thermal shock was found to be suppressed in a seed with a cross-section of $7 \times 7 \text{ mm}^2$ when the doped Ge concentration exceeded $9 \times 10^{19} \text{ cm}^{-3}$ [94]. Heavy Ge and boron co-doping (e.g. $[\text{Ge}] = 4 \times 10^{19} \text{ cm}^{-3}$, $[\text{B}] = 9 \times 10^{18} \text{ cm}^{-3}$) in silicon can also suppress dislocation generation significantly due to the increase of critical resolved shear stress for dislocation generation [269]. Moreover, the $\text{Si}_{1-x}\text{Ge}_x$ alloy also shows higher yield strength than pure silicon due to higher concentration of Ge in silicon, and the yield strength of the alloy increases with increasing Ge concentrations in the region $0 < x < 0.1$ [270].

Ge doping can also retard dislocation motion in silicon. The sizes of dislocation motion-induced rosettes in Ge doped CZ silicon are smaller than those in conventional CZ silicon [271]. In addition, as shown in Fig. 36, the rosette size decreases with increasing Ge concentrations [255,272].

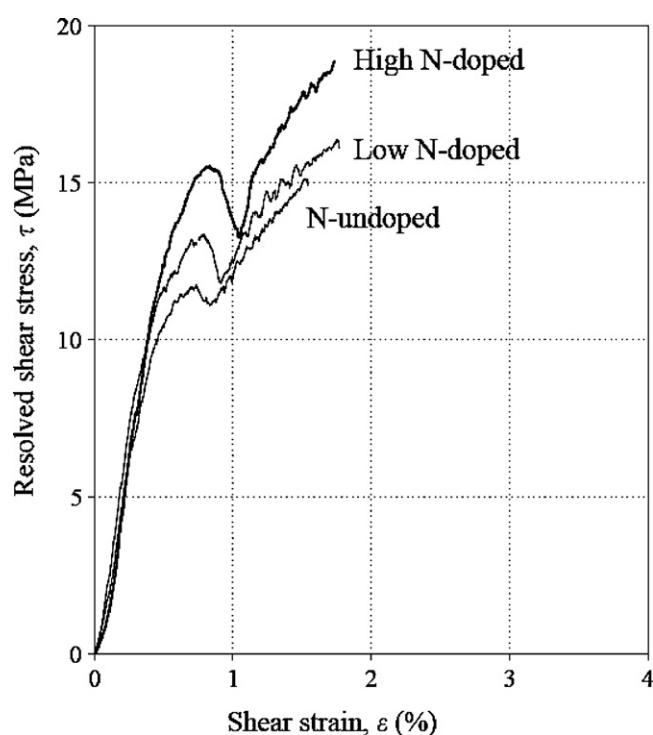


Fig. 35. Stress–strain curves of dislocation-free Czochralski silicon crystals deformed in the $<110>$ direction at 850°C under the shear strain rate $d\epsilon//dt = 7 \times 10^{-6} \text{ s}^{-1}$ for different N concentrations. The concentration of N in the samples is 3×10^{13} – $3 \times 10^{14} \text{ cm}^{-3}$ for low N-doped samples, 3×10^{14} – $3 \times 10^{15} \text{ cm}^{-3}$ for high N-doped samples and $<3 \times 10^{13} \text{ cm}^{-3}$ for the N-undoped samples [263].

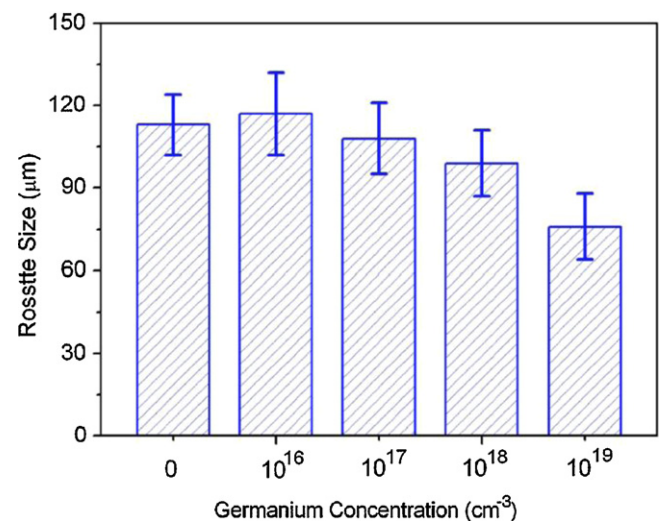


Fig. 36. Rosette sizes in CZ silicon wafer and the GCZ silicon wafers with different Ge concentrations subjected to $1100^\circ\text{C}/2 \text{ h}$ annealing after the 200 g indentation [255].

The influence of Ge doping on dislocation velocity depends on the doping concentrations. In the GCZ silicon with the Ge concentrations between 10^{19} and 10^{20} cm^{-3} , the dislocation velocity is almost comparable to that in Ge-free CZ silicon [269]. With Ge doping at a concentration of $2 \times 10^{20}\text{ cm}^{-3}$, the dislocation velocity is higher than that in conventional CZ silicon. With further higher Ge concentrations, for example 2.2% ($\sim 1.1 \times 10^{21}\text{ cm}^{-3}$) and 5.4% ($2.7 \times 10^{21}\text{ cm}^{-3}$), the dislocation velocity is lower than that in conventional CZ silicon [273].

As a substitutional impurity in silicon, Ge cannot lock dislocations as strongly as oxygen and N. The interaction energy between Ge atoms and dislocations is $0.34\text{ eV}/\text{\AA}$, much lower than those for oxygen ($1.80\text{ eV}/\text{\AA}$) and N ($1.66\text{ eV}/\text{\AA}$) [274]. Moreover, the diffusion coefficient of Ge in silicon is several orders of magnitude lower than that of oxygen [274]. Therefore, the dislocation locking by Ge can be ignored when oxygen is present in silicon even if the Ge concentration is 1–2 orders of magnitude higher than the typical oxygen concentration in CZ silicon ($\sim 10^{18}\text{ cm}^{-3}$). In addition to the direct interaction with dislocations, Ge can affect dislocation locking indirectly by influencing oxygen diffusion. It is found that the dislocation unlocking stress in Ge doped CZ silicon ([Ge]: $8 \times 10^{19}\text{ cm}^{-3}$) is lower than that in conventional CZ silicon. The strain introduced by Ge doping may retard oxygen diffusion in silicon, resulting in a lower unlocking stress [275].

C doping can also retard dislocation glide in silicon efficiently [276]. According to MD calculation, the binding energy of C-edge dislocation ($1.54\text{ eV}/\text{\AA}$) is close to those of oxygen and N [268]. This can account for the above-mentioned retarded dislocation glide and the increased yield strength in C-doped silicon. On the other hand, C can degrade the mechanical properties of silicon through enhancement of oxygen precipitation. It is found that the upper yield strength of the annealed silicon decreases with increasing C concentration from 10^{14} to 10^{16} cm^{-3} due to the C enhanced oxygen precipitation [277–279].

7. Conclusions

Impurity engineering based on the N, Ge and C co-doping technology is currently becoming the most effective way to control defects in CZ silicon used for modern ULSI industry. The investigation of co-doping technology in the past decades has set the framework of impurity engineering from the point view of material science and has attracted intensive industrial interest in the importance of device fabrication. The fundamental properties of co-dopants in CZ silicon have been understood well. They can interplay with oxygen and vacancy to form some kinds of complexes and further give strong influence on the dynamics of microdefects during crystal growth. The formation of TDs in the co-doped CZ silicon can be suppressed at some level, benefiting the electrical stability of silicon substrate. The most important issue is that two specific defects in current large diameter CZ silicon, i.e., oxygen precipitate and void, can be modulated by co-doping technology. The former is related to the device IG and the latter is associated with the device GOI. Oxygen precipitates in the co-doped silicon can be effectively enhanced for the application of IG technology, and meanwhile voids can be tailored into small sizes for the high quality DZ by annealing out. Besides, the co-dopants in CZ silicon can effectively lock the dislocations and therefore improve the mechanical strength of wafers. All these points put the co-doped silicon crystals at a strong position for their application as high quality substrates in advanced microelectronics. Since the application of co-doping technologies would not obviously increase the cost of crystal growth, some important wafer vendors including SEH, Wacker, are producing such kinds of products for microelectronic industry, such as NCZ silicon wafers. However, an

open issue is that the mechanism of the co-doped impurities interacting with point defects and further impacting the dynamics of microdefects in CZ silicon is not completely understood. It seems difficult to experimentally elucidate the initial process of defect formation. For further deeper understanding, first-principles calculations will provide “thought experiments” to figure out what species will be energetically favorable to form as the precursors of defect nuclei in the future.

Acknowledgments

This work is supported by National Natural Science Foundation of China (Nos. 50832006, 60906002 and 61274057), National Key Technology R&D Program (2011BAE03B13), and National 973 project (2013CB632100).

References

- [1] T. Sinno, E. Dornberger, W. von Ammon, R.A. Brown, F. Dupret, Materials Science and Engineering B 28 (2000) 149.
- [2] D. Yang, J. Chen, X. Ma, D. Que, Journal of Crystal Growth 311 (2009) 837.
- [3] Y. Yatsurugi, N. Akiyama, Y. Endo, T. Nozaki, The Journal of Electrochemical Society 120 (1973) 975.
- [4] Y. Itoh, T. Nozaki, T. Masui, T. Abe, Applied Physics Letters 47 (1985) 488.
- [5] Y. Tokumaru, H. Okushi, T. Masui, T. Abe, Japanese Journal of Applied Physics 21 (1982) L443.
- [6] P.L.F. Hemment, R.F. Peart, M.D. Yao, K.G. Stephens, Applied Physics Letters 46 (1985) 952.
- [7] P.H. Bucksbaum, J. Bokor, Physical Review Letters 53 (1984) 182.
- [8] R. Hockett, D. Sams, The Measurement of Nitrogen in Silicon Substrates by SIMS, 2000: International Society for Optical Engineering, 1999.
- [9] A. Karoui, G.A. Rozgonyi, Journal of Applied Physics 96 (2004) 3264.
- [10] T. Chao, M. Liaw, C. Chu, C. Chang, C. Chien, C. Hao, T. Lei, Applied Physics Letters 69 (1996) 1781.
- [11] P. Wagner, R. Oeder, W. Zulehner, Applied Physics A: Materials Science & Processing 46 (1988) 73.
- [12] M. Nakatsu, A. Hashimoto, A. Natsume, N. Inoue, in: C.L. Claeys (Ed.), High Purity Silicon VIII, The Electronical Society, 2004, p102.
- [13] H. Ono, M. Horikawa, Japanese Journal of Applied Physics 42 (2003) L261.
- [14] M. Porrini, M. Pretto, R. Scala, Materials Science and Engineering B 102 (2003) 228.
- [15] R. Jones, I. Hahn, J.P. Goss, P.R. Briddon, S. Oeberg, Structure and Electronic Properties of Nitrogen Defects in Silicon, Scitec Publications Ltd, 2004.
- [16] P.A. Schultz, J.S. Nelson, Applied Physics Letters 78 (2001) 736.
- [17] J.S. Nelson, P.A. Schultz, A.F. Wright, Applied Physics Letters 73 (1998) 247.
- [18] H. Sawada, Physical Review B 65 (2002) 75201.
- [19] N. Fujita, R. Jones, J.P. Goss, P.R. Briddon, T. Frauenheim, Applied Physics Letters 87 (2005) 021902.
- [20] N. Stoddard, P. Pichler, G. Duscher, W. Windl, Physical Review Letters 95 (2005) 25901.
- [21] A.H. Clark, J.D. MacDougall, K.E. Manchester, P.E. Roughan, F.W. Anderson, Bulletin of American Physical Society 13 (1968) 376.
- [22] N.V. Denisova, E.I. Zorin, P.V. Pavlov, D.I. Tetelbaum, A.F. Khokhlov, Neorganicheskie Materialy 11 (1975) 2236.
- [23] T. Itoh, T. Abe, Applied Physics Letters 53 (1988) 39.
- [24] R.S. Hockett, Applied Physics Letters 54 (1989) 1793.
- [25] G. Mannino, V. Privitera, S. Sciasse, S. Libertino, E. Napolitani, P. Pichler, N.E.B. Cowern, Electrochemical and Solid-State Letters 7 (2004) G161.
- [26] V.V. Voronkov, R.J. Falster, Solid State Phenomena 95 (2003) 83.
- [27] X. Niu, W. Zhang, E. Zhang, J. Sun, G. Lu, Journal of Crystal Growth 263 (2004) 167.
- [28] Z. Jiang, W. Zhang, X. Niu, Rare Metals 24 (2005) 226.
- [29] C.D. Thurmond, private communication.
- [30] S.N. Rea, J.D. Lawrence, J.M. Anthony, The Journal of Electrochemical Society 134 (1987) 752.
- [31] W. Zhang, S. Yan, Z. Ji, Journal of Crystal Growth 169 (1996) 598.
- [32] X. Niu, W. Zhang, G. Lu, Z. Jiang, Journal of Crystal Growth 267 (2004) 424.
- [33] P. Wang, X. Yu, P. Chen, X. Li, D. Yang, X. Chen, Z. Huang, Solar Energy Materials and Solar Cells 95 (2011) 2466.
- [34] G.L. McVay, A.R. DuCharme, Journal of Applied Physics 44 (1973) 1409.
- [35] D.A. Petrov, Yu.M. Shashkov, I.P. Akimchenko, Trudy II. Vop. Met. Fiz. Polaprov., Soveshch. Akad. Nauk SSSR, Moskva, 1957, p. 130.
- [36] M. Ogino, Y. Oana, M. Watanabe, Physica Status Solidi (a) 72 (1982) 535.
- [37] P. Pichler, Intrinsic Point Defects, Impurities, and Their Diffusion in Silicon, Springer, Berlin, 2004.
- [38] G. Hettich, H. Mehrer, K. Maier, in: J.H. Albany (Ed.), Defects and Radiation Effects in Semiconductors 1978, Inst. Phys. Conf. Ser. 46, Institute of Physics, London, 1979, p. 500.
- [39] P. Dorner, W. Gust, B. Predel, U. Roll, A. Lodding, H. Odelius, Philosophical Magazine 49 (1984) 557.
- [40] A. Bouchetout, N. Tabet, E. Monty, in: H.J. von Bardeleben (Ed.), Proceedings of the Fourteenth International Conference on Defects in Semiconductors, Trans. Tech., Switzerland, 1986, p. 127.

- [41] P. Fahey, S. Iyer, G. Scilla, *Applied Physics Letters* 54 (1989) 843.
- [42] T. Nozaki, Y. Yatsurugi, N. Akiyama, Y. Endo, Y. Makida, *Journal of Radioanalytical Chemistry* 19 (1974) 109.
- [43] T. Nozaki, Y. Yatsurugi, N. Akiyama, *The Journal of Electrochemical Society* 117 (1970) 1566.
- [44] A.R. Bean, R.C. Newman, *Journal of Physical Chemistry Solids* 32 (1971) 1211.
- [45] R.C. Newman, J.B. Willis, *Journal of Physical Chemistry Solids* 26 (1965) 373.
- [46] J.L. Regolini, J.P. Stoguert, C. Ganter, P. Siffert, *The Journal of Electrochemical Society* 133 (1986) 2165.
- [47] R.C. Newman, J. Wakefield, in: J.B. Schroeder (Ed.), *Metallurgy of Semiconductor Materials*, 15, Interscience, New York, 1962, p. 201.
- [48] F. Rollert, N.A. Stolwijk, H. Mehrer, *Materials Science Forum* 38–41 (1989) 753.
- [49] J.P. Kalejs, L.A. Ladd, U. Gosele, *Applied Physics Letters* 45 (1984) 268.
- [50] L.A. Ladd, J.P. Kalejs, U. Gosele, *Materials Research Society Symposium Proceedings* 36 (1985) 89.
- [51] A.K. Tipping, R.C. Newman, *Semiconductor Science and Technology* 2 (1987) 315.
- [52] S.P. Chappell, G. Davies, E.C. Lightowers, R.C. Newman, *Materials Science Forum* 38–41 (1989) 481.
- [53] W. Kaiser, C.D. Thurmond, *Journal of Applied Physics* 30 (1959) 427.
- [54] D. Que, L. Li, Y. Lin, Chinese Patent, CN85100295, 1985.
- [55] D. Que, L. Li, X. Chen, Chinese Patent, CN87105811, 1987.
- [56] D. Que, L. Li, X. Chen, Y. Lin, J. Zhang, X. Zhou, J. Yang, *Science in China (Series A)* 34 (1991) 1017.
- [57] J. Carle, K. Francols, D.J. Henrl, European Patent, EP0191111, 1986.
- [58] F. Schmid, C.P. Khattak, *Journal of the Electrochemical Society* 126 (1979) 935.
- [59] X. Yu, D. Yang, K. Hoshikawa, *Journal of Crystal Growth* 318 (2011) 178.
- [60] C.R. Alpass, J.D. Murphy, R.J. Falster, P.R. Wilshaw, *Journal of Applied Physics* 105 (2009) 013519.
- [61] W. von Ammon, R. Hözl, J. Virbulis, E. Dornberger, R. Schmolke, D. Gräf, *Journal of Crystal Growth* 226 (2001) 19.
- [62] X. Yu, D. Yang, X. Ma, J. Yang, L. Li, D. Que, *Journal of Applied Physics* 92 (2002) 1.
- [63] M. Suezawa, K. Sumino, H. Harada, T. Abe, *Japanese Journal of Applied Physics* 25 (1986) L859.
- [64] M. Suezawa, K. Sumino, H. Harada, T. Abe, *Japanese Journal of Applied Physics* 27 (1988) 62.
- [65] H. Ch.Alt, H.E. Wagner, *Physical Review B* 82 (2010) 115203.
- [66] H.E. Wagner, H. Ch.Alt, W. von Ammon, F. Bittersberger, A. Huber, L. Koester, *Applied Physics Letters* 91 (2007) 152102.
- [67] H.Ch. Alt, Y.V. Gomeniuk, F. Bittersberger, A. Kempf, D. Zemke, *Materials Science in Semiconductor Processing* 9 (2006) 114.
- [68] C.P. Ewels, R. Jones, S. Öberg, J. Miro, P. Deák, *Physical Review Letters* 77 (1996) 865.
- [69] A. Hara, T. Fukuda, T. Miyabu, I. Hirai, *Japanese Journal of Applied Physics* 28 (1988) 142.
- [70] M.W. Qi, S.S. Tan, B. Zuh, P.X. Cai, W.F. Gu, X.M. Xu, T.S. Shi, *Journal of Applied Physics* 69 (1990) 3775.
- [71] R. Jones, C. Ewels, J.P. Goss, J. Miro, P. Deák, S. Öberg, F. Berg Rasmussen, *Semiconductor Science and Technology* 9 (1994) 2145.
- [72] N. Fujita, R. Jones, S. Öberg, P.R. Briddon, *Physica B* 401 (2007) 159.
- [73] D. Yang, X. Ma, R. Fan, D. Li, J. Zhang, L. Li, D. Que, K. Sumino, *Materials Science and Engineering B* 72 (2000) 121.
- [74] R. Jones, S. Öberg, A. Umerski, *Materials Science Forum* 65–66 (1991) 287.
- [75] A. Gali, J. Miro, P. Deák, C.P. Ewels, R. Jones, *Journal of Physics: Condensed Matter* 8 (1996) 7711.
- [76] A. Hara, A. Masaki, M. Koizuka, T. Fukuda, *Journal of Applied Physics* 75 (1994) 2929.
- [77] D. Yang, R. Fan, L. Li, D. Que, K. Sumino, *Applied Physics Letters* 68 (1996) 487.
- [78] N. Fujita, R. Jones, S. Öberg, P.R. Briddon, *Journal of Materials Science. Materials in Electronic 18* (2007) 683.
- [79] N. Inoue, M. Nakatsu, H. Ono, Y. Inoue, *Materials Science and Engineering B* 134 (2006) 202.
- [80] M. Li, D. Yang, X. Ma, C. Cui, D. Que, *Physical Status Solidi (c)* 4 (2007) 3090.
- [81] L.S. Adam, M.E. Law, S. Szpala, P.J. Simpson, D. Lawther, O. Dokumaci, S. Hegde, *Applied Physics Letters* 79 (2001) 624.
- [82] N. Fuma, K. Tashiro, K. Kakimoto, Y. Takano, *Japanese Journal of Applied Physics* 35 (1996) 1993.
- [83] H. Sawada, K. Kawakami, *Physical Review B* 62 (2000) 1851.
- [84] H. Kageshima, A. Taguchi, K. Wada, *Applied Physics Letters* 76 (2000) 3718.
- [85] J.P. Goss, I. Hahn, R. Jones, P.R. Briddon, S. Öberg, *Physical Review B* 67 (2003) 045206.
- [86] A. Karoui, F. Sahtout Karoui, G.A. Rozgonyi, M. Hourai, K. Sueoka, *The Journal of Electrochemical Society* 150 (2003) G771.
- [87] H. Kageshima, A. Taguchi, K. Wada, *Physica B* 340–342 (2003) 626.
- [88] F.S. Karoui, A. Karoui, *Journal of Applied Physics* 108 (2010) 033513.
- [89] H.J. Stein, *Applied Physics Letters* 47 (1985) 1339.
- [90] A. Taguchi, H. Kageshima, K. Wada, *Journal of Applied Physics* 97 (2005) 053514.
- [91] J. Chen, T. Wu, X. Ma, L. Wang, D. Yang, *Journal of Applied Physics* 103 (2008) 123519.
- [92] B. Pejcincovic, B. Kay, L.E. Tang, T.W. Navon, *Electron Devices, IEEE Transactions On* 36 (1989) 2129.
- [93] A. Brelot, J. Charlemagne, *Radiation Effects* 9 (1971) 65.
- [94] T. Taishi, X. Huang, K. Hoshikawa, *Materials Science in Semiconductor Processing* 5 (2002) 409.
- [95] C.M. Carbonaro, V. Fiorentini, F. Bernardini, *Physical Review B* 66 (2002) 233201.
- [96] L.I. Khirunenko, O.O. Kobzar, Y.V. Pomozov, M.G. Sosnin, G. Weyer, *Physica B: Condensed Matter* 340–342 (2003) 546.
- [97] G.D. Watkins, *Nuclear Science IEEE Transactions On* 16 (1969) 13.
- [98] C.V. Budtz-Jørgensen, P. Kringhøj, A.N. Larsen, N.V. Abrosimov, *Physical Review B* 58 (1998) 1110.
- [99] A. Chroneos, R.W. Grimes, H. Bracht, *Journal of Applied Physics* 105 (2009) 016102.
- [100] J. Vanhellemont, M. Suezawa, I. Yonenaga, *Journal of Applied Physics* 108 (2010) 016105.
- [101] G.D. Watkins, *Physical Review B* 12 (1975) 4383.
- [102] D.W. George, *Materials Science in Semiconductor Processing* 3 (2000) 227.
- [103] L. Wang, D. Yang, *Physica B: Condensed Matter* 404 (2009) 58.
- [104] A. Chroneos, C.A. Londos, *Journal of Applied Physics* 107 (2010) 093518.
- [105] D. Yang, J. Chen, *Defects and Diffusion in Ceramics: An Annual Retrospective* VII 242–244 (2005) 169.
- [106] H. Yamada-Kaneta, C. Kaneta, T. Ogawa, *Physical Review B* 47 (1993) 9338.
- [107] L.I. Khirunenko, M.G. Sosnin, N.V. Abrosimov, M. Höhne, W. Shröder, Yu.V. Pomozov, *Physica B: Condensed Matter* 273–274 (1999) 305.
- [108] J. Humlíček, R. Štoudek, A. Dubroka, *Physica B: Condensed Matter* 376–377 (2006) 212.
- [109] L.I. Khirunenko, V.A. Zasuhu, Yu. V. Pomozov, M.G. Sosnin, *Physica B: Condensed Matter* 308–310 (2001) 301.
- [110] S. Hao, L. Kantorovich, G. Davies, *Physical Review B* 69 (2004) 155204.
- [111] V.P. Markevich, A.R. Peaker, J. Coutinho, R. Jones, V.J.B. Torres, S. Öberg, P.R. Briddon, L. Dobaczewski, N.V. Abrosimov, *Physical Review B* 69 (2004) 125218.
- [112] C.A. Londos, A. Andrianakis, V.V. Emtsev, G.A. Oganesyan, H. Ohya, *Physica B: Condensed Matter* 404 (2009) 4693.
- [113] C.A. Londos, A. Andrianakis, V.V. Emtsev, H. Ohya, *Journal of Applied Physics* 105 (2009) 123508.
- [114] Yu.G. Semenov, V.A. Stephanovich, *Semiconductors* 26 (1992) 324.
- [115] K. Schmalz, V.V. Emtsev, *Applied Physics Letters* 65 (1994) 1575.
- [116] L. Song, X. Zhan, B. Benson, G. Watkins, *Physical Review B* 42 (1990) 5765.
- [117] J. Trombetta, G. Watkins, *Applied Physics Letters* 51 (1987) 1103.
- [118] P. Mooney, L. Cheng, M. Süli, J. Gerson, J. Corbett, *Physical Review B* 15 (1977) 3836.
- [119] G. Davies, E. Lightowers, R. Woolley, R. Newman, A. Oates, *Journal of Physics C: Solid State Physics* 17 (1984) L499.
- [120] K. Thonke, G. Watkins, R. Sauer, *Solid State Communications* 51 (1984) 127.
- [121] L. Murin, J. Lindström, G. Davies, V. Markevich, *Nuclear Instruments and Methods in Physics Research Section* 253 (2006) 210.
- [122] J. Lindström, L. Murin, T. Hallberg, V. Markevich, B. Svensson, M. Kleverman, J. Hermansson, *Nuclear Instruments and Methods in Physics Research Section* 186 (2002) 121.
- [123] G. Davies, A. Oates, R. Newman, R. Woolley, E. Lightowers, M. Binns, J. Wilkes, *Journal of Physics C: Solid State Physics* 19 (1986) 841.
- [124] D. Backlund, S. Estreicher, *Physica B: Condensed Matter* 401 (2007) 163.
- [125] R. Jones, S. Öberg, *Physical Review Letters* 68 (1992) 86.
- [126] C. Londos, E. Sgourou, A. Chroneos, V. Emtsev, *Semiconductor Science and Technology* 26 (2011) 105024.
- [127] G. Davies, E. Lightowers, R. Newman, A. Oates, *Semiconductor Science and Technology* 2 (1987) 524.
- [128] K. O'Donnell, K. Lee, G. Watkins, *Physica* 116 (1983) 258.
- [129] A. Yukhnovich, V. Tkachev, *Soviet Physics: Solid State* 8 (1966) 1264.
- [130] A. Bean, R. Newman, R. Smith, *Journal of Physical Chemistry Solids* 31 (1970) 739.
- [131] G. Watkins, in: P. Baruch (Ed.), *Radiation Damage in Semiconductors*, Paris, 1965, p. 97.
- [132] K. Brower, *Physical Review B* 9 (1974) 2607.
- [133] K. Natarajan, E. Heasell, *Physical Status Solidi A* 28 (1975) 603.
- [134] G. Jellison, *Journal of Applied Physics* 53 (1982) 5715.
- [135] G. Davies, R.C. Newman, in: T.S. Moss (Ed.), *Handbook on Semiconductors*, vol. 3b, Elsevier Science, Amsterdam, 1994, p. 1557.
- [136] E. Wong, B. Streetman, *Journal of Applied Physics* 42 (1971) 5882.
- [137] E. Lavrov, L. Hoffmann, B. Bech Nielsen, *Physical Review B* 60 (1999) 8081.
- [138] C.S. Fuller, J.W. Dietzenberger, N.B. Hannay, E. Buehler, *Physical Review* 96 (1954) 833.
- [139] C.S. Fuller, R.A. Logan, *Journal of Applied Physics* 28 (1957) 1427.
- [140] W. Götz, G. Pensl, *Physical Review B* 46 (1992) 4312.
- [141] W. Kaiser, H.L. Frisch, H. Reiss, *Physical Review* 112 (1958) 1546.
- [142] V. Cazcarra, P. Zunino, *Journal of Applied Physics* 51 (1980) 4206.
- [143] P. Deák, L.C. Snyder, J.W. Corbett, *Physical Review Letters* 66 (1991) 747.
- [144] D. Yang, D. Que, K. Sumino, *Journal of Applied Physics* 77 (1995) 943.
- [145] E. Hild, P. Gaworowski, M. Franz, K. Pressel, *Applied Physics Letters* 72 (1998) 1362.
- [146] H. Li, D. Yang, X. Yu, X. Ma, D. Tian, L. Li, D. Que, *Journal of Physics: Condensed Matter* 16 (2004) 5745.
- [147] J.W. Cleland, *The Journal of Electrochemical Society* 129 (1982) 2127.
- [148] W. Wijaranakula, *Journal of Applied Physics* 69 (1991) 2737.
- [149] J.A. Griffin, J. Hartung, J. Weber, H. Navarro, L. Genzel, *Applied Physics A* 48 (1989) 41.
- [150] C. Chen, C. Li, H. Ye, S. Shen, D. Yang, *Journal of Applied Physics* 76 (1994) 3347.
- [151] J.L. Lindström, T. Hallberg, *Physical Review Letters* 72 (1994) 2729.
- [152] R.C. Newman, A.S. Oates, F.M. Livingston, *Journal of Physics C: Solid State Physics* 16 (1983) 667.

- [153] U. Gösele, T.Y. Tan, *Applied Physics A: Materials Science & Processing* 28 (1982) 79.
- [154] W. Kürner, R. Suesr, A. Dörnen, K. Thonke, *Physical Review B* 39 (1989) 13327.
- [155] J. Coutinho, R. Jones, P.R. Briddon, S. Öberg, L.I. Murin, V.P. Markevich, J.L. Lindström, *Physical Review B* 65 (2001) 014109.
- [156] A.R. Bean, R.C. Newman, *Journal of Physical Chemistry Solids* 33 (1972) 255.
- [157] C. Cui, D. Yang, X. Ma, M. Li, D. Que, *Materials Science in Semiconductor Processing* 9 (2006) 110.
- [158] D. Yang, J. Chen, H. Li, X. Ma, D. Tian, L. Li, D. Que, *Physical Status Solidi (a)* 203 (2006) 685.
- [159] T. Tan, E. Gardner, W. Tice, *Applied Physics Letters* 20 (1977) 175.
- [160] B. Leroy, C. Plougonven, *The Journal of Electrochemical Society* 127 (1980) 961.
- [161] S. Kishino, Y. Matsushita, M. Kanamori, T. Iizuka, *Japanese Journal of Applied Physics* 21 (1981) 1.
- [162] M. Hasebe, Y. Takeoka, S. Shioyama, S. Naito, in: K. Sumino (Ed.), *Defect Control in Semiconductors*, North-Holland, Amsterdam, 1990, p. 157.
- [163] Z. Zeng, X. Ma, J. Chen, D. Yang, I. Ratschinski, F. Hevrot, H.S. Leipner, *Journal of Crystal Growth* 312 (2010) 169.
- [164] A. Karoui, F. Sahtout Karoui, G.A. Rozgonyi, D. Yang, *Journal of Applied Physics* 96 (2004) 3255.
- [165] K. Aihara, H. Takeno, Y. Hayamizu, M. Tamatsuka, T. Masui, *Journal of Applied Physics* 88 (2000) 3705.
- [166] K. Nakai, Y. Inoue, H. Yokota, A. Ikari, J. Takahashi, A. Tachikawa, K. Kitahara, Y. Ohta, W. Ohashi, *Journal of Applied Physics* 89 (2001) 4301.
- [167] X. Yu, D. Yang, X. Ma, D. Que, *Microelectronic Engineering* 69 (2003) 97.
- [168] H. Fujimori, H. Fujisawa, Y. Hirano, T. Okabe, *Journal of Crystal Growth* 237 (2002) 338.
- [169] F. Shimura, R.S. Hockett, *Applied Physics Letters* 48 (1986) 224.
- [170] J. Vanhellemont, C. Claeys, *Journal of Applied Physics* 62 (1987) 3960.
- [171] K. Wada, H. Nakanishi, H. Takaoka, N. Inoue, *Journal of Crystal Growth* 57 (1982) 535.
- [172] D. Yang, X. Ma, R. Fan, J. Zhang, L. Li, D. Que, *Physica B* 273 (1999) 308.
- [173] L. Li, D. Yang, *Microelectronic Engineering* 56 (2001) 205.
- [174] G.A. Rozgonyi, A. Kroui, A. Kvitt, G. Duschner, *Microelectronic Engineering* 66 (2003) 305.
- [175] T. Abe, T. Masui, H. Harada, J. Chikawa, in: W.M. Bullis, S. Broydo (Eds.), *VLSI Science and Technology 1985*, Electrochemical Society, Pennington, NJ, 1985, p. 543.
- [176] H. Kageshima, A. Taguchi, K. Wada, *Physica B* 340 (2003) 626.
- [177] A. Taguchi, H. Kageshima, K. Wada, *Journal of Applied Physics* 97 (2005) p.053514.
- [178] A. Karoui, F.S. Karoui, A. Kvitt, G.A. Rozgonyi, D. Yang, *Applied Physics Letters* 80 (2002) 2114.
- [179] D. Yang, X. Yu, *Defect and Diffusion Forum* 230–232 (2004) 199.
- [180] C. Cui, X. Ma, D. Yang, *Journal of Applied Physics* 104 (2008) 123523.
- [181] J. Chen, D. Yang, H. Li, X. Ma, D. Que, *Journal of Crystal Growth* 291 (2006) 66.
- [182] J. Chen, D. Yang, H. Li, X. Ma, D. Que, *Journal of Applied Physics* 99 (2006) 073509.
- [183] H. Li, D. Yang, X. Ma, X. Yu, D. Que, *Journal of Applied Physics* 96 (2004) 4161.
- [184] J. Chen, X. Ma, D. Yang, *Thin Solid Films* 518 (2010) 2334.
- [185] J. Chen, D. Yang, H. Li, X. Ma, D. Que, *Materials Science in Semiconductor Processing* 9 (2006) 600.
- [186] V.V. Voronkov, R. Falster, *Journal of Crystal Growth* 194 (1998) 76.
- [187] V.V. Voronkov, R. Falster, *Materials Science in Semiconductor Processing* 5 (2002) 387.
- [188] P. Wu, J. Chen, X. Ma, D. Yang, *Journal of Applied Physics* 107 (2010) 073518.
- [189] D. Yang, X. Yu, X. Ma, J. Xu, L. Li, D. Que, *Journal of Crystal Growth* 243 (2002) 371.
- [190] D. Yang, *Physical Status Solidi (a)* 202 (2005) 931.
- [191] A. Borghesi, B. Pivac, A. Sassella, A. Stella, *Journal of Applied Physics* 77 (1995) 4169.
- [192] K. Sueoka, N. Ikeda, T. Yamamoto, S. Kobayashi, *Journal of Applied Physics* 74 (1993) 5437.
- [193] C.A. Londos, A. Andrianakis, V.V. Emtsev, H. Ohya, *Semiconductor Science and Technology* 24 (2009) 075002.
- [194] C.A. Londos, A. Andrianakis, V.V. Emtsev, G.A. Oganesyan, H. Ohya, *Physica B* 44 (2009) 4693.
- [195] S. Kishino, Y. Matsushita, M. Kanamori, T. Iizuka, *Japanese Journal of Applied Physics* 121 (1982) 1.
- [196] M. Ogino, *Applied Physics Letters* 41 (1982) 847.
- [197] T.Y. Tan, E.E. Gardner, W.K. Tice, *Applied Physics Letters* 30 (1977) 175.
- [198] T.Y. Tan, C.Y. Kung, *Journal of Applied Physics* 59 (1986) 917.
- [199] F. Shimura, R.S. Hockett, D.A. Reed, D.H. Wayne, *Applied Physics Letters* 47 (1985) 794.
- [200] F. Shimura, J.P. Baiardo, P. Fraundorf, *Applied Physics Letters* 46 (1985) 941.
- [201] F. Shimura, *Journal of Applied Physics* 59 (1986) 3251.
- [202] Q. Sun, K.H. Yao, J. Lagowski, H.C. Gatos, *Journal of Applied Physics* 67 (1990) 4313.
- [203] P. Liu, X. Ma, J. Zhang, L. Li, D. Que, *Journal of Applied Physics* 87 (2000) 3669.
- [204] H.L. Tsai, in: H.R. Huff, T. Abe, B. Kolbesen (Eds.), *Semiconductor Silicon 1986*, The Electrochemical Society, Pennington, NJ, 1986, p. 790.
- [205] S. Hahn, S. Shatas, H.J. Stein, Z.U. Rek, W.A. Tiller, *Journal of Applied Physics* 64 (1988) 849.
- [206] C.A. Londos, M.S. Potsidi, V.V. Emtsev, *Physical Status Solidi (c)* 2 (2005) 1963.
- [207] S. Huth, O. Breitenstein, A. Huber, U. Lambert, *Journal of Applied Physics* 88 (2000) 4000.
- [208] E. Dornberger, D. Temmler, W. Von Ammon, *The Journal of Electrochemical Society* 149 (2002) 226.
- [209] K. Nakamura, T. Saishoji, T. Kubota, T. Iida, Y. Shimanuki, T. Kotooka, J. Tomioka, *Journal of Crystal Growth* 180 (1997) 61.
- [210] J. Ryuta, E. Morita, T. Tanaka, Y. Shimanuki, *Japanese Journal of Applied Physics* 29 (1990) L1947.
- [211] H. Yamagishi, I. Fusegawa, N. Fujimaki, M. Katayama, *Semiconductor Science and Technology* 7 (1992) 135.
- [212] S. Umeho, S. Sadamitsu, H. Murakami, M. Hourai, S. Sumita, T. Shigematsu, *Japanese Journal of Applied Physics* 32 (1993) 699.
- [213] T. Ueki, M. Itsumi, T. Takeda, *Applied Physics Letters* 70 (1997) 1248.
- [214] M. Itsumi, H. Akiya, T. Ueki, M. Tomita, M. Yamawaki, *Journal of Applied Physics* 78 (1995) 5984.
- [215] V. Voronkov, R. Falster, *The Journal of Electrochemical Society* 149 (2002) G167.
- [216] K. Takano, M. Iida, E. Iino, M. Kimura, H. Yamagishi, *Journal of Crystal Growth* 180 (1997) 363.
- [217] V. Voronkov, *Journal of Crystal Growth* 59 (1982) 625.
- [218] W. Wijaranakula, *Journal of Applied Physics* 75 (1994) 3678.
- [219] B. Park, G. Seo, G. Kim, *Journal of Crystal Growth* 222 (2001) 74.
- [220] X. Yu, D. Yang, X. Ma, L. Li, D. Que, *Semiconductor Science and Technology* 18 (2003) 399.
- [221] J. Chen, D. Yang, H. Li, X. Ma, D. Tian, L. Li, D. Que, *Journal of Crystal Growth* 306 (2007) 262.
- [222] V. Voronkov, R. Falster, *Materials Science and Engineering B* 114 (2004) 130.
- [223] K. Nakai, K. Kitahara, Y. Ohta, A. Ikari, M. Tanaka, *Japanese Journal of Applied Physics* 43 (2004) 1241.
- [224] M. Porri, V. Voronkov, R. Falster, *Materials Science and Engineering B* 134 (2006) 185.
- [225] J. Takahashi, K. Nakai, K. Kawakami, Y. Inoue, H. Yokota, A. Tachikawa, A. Ikari, W. Ohashi, *Japanese Journal of Applied Physics* 42 (2003) 363.
- [226] X. Yu, X. Ma, C. Li, J. Yang, D. Yang, *Japanese Journal of Applied Physics* 43 (2004) 4082.
- [227] X. Ma, L. Fu, D. Tian, D. Yang, *Journal of Applied Physics* 98 (2005) 084502.
- [228] F. Shimura, T. Higuchi, R. Hockett, *Applied Physics Letters* 53 (1988) 69.
- [229] R. Falster, V.V. Voronkov, F. Quast, *Physical Status Solidi (b)* 222 (2000) 219.
- [230] Q. Shui, D. Yang, L. Li, X. Pi, D. Que, *Physica B: Condensed Matter* 307 (2001) 40.
- [231] C. Cui, D. Yang, X. Yu, X. Ma, L. Li, D. Que, *Semiconductor Science and Technology* 19 (2004) 548.
- [232] C. Cui, D. Yang, X. Ma, D. Que, *Japanese Journal of Applied Physics* 45 (2006) 4903.
- [233] C. Cui, D. Yang, X. Ma, R. Fan, L. Li, D. Que, *Physica B: Condensed Matter* 376 (2006) 216.
- [234] D. Yang, M. Li, C. Cui, X. Ma, D. Que, *Materials Science and Engineering B* 134 (2006) 193.
- [235] X. Yu, D. Yang, X. Ma, H. Li, Y. Shen, D. Tian, L. Li, D. Que, *Journal of Crystal Growth* 250 (2003) 359.
- [236] J. Chen, D. Yang, X. Ma, R. Fan, D. Que, *Journal of Applied Physics* 102 (2007) 066102.
- [237] J. Chen, D. Yang, X. Ma, H. Li, D. Que, *Journal of Applied Physics* 101 (2007) 033526.
- [238] J. Chen, D. Yang, X. Ma, D. Que, *Applied Physics A: Materials Science & Processing* 94 (2009) 905.
- [239] J. Chen, D. Yang, X. Ma, W. Wang, Y. Zeng, D. Que, *Journal of Applied Physics* 101 (2007) 113512.
- [240] J. Chen, D. Yang, *Physical Status Solidi (c)* 6 (2009) 625.
- [241] J. Chen, D. Yang, X. Ma, D. Que, *Journal of Physics: Condensed Matter* 18 (2006) 11131.
- [242] K. Nakai, K. Kitahara, Y. Ohta, A. Ikari, M. Tanaka, *Japanese Journal of Applied Physics* 43 (2004) 1247.
- [243] X. Ma, X. Yu, R. Fan, D. Yang, *Applied Physics Letters* 81 (2002) 496.
- [244] L. Gong, X. Ma, D. Tian, L. Fu, D. Yang, *Semiconductor Science and Technology* 20 (2005) 228.
- [245] G. Kissinger, J. Vanhellemont, U. Lambert, D. Gräf, E. Dornberger, H. Richter, *The Journal of Electrochemical Society* 145 (1998) L75.
- [246] R. Cook, *Journal of Material Science* 41 (2006) 841.
- [247] X. Brun, S. Melkote, *Solar Energy Materials and Solar Cells* 93 (2009) 1238.
- [248] P. Hirsch, S. Roberts, J. Samuels, *Proceedings of the Royal Society of London Series A-Mathematical Physical and Engineering Sciences* 421 (1989) 25.
- [249] J. Samuels, S. Roberts, *Proceedings of the Royal Society of London Series A-Mathematical Physical and Engineering Sciences* 421 (1989) 1.
- [250] H. Shimizu, S. Isomae, K. Minowa, T. Satoh, T. Suzuki, *The Journal of Electrochemical Society* 145 (1998) 2523.
- [251] A. Karoui, G. Rozgonyi, T. Ciszek, in: P.M. Anderson, et al. (Eds.), *Nanoscale Materials and Modeling-Relations among Processing, Microstructure and Mechanical Properties*, 2004, p. 123.
- [252] J. Vedde, P. Gravesten, *Materials Science and Engineering B* 36 (1996) 246.
- [253] G. Wang, D. Yang, D. Li, Q. Shui, J. Yang, D. Que, *Physica B-Condensed Matter* 308 (2001) 450.
- [254] J. Chen, D. Yang, X. Ma, Z. Zeng, D. Tian, L. Li, D. Que, L. Gong, *Journal of Applied Physics* 103 (2008) 123521.
- [255] P. Wang, X. Yu, Z. Li, D. Yang, *Journal of Crystal Growth* 318 (2010) 230.
- [256] W. Xu, J. Chen, X. Ma, D. Yang, L. Gong, D. Tian, *Crystal Research and Technology* 46 (2011) 10.
- [257] Z. Zeng, L. Wang, X. Ma, S. Qu, J. Chen, Y. Liu, D. Yang, *Scripta Materialia* 64 (2011) 832.
- [258] S. Danyluk, D. Lim, J. Kalejs, *Journal of Material Science Letters* 4 (1985) 1135.
- [259] I. Yonenaga, K. Sumino, *Japanese Journal of Applied Physics* 23 (1984) L590.
- [260] S. Hu, W. Patrick, *Journal of Applied Physics* 46 (1975) 1869.

- [261] I. Yonenaga, K. Sumino, K. Hoshi, *Journal of Applied Physics* 56 (1984) 2346.
- [262] H. Lu, D. Yang, L. Li, Z. Ye, D. Que, *Physical Status Solidi (a)* 169 (1998) 193.
- [263] V. Orlov, H. Richter, A. Fischer, J. Reif, T. Muller, R. Wahlich, *Materials Science in Semiconductor Processing* 5 (2002) 403.
- [264] D. Li, D. Yang, D. Que, *Physica B* 274 (1999) 553.
- [265] K. Sumino, I. Yonenaga, M. Imai, T. Abe, *Journal of Applied Physics* 54 (1983) 5016.
- [266] J. Murphy, C. Alpass, A. Giannattasio, S. Senkader, R.J. Falster, P. Wilshaw, *Nuclear Instruments and Methods in Physics Research Section B* 253 (2006) 113.
- [267] I. Yonenaga, *Materials Science and Engineering B* 124 (2005) 293.
- [268] A. Karoui, in: P. Pichler, et al. (Eds.), *Silicon Front-End Junction Formation-Physics and Technology*, 2004, p. 387.
- [269] I. Yonenaga, T. Taishi, X. Huang, K. Hoshikawa, *Journal of Crystal Growth* 275 (2005) 501.
- [270] I. Yonenaga, *Journal of Crystal Growth* 275 (2005) 91.
- [271] T. Fukuda, A. Ohsawa, *Applied Physics Letters* 60 (1992) 1184.
- [272] D. Li, Y. Zhao, D. Yang, *Journal of Rare Earths* 24 (2006) 83.
- [273] I. Yonenaga, *Journal of Material Science* 10 (1999) 329.
- [274] W. Scotten, *Diffusion in Silicon*: IC Knowledge LLC, 2008, p. 71.
- [275] Z. Zeng, J. Murphy, R. Falster, X. Ma, D. Yang, P. Wilshaw, *Journal of Applied Physics* 109 (2011) 063532.
- [276] M. Akatsuka, K. Sueoka, *Japanese Journal of Applied Physics* 40 (2001) 1240.
- [277] T. Fukuda, *Applied Physics Letters* 65 (1994) 1376.
- [278] T. Fukuda, M. Koizuka, *Journal of Applied Physics* 74 (1993) 2420.
- [279] T. Fukuda, A. Ohsawa, *Journal of Applied Physics* 73 (1993) 112.